NUI Galway
OÉ Gaillimh

Investigating the Role of IRE1α RNase Activity in Breast Cancer

A thesis submitted to the National University of Ireland Galway in fulfilment of the requirement for the degree of

Doctor of Philosophy

By

Eoghan Patrick McGrath

Discipline of Biochemistry, School of Natural Sciences,

National University of Ireland, Galway

Thesis Supervisor: Professor Afshin Samali

Head of School: Professor Ciaran Morrison

September 2018

Table of Contents

Declaration

This thesis is a presentation of my own original research work. Wherever contributions of others are involved, every effort has been made to indicate this clearly at the outset of each chapter.

This work was done under the supervision of Professor Afshin Samali, at the National University of Ireland, Galway.

Work described in chapter IV was co-supervised by Dr. Claudio Hetz at the Laboratory of Proteostasis Control and Biomedicine, at the Institute of Biomedical Sciences, Faculty of Medicine, Universidad de Chile.

Acknowledgements

I have a lot of people to thank who have helped me over the past five years and without whom I couldn't have done any of this work, and definitely wouldn't have had as much craic.

Firstly, thank you Afshin for giving me the opportunity to do my PhD in your lab. You pushed me a lot and had faith in me to follow my own ideas. I'm really grateful for the opportunities you gave me to travel during my PhD. It has given me opportunities I wouldn't have believed possible five years ago, so thanks a lot.

Susan, thank you so much for all of your help. You always set the highest standards and I'm a much better scientist for having worked with you. I really appreciate all of the guidance and advice you've given me. You're going to be an awesome PI.

I want to thank all of the other Samali/Gorman lab, ARC and Bioscience members who helped me along the way and were always willing to share their time and expertise. In particular Adrienne, Kasia, Shane, Marion, Alex, and Enda.

Most of the work in this thesis was done in Galway, but I finished it in Santiago, Chile, where I made a lot of friends and lived in constant fear of earthquakes.

Thank you Claudio for giving me the opportunity to come to your lab. I don't know how many other PI's would invest so much time and energy in a visiting student. I really appreciate all of your advice and guidance. I had a great time and gained invaluable perspective. Thank you.

Hery (YOOO), thank you for taking so much of your time to train me and give me advice on experiments and everything. The quality of my work improved so much under your guidance. You were always positive, and willing to share your knowledge. Thanks a lot.

I want to thank all of the other postdocs in Claudio's lab and the UPR team (the best team), especially Phillipe, Yannis, and Younis, for all of the advice they gave me about experiments and about pursuing a career in academia. Thank you to all the other friends I made in Claudio's lab. It's nice to know that people on the other side of the planet are also making terrible UPR-based jokes.

Aitor, Brian, Chetan, Stuart (aka “The Squad”). You were such great additions to the lab in terms of science and in terms of craic. I think I learned a lot more from you than you did from me. Thank you to all of my other friends in ARC, biochemistry and beyond; Argha, Ben, Emma, Eimear, Shiva, Higgo, Antonio, Karen, and the board game crew for your support.

Thank you Sveta and Trish for training me, giving me all of the advice, and basically taking care of me in my first year. You scared me a lot at the start, but it looks like it all worked out in the end, just like you said it would. You were always supportive and made me feel welcome even when I was the only guy surrounded by five girls; which in retrospect doesn’t seem so bad.

Thank you Elena for your constant positivity and for reminding me to follow my own advice.

Izabela, somehow we made it through. You were there the whole way and always willing to offer support and advice (not only on scientific matters). I don’t know if I would have made it through the first two years without your friendship and support (though I nearly died at your wedding). Thank you.

Well, it was a lucky day for me when Aaron started in the lab. I won’t pretend we gave each other any great scientific advice (apart from plakogoblin) which was a miracle), but you always managed to find the humour in the bleakest situations, which made all the difference. You were always supportive and free for pints. Suffice it to say, you were actually class.

Thank you to my Dublin friends Kareem and Richie for keeping me grounded, and always making sure I saw the bigger picture when I inevitably descended into the biannual rut. I’ll never forget the help you gave me Kareem, especially towards the end.

Mum and Dad, I couldn’t ask for better parents. You’ve been such an unshakable rock of support over the past five years and always. None of this would have been possible without you. Thank you.

Publications

Research Articles:

Logue, S. E. *et al.* Inhibition of IRE1 RNase activity modulates the tumor cell secretome and enhances response to chemotherapy. *Nature communications* 9, 3267, doi:10.1038/s41467-018-05763-8 (2018).

McGrath EP**,** Urra H, Almanza A, Leuzzi B, Chevet E, Logue SE, Hetz C, Samali A. IRE1 regulates breast cancer cell migration through cleavage of junction plakoglobin (JUP) mRNA. *In Preparation*

Reviews:

Maurel, M. *et al.* Controlling the unfolded protein response-mediated life and death decisions in cancer. *Seminars in cancer biology* 33, 57-66, doi:10.1016/j.semcancer.2015.03.003 (2015).

McGrath, E. P. *et al.* The Unfolded Protein Response in Breast Cancer. *Cancers* **10**, doi:10.3390/cancers10100344 (2018).

Abstract

Metastatic, drug resistant disease poses the greatest threat to the survival of breast cancer patients. Thus, elucidating and targeting mechanisms which govern this phenotype is a primary goal of the breast cancer field. Breast cancers manipulate cellular stress pathways to gain a survival advantage and fuel their growth. The unfolded protein response (UPR) is a major cell stress pathway responsible for the genesis and growth of many breast cancers. The most evolutionarily conserved transducer of the unfolded protein response is a protein called inositol-requiring enzyme 1 (IRE1), which is an important player in both luminal and basal-like breast cancers. Pro-tumour roles of IRE1 are mediated through its endoribonuclease (RNase) domain which has two functions, X-box binding protein 1 (*XBP1*) splicing and regulated IRE1-dependent decay (RIDD). In this thesis we have determined that the IRE1 RNase is particularly active in triple negative breast cancer (TNBC), a subtype with a poor prognosis and limited treatment options. We have discovered novel targets of the IRE1 RNase domain, namely C-X-C motif chemokine ligand 1 (*CXCL1*) which we have shown to govern a drug-resistant and stem cell-like phenotype. We also identified the first RIDD substrate in breast cancer (junction plakoglobin (*JUP*)) and found that its degradation by IRE1 may promote migration of TNBC cells. We employed MKC8866, a small molecule with clinical potential, to show that both of these processes can be blocked. This work highlights the promise of targeting IRE1 in the clinic to prolong and improve the lives of breast cancer patients.

Abbreviations

ABL	ABL proto-oncogene 1, non-receptor tyrosine kinase 1
ACTD	Actinomycin D
ASK1	Apoptosis-signalling kinase 1
ATF6	Activating transcription Factor 6
ATG5	Autophagy Related 5
ATGL16	Autophagy Relation 16 like 1
ATP	Adenosine Triphosphate
BCL2	BCL2, Apoptosis Regulator
Bfa	Brefeldin A
BI-1	Bax-Inhibitor 1
Bp	Base Pair
Carboxy-terminal of HSP70-Interacting Protein	CHIP
CB	Cytochalasin B
CCNG2	Cyclin G2
CD59	CD59 Molecule (CD9 Blood Group)
CDON	Cell Adhesion Associated Oncogene Regulated
CNX	Calnexin
CRT	Calreticulin
CSC	Cancer Stem Cell
Ct	Cycle Threshold
CXCL1	C-X-C motif Chemokine Ligand 1
DEPC	Diethyl Pyrocarbonate
DN	Dominant Negative
DNA	Deoxyribonucleic Acid
DTT	Dithiothreitol
EIF2A	Eukaryotic Translation Initiation Factor 2 Alpha
EIF2AK3	EIF2A Kinase 3
ER	Endoplasmic Reticulum
ERAD	Endoplasmic Reticulum Associated Degradation
ERDJ4 (DNAJB9)	DnaJ heat shock protein family (Hsp90) member B9
ERO1	ER Oxidoreductin 1
ESR1	Estrogen Receptor Alpha
FLNA	Filamin A
FOXO	Forkhead Box O
GMCSF	Colony Stimulating Factor 2
GRP78	Glucose Regulated Protein 78kDa
HER2	Human Epithelial Growth Factor Receptor 2
HERP	Homocysteine Inducible ER protein with ubiquitin-like domain 1
HSP	Heatshock Protein
HUVEC	Human Ubilical Vein Endothelial Cells
IL6	Interleukin 6
IL8	Interleukin 8

ING4	Inhibitor of Growth Family Member 4
IRE1/ERN1	Inositol-Requiring Enzyme 1/Endoplasmic Reticulum Signalling to Nucleus 1
JNK	C-JUN N-Terminal Kinase
JUN	Jun Proto-oncogene, AP-1 Transcription Factor Subunit
JUP	Junction Plakoglobin
KD	Knockdown
KO	Knockout
MCL1	MCL1, BCL2 Family Apoptosis Regulator
MFE	Mammosphere Formation Efficiency
miRNA	Micro RNA
mRNA	Messenger RNA
MRPL19	Mitochondrial Ribosomal Protein L19
NCK1	NCK Adaptor Protein 1
NFKB	Nuclear Factor kappa-light-chain-activator of B-cells
NMHCIIB	Non-muscle Myosin IIB
N-MYC Interactor	NMI
NRF2	Nuclear Factor Erythroid 2, Related Factor 2
OTUB1	OUT deubiquitinase, ubiquitin aldehyde binding 1
PARP16	Poly-ADP Ribose Polymerase
PCR	Polymerase Chain Reaction
PDI	Protein Disulfide Isomerase
PDIA6	Protein Disulfide Isomerase 6
PERK/EIF2AK3	PRK-like ER Kinase/EIF2A Kinase 3
PGR	Progesterone Receptor
PP2A	Protein Phosphatase 2A
PPIA	Peptidylprolyl isomerase A
PPM1L	Protein Phosphatase 1-like gene
Protein Kinase A	PKA
qPCR	Quantitative Polymerase Chain Reaction
RIDD	Regulated IRE1 Dependant Decay
RNA	Ribonucleic Acid
RNAi	RNA interference
RNase	Endoribonuclease
RPL19	Ribosomal Protein L19
RTCB	RNA 2’,3’-cyclic phosphate and 5’-OH ligase
RT-PCR	Reverse Transcription Polymerase Chain Reaction
SEL1L	ERAD E3 ligase adaptor unit
SERCA	sarco/endoplasmic reticulum Ca^{2+} ATPase
siRNA	Small interfering RNA
SRP	Signal Recognition Particle
STAT3	Signal Transducer and Activator of Transcription 3
TERS	Transmissible ER Stress
Tg	Thapsigargin
TGFB	Transforming Growth Factor Beta
TIMP3	TIMP Metallopeptidase inhibitor 3

Tm	Tunicamycin
TNBC	Triple Negative Breast Cancer
TNF	Tumour Necrosis Factor
TRAF2	TNF Receptor Associated Factor 2
TRAF6	TNF Receptor Associated Factor 6
UPR	Unfolded Protein Response
VEGFA	Vascular Endothelial Growth Factor A
XBP1	X-box Binding Protein 1
XBP1s	Spliced X-box Binding Protein 1
XBP1u	Unspliced X-box Binding Protein 1

Chapter I: Introduction

1.1 The Endoplasmic Reticulum

Keith R. Porter coined the term endoplasmic reticulum (ER) after originally observing a "lace-like reticulum" in fibroblast-like cells from a chick embryo in 1945 using electron microscopy[1]. Later work by Palade *et al* would identify two types of ER; rough ER, containing associated "small granules" (ribosomes), and smooth ER[2,3]. Early work showed that labelled amino acids were more readily incorporated into microsomal proteins than those of other fractions[4], and that dissociation of ribosomes from the ER could prevent protein synthesis[5]. This paved the way for later studies which elucidated the mechanics of mRNA translation at the ER[6].

Today we know the ER is a large membrane-bound perinuclear organelle with many biological functions, and that the two types of ER are specialized for different processes. The rough ER is comprised of a network of tubules and sacs and the cytosolic face of its membrane is dotted with ribosomes. At ER-localised ribosomes, nascent peptides encoding membrane and secreted proteins are cotranslationally translocated, via a complex called the translocon, into the ER lumen where they begin folding. The smooth ER has a more flattened sheet-like structure compared to the rough ER, and is responsible for calcium regulation, drug detoxification, and the synthesis of lipids and hormones[7].

The ratio of rough to smooth ER varies between cell types, depending on the function of that cell. For instance, plasma cells have enlarged rough ER as they are responsible for producing and secreting huge quantities of antibodies. Conversely, ovarian and testicular cells, which are responsible for producing lipid-containing hormones, have an increased abundance of smooth ER[7].

Correct protein folding and maturation is essential for proper cellular, and thus organismal, function. The maintenance of correct protein folding, as well the detection and degradation of unfolded or incorrectly folded proteins is mediated by many interconnected cellular processes. Collectively these processes are called the proteostasis (proteome and homeostasis) network. Proteostasis is required for

cellular function and disturbance of cellular proteostasis underlies many diseases (see section 1.12).

1.2 Protein Folding in the ER

Proteins must fold correctly to function properly. The compartmentalisation of the ER from the cytosol is necessary to allow proteins destined for extracellular secretion, or the lumen of certain cellular organelles, to adopt a native structure appropriate to the environment in which they function. As such, the ER lumen harbours ion concentrations and a redox potential that are comparable to the extracellular space but not to the cytosol[8]. This means that the cell must have mechanisms in place that ensure that secretory pathway peptides which are translated in the cytosol are exposed only to the specialised ER folding environment, and other machinery which ensures that the ER folding environment is maintained.

1.2.1 Co-translational Translocation

ER-destined peptides contain a signal recognition sequence at their N-termini. This sequence is recognised by the signal-recognition particle (SRP) which binds to the nascent ribosome-associated peptide, and to an SRP receptor on the ER membrane. Binding of the SRP to the signal sequence halts translation, thus ensuring that no folding is allowed to occur in the cytosol, and further ensures that enzymes like lysozyme are not allowed to enter the cytosol. The SRP-ribosome complex interacts with a complex called the SEC61 translocon which forms a pore through which the growing peptide is cotranslationally translocated into the ER lumen[9].

1.2.2 Chaperones

The correct folding of nascent peptides within the ER is accomplished by free-energy reactions (e.g. hydrophobic interactions), chaperone proteins which directly interact with nascent peptides, enzymes which add prosthetic groups like sugars and lipids, and by other proteins which maintain the correct folding environment in the ER. Heat shock protein (HSP) 70 and HSP90 family chaperone proteins are abundant in the ER lumen. Glucose-regulated protein 78 (GRP78, aka HSPA5, BiP) is a HSP70 family member with diverse roles within the ER. As a chaperone, it binds to exposed hydrophobic regions of folding proteins, preventing their aggregation and/or misfolding. HSP40 members co-ordinate the function and localisation of HSP70 members, and also have chaperone activity[10]. Among them, DnaJ heat shock

protein family (Hsp40) member B9 DnaJ (DNAJB9, aka ERDJ4) has a crucial role in co-ordinating GRP78 within the ER lumen[11].

1.2.3 N-linked Glycosylation & Protein Quality Control

Addition of oligosaccharides residues to nascent peptides helps to define their function and solubility. These residues also act as molecular beacon of protein folding fidelity. Core oligosaccharide chains (consisting of two N-acetylglucosamine residues, nine mannose residues, and three terminal glucose residues) are assembled on a lipid known as dolichol at the ER membrane before being transferred to asparagine residues of nascent peptides within the ER lumen by oligosaccharyltransferase (N-linked glycosylation)[12]. Upon transfer, two terminal glucose moieties of the N-linked chain are sequentially removed and the nascent peptide is transiently bound by two ER resident calcium dependent chaperones known as calreticulin (CRT) and calnexin (CNX). In concert with other ER chaperones, CRT and CNX facilitate protein folding, and cleavage of the third terminal glucose residue. This cleavage prevents CNX from binding to the client protein. Proteins which have failed to achieve native conformation are subsequently reglucosylated by the ER resident UDP-glucose:glycoprotein glucosyltransferase and rebound by CNX, while correctly folded proteins are transported to the Golgi[13]. Folding proteins cycle between unglycosylated and reglycosylated states until they reach their native conformation, or are deemed unfoldable and exported to the cytoplasm for destruction in proteasomes through a process called ER-associated degradation (ERAD) (see section 1.3.1). Peptides are earmarked for destruction by sequential removal of mannose residues from the N-linked glycan, until the α-1,6-linked mannose is exposed, and delivered to ERAD export machinery[13].

1.2.4 Oxidative Folding

The oxidising environment within the ER favours the formation of disulphide bonds between cysteine residues within nascent peptides. Disulphide bond formation is catalysed by protein disulphide isomerases (PDIs) which also possess oxidoreductase activity, thus allowing PDI to unfold and correctly refold nascent peptides. The specific function of a PDI molecule depends on its own redox state and the type of client protein. ER oxidoreductin 1 (ERO1), the most well-conserved PDI disulphide donor, uses free O_2 within the ER lumen to generate disulphide bonds, which it transfers to reduced PDI, thereby enabling PDI to oxidise cysteines on folding

peptides to create disulphide bonds. Electrons released by the oxidation event are transferred back from folding peptide to PDI to ERO1 to O_2, generating H_2O_2. Activity of the anti-oxidant glutathione (GSH) and its oxidised form (GSSG) contribute to maintenance of appropriate redox balance in many cell compartments, including the ER. Indeed, the [GSH]:[GSSH] ratio is lower in the secretory compartment than other cellular compartments, thus maintaining a relatively strong oxidising environment[14]. Several other mechanisms contribute to redox maintenance in the ER[15].

1.2.5 Calcium Homeostasis

As mentioned previously the ER lumen is the primary site of calcium storage in cells. Indeed, calcium concentrations can be one-thousand times greater in the ER than in the cytosol (about 100 μM and 100 nM respectively). This gradient is maintained by sarcoplasmic/endoplasmic reticulum Ca^{2+} ATPase (SERCA) pumps, which actively import calcium into the ER lumen from the cytosol. Within the ER, CRT, CNX, GRP78, and PDI (among others) sequester large amounts Ca^{2+}, thus acting as buffers to maintain ER calcium homeostasis. Furthermore, each of these proteins requires Ca^{2+} for their activity. Ca^{2+} release from the ER is associated with stress, and is associated with a programmed mode of cell death called apoptosis (see section 1.10.1). Thus, calcium homeostasis within the ER is a prerequisite for correct protein folding and for the overall health of cells[16].

1.3 Protein Degradation Pathways

Even if ER folding homeostasis is successfully maintained, many proteins do not achieve their native conformation. The fidelity of protein folding is so tightly controlled in fact, that even correctly folded proteins are often targeted for degradation. This redundancy is likely an evolutionary overreaction to the deleterious threats incorrectly folded proteins can pose to the entire organism (see section 1.12). To rid the ER lumen of misfolded proteins, cells possess two protein degradation pathways; ER-associated degradation (ERAD) and autophagy. Both processes occur basally in cells, but become more active in response to cellular stressors.

1.3.1 ERAD

ERAD is a process by which unfolded or misfolded proteins within the ER lumen are recognised, exported to the cytosol, and degraded by the ubiquitin proteasome system. In mammals, ERAD is a complex system and different ERAD pathways are responsible for the recognition and export of different proteins. Though many essential ERAD proteins have been characterised, the precise signalling and interactive mechanisms which mediate ERAD remain to be elucidated. As mentioned in section 1.2.3, peptides can be marked for destruction by the sequential removal of mannose residues from the core N-linked glycan. ER chaperones including GRP78, osteosarcoma amplified 9, and ER degradation-enhancing α-mannosidase-like protein 1, bind to misfolded proteins and deliver them to ERAD export machinery. Ubiquitin E3 ligases are responsible for the ubiquitination of many proteins, which leads to their proteasomal degradation in many cases. In ERAD the E3 ubiquitin ligase synoviolin 1 (SYNV1) forms a complex with ERAD E3 ligase adaptor unit (SEL1L) which provides the channel through which ERAD substrates are exported to the cytoplasm. In the cytoplasm, the ligase domain of SYNV1 ubiquitinates ERAD substrates. The ub-tagged substrates are subsequently degraded in proteasomes[17].

1.3.2 Autophagy

Autophagy is a complex and highly regulated process in which cellular contents are degraded and recycled. Autophagy is not an ER-specific process, but can be activated in response to a variety of cellular stresses, most notably, starvation. Nevertheless, autophagy is a mechanism through which misfolded proteins are removed from the ER lumen.

During autophagy, specific cellular contents are packaged inside membrane-bound structures called autophagosomes which fuse with lysosomes to form a structure called an autolysosome in which the cargo is finally degraded. The mature autophagosome is formed by the elongation of an immature membrane structure called a phagophore. The origin of the phagophore is still a subject of debate in the field but it can be derived from the ER, plasma, golgi and mitochondrial membranes. The maturation of the phagophore is a complex process requiring multiple proteins working in concert. Specific receptors, known as autophagy receptors, are embedded in the phagophore and bind to specific cargo proteins. This receptor mediated

"selective autophagy" is a relatively recent discovery, before which autophagy was generally considered to be a non-specific process[18,19].

1.4 ER Stress

As illustrated above, maintenance of a correct folding environment with in the ER is contingent on the function of individual proteins as well as the interplay of many cellular processes. If ER folding homeostasis is disturbed, misfolded and unfolded proteins build-up in the ER lumen. When this occurs, the ER is said to be stressed.

ER stress is caused by many physiological and pathological conditions. Physiological ER stress is observed in professional secretory cells which produce large amounts of secreted proteins such as antibody-secreting plasma cells, and insulin-secreting pancreatic β cells. In such contexts it is important that cells maintain a basal level of stress to avail of stress signalling which enhances the folding capacity of the ER. Markers of ER stress are also observed in a plethora of diseases such as neurodegenerative diseases[20], diabetes[21], cystic fibrosis[22], and many types of cancer (see section 1.12)[23].

In the laboratory setting, ER stress is triggered pharmacologically with compounds such as; tunicamycin (Tm), thapsigargin (Tg), dithiothreitol (DTT), and Brefeldin A (Bfa). Such chemical approaches are informative in mechanistic studies of ER stress and downstream signalling, but are often criticised for their inability to recapitulate physiological and pathological ER stress. More physiologically relevant alternatives include inducing ER stress by expressing chronically misfolding proteins which accumulate in the ER[24]. These are especially useful in studying diseases such as Parkinson's disease which are characterised at the molecular level by the accumulation of misfolded proteins (see section 1.12.1).

1.5 The Unfolded Protein Response

The UPR is the cellular response to ER stress. Since cells need correctly folded proteins to function, they must be able to monitor homeostasis within the ER and adjust its capacity to fold and export proteins according to need. Conversely, cells must also have a method of engaging cell death programs under conditions of irremediable ER stress which threaten tissue homeostasis. The UPR fulfils both of

these roles, acting as either an adaptive or a pro-death pathway depending on the cell context and the nature/duration of the stressor[25,26].

1.5.1 Discovery of the UPR

The UPR was initially observed, though unknowingly, in the 1970s when researchers found that depletion of glucose from cell culture medium led to the induction of GRP78 and GRP94[27]. It was more than a decade later that the mechanism of GRP induction by glucose depletion was identified. Kozutsumi *et al* demonstrated that a chronically misfolding influenza hemagglutinin mutant was able to induce GRP expression in simian cells[28]. To find the mechanism linking misfolded proteins in the ER to transcriptional induction of GRPs, researchers employed the yeast strain *Saccharomyces cerevisiae* as a model organism, correctly assuming that the yeast UPR would be simpler and thus easier to study than its mammalian counterpart.

In 1993, Kazutoshi Mori and Peter Walter independently discovered that a transmembrane kinase was responsible for UPR induction in yeast[29,30]. The kinase was found to be identical to Inositol-requiring enzyme 1 (IRE1 aka ERN1) which had been identified one year earlier in a different context[31]. In 1996, both Mori and Walter discovered that the HAC1 (XBP1 in mammals) transcription factor was required for UPR induction in yeast[32], with Walter finding that it was activated through a post-transcriptional splicing event[33]. One year later, Walter reported that *HAC1* was cleaved through an unconventional splicing mechanism mediated by IRE1 itself[34]. For these and other discoveries, Walter and Mori are credited with founding the UPR field[35].

1.5.2 Activation of UPR Sensors

In mammals, UPR signalling originates from IRE1[36,37,38], and two other sensors; Activating Transcription Factor 6 (ATF6) [39,40], and PKR-like ER Kinase (PERK, also known as EIF2AK3)[41]. The classical model of UPR activation involves the regulation of all three sensors by GRP78. In this model all three sensors are bound by GRP78 under non-stress conditions and are thus maintained in an inactive state. However, upon ER stress, GRP78 favours binding to unfolded proteins and detaches from the sensors leading to their activation. Other models have been proposed in which IRE1 and PERK are directly bound by unfolded proteins and thereby activated[42]. Recently, a unifying model was proposed in which IRE1 activation was dependent on the binding of unfolded peptides to the IRE1 luminal domain. In the

unified model, GRP78 binds during the early stages of stress, and upon its dissociation, unfolded proteins bind to IRE1 and trigger oligomerisation. In this way GRP78 does lead to activation of IRE1 under ER stress, but the binding of unfolded proteins is also required[43-45]. The precise activation mode of the UPR sensors remains controversial.

Through a transcriptional program, the UPR promotes cell adaptation and survival by driving expansion of the ER, an increase in the abundance of protein chaperones (such as GRP78 and ERDJ4), and the engagement of protein degradation machinery (ERAD and autophagy). The UPR also restricts protein production and halts the cell cycle. If these mechanisms fail to restore homeostasis, the UPR switches to a modality which promotes cell death. Temporal regulation of IRE1, PERK, and ATF6 governs this switch[46]. The current model of cell fate regulation by the UPR in normal cells consists of an early pro-adaptive response mediated by all three UPR arms that gives way to pro-death signalling regulated by PERK and IRE1[46]. The precise regulation and signalling outputs of each sensor as they pertain to adaptation or cell death are described below.

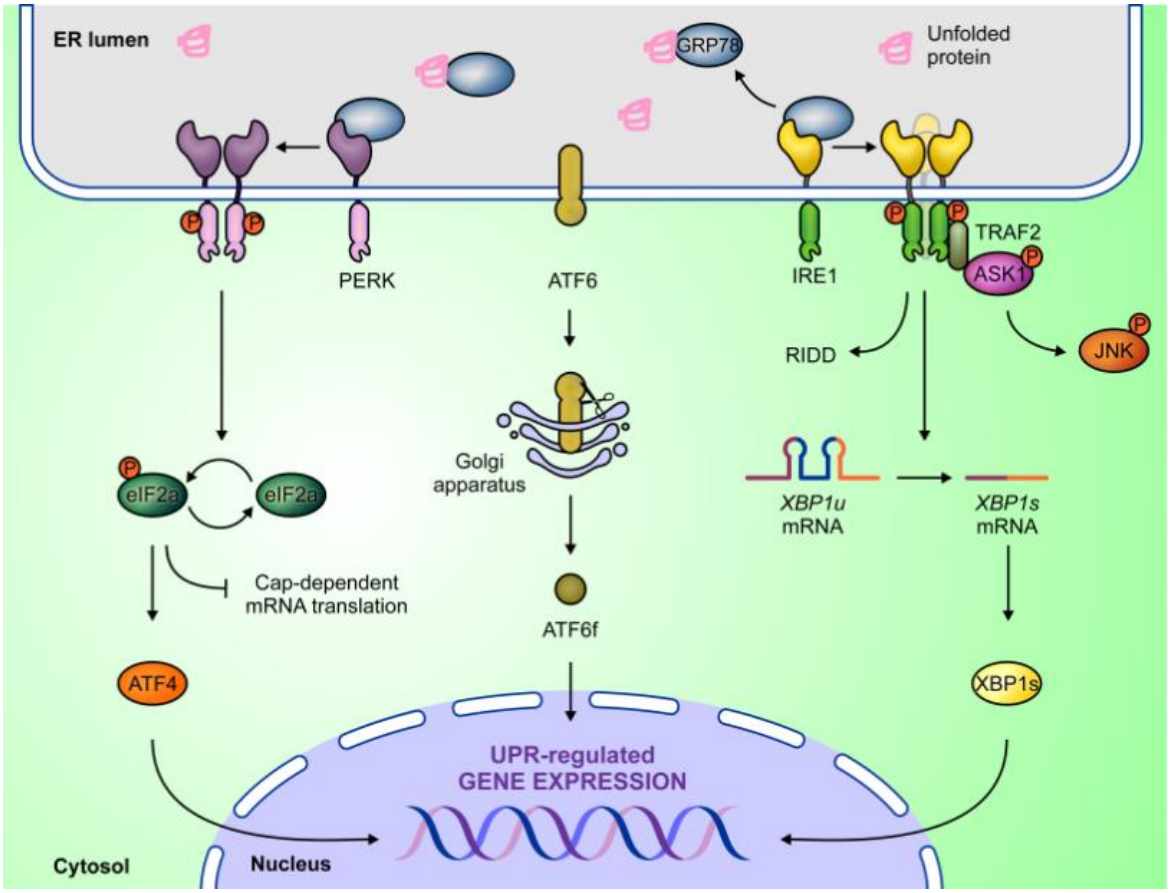

Figure 1.1. The Unfolded Protein Response. Build-up of unfolded proteins within the ER lumen leads to activation of ER stress sensors by sequestering GRP78. ATF4, ATF6f, and XBP1s are adaptive transcription factors activated by the PERK, ATF6, and IRE1 signalling branches respectively, and promotes expression of chaperones and protein degradation pathway components. The UPR also engages degradation of cytosolic RNA and activation of JNK through IRE1, and inhibition of global protein synthesis through PERK. Figure prepared by Katarzyna Mnich.

1.6 ATF6

ATF6 is a pro-survival transcription factor which becomes activated upon ER stress, firstly by cleavage from the ER membrane and secondly by processing in the Golgi apparatus by site-1 and site-2 proteases[47,48]. Once it has achieved its transcriptionally active form (ATF6f), ATF6f translocates to the nucleus and upregulates a subset of genes which help to restore homeostasis to the ER, including chaperones and *XBP1*. In fact, ATF6f shares many transcriptional targets with XBP1s and binds XBP1s to synergistically promote ER homeostasis[47,49]. ATF6 has some pro-death activity through the indirect downregulation of the pro-survival Bcl-2 family member MCL1, BCL2 family apoptosis regulator[50].

1.7 PERK

PERK dimerizes upon ER stress and GRP78 dissociation and becomes activated through transautophosphorylation, mediating UPR signalling through its cytoplasmic kinase domain. PERK phosphorylates eukaryotic initiation factor 2α (EIF2α), causing a block in global mRNA translation. This block promotes cell survival by lowering the requirement of the ER to fold proteins, and halts cell cycle progression by expediting the depletion of cyclin D1. However, phosphorylation of EIF2α blocks assembly of the pre-initiation complex which is required for normal mRNA translation. However, some mRNA, such as activating transcription factor 4 (*ATF4*) mRNA and its transcriptional targets have a second upstream open reading frame are selectively translated upon EIF2α phosphorylation[51]. Some ATF4 target genes, like Autophagy Related 5 (*ATG5*), encode proteins necessary for autophagy. Another ATF4 target, C/EBP Homologous Protein (*CHOP*, also known as *DDIT3*), promotes death following prolonged ER stress by directly upregulating pro-apoptotic proteins and relieving the blockade of global protein synthesis[52]. Other direct PERK kinase substrates include nuclear factor erythroid 2-related factor 2 (NRF2) a vital component of the anti-oxidant response, the transcription factor forkhead Box O (FOXO), which has a role in promoting hormone-independent growth in breast cancer, and diacylglycerol which has diverse roles as a second messenger and substrate in cells[25,44,53-55].

1.8 IRE1

IRE1 is a bi-functional type-1 transmembrane protein, and is the most conserved arm of the UPR, being present in yeast. Two isoforms of IRE1 are found in mammals, IRE1α and IRE1β. IRE1α is ubiquitously expressed while IRE1β is only found in the bronchial epithelium and the gut. The IRE1 referred to throughout this thesis is IRE1α[56]. Upon ER stress, IRE1 monomers come into close proximity, brining two cytoplasmic kinase domains on opposing monomers into close proximity enabling transautophosphorylation. This triggers IRE1 dimerization and activation of the cytosolic IRE1 RNase domain[57,58]. It is important to note that activation of IRE1 and its RNase has been reported to occur independently of ER stress (see section 1.8.6)[59,60].

1.8.1 XBP1s

Once active, the IRE1 RNase domain splices a 26 nucleotide intron from mRNA transcribed from the *XBP1* gene. Spliced *XBP1* mRNA is subsequently ligated by RNA 2',3'-Cyclic Phosphate and 5'-OH Ligase (RTCB) [61]. The spliced and ligated mRNA of *XBP1* is translated into a pro-survival transcription factor called XBP1 spliced (XBP1s) [37] The unspliced *XBP1* mRNA is also translated, yielding a short-lived protein called XBP1 unspliced (XBP1u), which can regulate XBP1s levels by (1) promoting the association of XBP1 with the ER membrane and promoting its splicing through IRE1 and (2) binding to XBP1s and preventing its translocation to the nucleus[62-64].

XBP1s is a well-studied pro-survival transcription factor with significance in a variety of diseases[65-67]. Within the context of the UPR, XBP1s upregulates genes responsible for restoring ER homeostasis and thus promotes adaptation to stress. XBP1s transcriptional targets in this regard include protein chaperones such as such as *DNAJB9* and components of the ERAD system such as homocysteine-inducible, ER stress-inducible, ubiquitin-like domain member 1 (*HERP*) [68]. XBP1s also drives expansion of the ER lumen, which provides more space for protein folding[69,70]. However, XBP1s may have a pro-death role in some circumstances such as in human umbilical vein endothelial cells (HUVEC) cells, where its overexpression promotes apoptosis[71].

It is important to note that the XBP1s transcriptional network is cell-type and stress-type specific[72]. Thus it is essential that a distinction be made between temporal XBP1s activation in the context of a UPR response, and both the tissue specific physiological functions of XBP1s in processes like development (section 1.11.1), and constitutive XBP1s activation in some disease states (see section 1.12).

1.8.2 RIDD

In addition to XBP1 splicing, the RNase of IRE1 cleaves cytosolic RNAs through a process called RIDD. RIDD substrates (i.e. RNA species cleaved by IRE1) are sequence- cell- and stress-type specific[73,74]. RIDD is a less characterized process than XBP1 splicing, though it is believed to promote ER homoeostasis by cleaving ER-localizing mRNA, thus lowering the amount of nascent peptides entering the ER to confer context-specific survival advantages, such as in pancreatic β-cells where IRE1 cleaves mRNA encoding pro-insulin, thus relieving stress in the ER[75]. Upon prolonged ER stress however, RIDD is thought to become maladaptive, cleaving a wider variety of mRNA substrates and ultimately promoting apoptosis through an undefined mechanism, though a controversial mechanism has been reported wherein IRE1 cleaves the miRNAs which repress caspase-2, thus promoting apoptosis[76].

The kinetics of RIDD activity, its regulators, and its role in promoting death have not been properly characterized[73]. Since RIDD substrates are cell-type specific and stress-type specific, the kinetics of RIDD will depend on the cell type and the substrate being cleaved. Indeed, different RIDD substrates show different kinetics of regulation under identical treatment in the same cell. To date, no RIDD substrates have been reported in breast tissue, healthy or otherwise.

1.8.3 RNase Regulation: XBP1 Splicing or RIDD (or both)

The mechanisms which govern whether IRE1 activation favours *XBP1* splicing and/or RIDD have been actively investigated since RIDD was discovered in 2006[74]. Reports suggest that increased oligomerisation of IRE1 within the ER membrane facilitates an extension of its substrate range beyond *XBP1* mRNA and into RIDD substrates[77]. Another report suggests that dimeric IRE1 favours RIDD activity wherein IRE1 monomers dimerise in a back-to-back conformation, while increased oligomerisation leads to front-to-front and back-to-back conformations favouring *XBP1* splicing[78]. Cumulatively, the literature suggests that *XBP1* splicing and RIDD, while having distinct catalytic mechanisms, can occur simultaneously under ER

stress. Since RIDD is such an ill-defined and context-specific process, claims about whether it is active or inactive in a certain context should be made with caution.

1.8.4 IRE1 Kinase & UPRosome

The kinase domain of IRE1 acts as a platform for a dynamic and multi-functional complex known as the UPRosome[46,79]. The pro-death modality of IRE1 has been attributed to the interaction of IRE1 with TNF receptor-associated factor 2 (TRAF2). TRAF2 binds apoptosis-signalling kinase 1 (ASK1) which activates c-JUN N-terminal kinase (JNK) signalling which promotes apoptosis through phosphorylation of c-JUN and upregulation of pro-apoptotic BCL2 family members. IRE1 can also act as a platform for NCK adaptor protein-mediated regulation of extracellular signal-related kinase and nuclear factor kappa-light-chain-activator of B-cells (NFκB) signalling[80,81]. Furthermore, IRE1 directly binds Signal Transducer and activator of transcription 3 (STAT3), and is important for STAT3 phosphorylation and activity under interleukin 6 (IL6) stimulation[82].

1.8.5 Regulators of IRE1

Activation of IRE1 under ER stress is dependent on several proteins, besides unfolded proteins and GRP78. Poly-ADP Ribose Polymerase 16 (PARP16) is found in the ER membrane and is essential for IRE1 RNase activity under ER stress. Knockdown of PARP16 abolishes *XBP1* splicing after Tm treatment[83]. Non-muscle myosin IIB (NMHCIIB) interacts with IRE1 during ER stress and promotes XBP1 splicing and IRE1 oligomerisation[84]. In hepatocytes, IRE1 is phosphorylated by protein kinase A (PKA) in response to glucagon stimulation[85].

Several proteins modulate the mode of IRE1 activation. Recently, ABL proto-oncogene 1, non-receptor tyrosine kinase (ABL) was shown to bind to IRE1 during ER stress and hyperactivate its RNase activity, leading to enhanced RIDD and promoting apoptosis[86]. N-MYC interactor (NMI) binds to IRE1 and diverts its activity towards JNK activation while blocking *XBP1* splicing[87]. IRE1 interaction with the SEC61 translocon is critical for the splicing of *XBP1*[88], however the binding of SEC61 prevents hyperactivation of IRE1, regulating the extent of *XBP1* splicing[89]. IRE1 is a target of the E3 ubiquitin ligase carboxyl terminal of HSP70 – interacting protein (CHIP) and of OTU deubiquitinase, ubiquitin aldehyde binding 1 (OTUB1). Under ER stress, CHIP ubiquitinates IRE1. However, subsequent

deubiquitination by OTUB1 diminished IRE1-mediated JNK activation, thus suggesting that CHIP controls IRE1 activation modes[55].

IRE1 can be switched off by many interacting proteins. IRE1 is dephosphorylated and thus deactivated by protein phosphatase 2A (PP2A) and protein phosphatase 1-like gene (PPM1l). However, while knock-out of PPM1l reduced ER stress-induced XBP1 splicing, knock-out under basal (non-stressed) conditions resulted in enhanced splicing[90]. Other proteins which directly bind and inactivate IRE1 include Bax inhibitor 1 (BI-1)[91], protein disulphide isomerase 6 (PDIA6)[92] and fortilin[93].

Of note, IRE1 is turned over by both autophagy (ATGL16L1[94]) and ERAD[95].

1.8.6 ER Stress-independent IRE1 Activation

In addition to what might be considered 'classical' activation of IRE1 by ER stress, there are several other mechanisms through which IRE1 becomes active. Zheng *et al* found at vascular endothelial growth factor (VEGF) induced internalisation of VEGF receptor 2 (VEGFR2, gene name *KDR*) which subsequently bound and activated IRE1, inducing the splicing of *XBP1*[96]. Both toll-like receptor 2 (TLR2) and TLR4 were shown by Laurie Glimcher's group to activate *XBP1* splicing independently of ER stress[59]. Lipid saturation has been observed to activate IRE1 activity, but not IRE1 clustering. PERK is also activated in this context, but ATF6 is not[97]. IRE1 can become pre-emptively activated in certain physiological contexts before the induction of ER stress, such as in plasma cells[98], and in cells stimulated with estrogen[99]. IRE1 becomes active when cells are depleted of XBP1. IRE1 has increased RIDD activity in this context, but the mechanism through which this occurs has not been formally addressed[100].

1.9 Defining UPR Activation

1.9.1 ATF6

ATF6 is activated through post-translational translocation and cleavage mechanisms[101] but there is no evidence that *ATF6* is transcriptionally upregulated in response to ER stress. Thus, presence of the ATF6f protein is the best readout for ATF6 activation. Alternatively, an ATF6f gene signature could be employed to determine activity, but this has not been reported to date.

1.9.2 PERK

PERK mRNA levels and PERK protein levels are not informative of PERK activity. Furthermore, high throughput transcriptomic analyses have limited utility since PERK targets such as ATF4 and CHOP are activated downstream of eIF2α phosphorylation, which can be mediated by three other kinases besides PERK[102]. Thus, the only *bona fide* read-out of PERK activation is the level of phosphorylated PERK (p-PERK). However, a PERK gene signature (determined by treating cells with PERK kinase inhibitor GSK2606414 and performing transcriptome analyses) has been reported and correlated with higher tumour grade and worse patient survival in breast cancer[103].

1.9.3 IRE1

Elevated levels of *IRE1* mRNA or protein do not necessarily imply IRE1 activation. Thus, researchers favour examination of XBP1s levels as a readout of IRE1 activity. In fact, investigations into the role of IRE1 RNase have focussed almost exclusively on XBP1s and no data implying roles for RIDD activity have been reported in many contexts such as breast cancer, although RIDD was identified over a decade ago. Unfortunately, probes which differentiate between the spliced and unspliced *XBP1* isoforms are absent from most (if not all) high throughput gene arrays. Since the two XBP1 isoforms have different and even opposing functions[62], total XBP1 levels inform neither XBP1s activity nor IRE1 activation. To circumvent this limitation, researchers have begun examining XBP1s gene signature (i.e. a set of genes known to be transcriptionally regulated by XBP1s)[104]. Immunohistochemical screens have also been hampered due to the lack of suitable antibodies specific to XBP1s. Thus, older studies in which total XBP1 was taken as a readout of IRE1 RNase activity should be interpreted cautiously.

1.9.4 GRP78

As with the three UPR sensors, GRP78 expression data should be interpreted cautiously. Elevated GRP78 levels are often taken as a readout of UPR activation since GRP78 is reregulated by all three UPR arms; IRE1/XBP1s, PERK/ATF4 and AFT6f[37,105]. However, *GRP78* is also a reported IRE1/RIDD substrate[106] and can be regulated in a UPR-independent manner by at least six other transcription factors[107-112]. Therefore, elevated GRP78 levels are at best only suggestive of UPR activity.

1.10 ER Stress-Induced Cell Death

As mentioned previously, unresolved ER stress can lead to cell death. The UPR mediates the switch from a pro-survival modality to a cell death modality by directly regulating cell death machinery. When normal cells experience unresolvable ER stress, the UPR triggers intrinsic apoptotic cell death, though it has a role in controlling other cell death modalities under different circumstances. For instance, previous work from our laboratory has shown that in the absence of intrinsic cell death machinery (i.e. caspase 9 (CASP9)), the UPR can trigger an autophagy- and caspase 8- dependant mode of cell death[113].

1.10.1 Intrinsic Apoptosis

Intrinsic apoptosis is a mode of programmed cell death initiated in response to intracellular stimuli such as excessive DNA damage or excessive ER stress. Intrinsic apoptosis is triggered by the permeabilisation of the outer membrane of mitochondria (MOM) which causes cytochrome C to be released into cytoplasm. This leads to the assembly of a wheel-like complex consisting of cytochrome C, apoptotic peptidase activator 1, and CASP9. This complex is called the apoptosome. At the apoptosome, CASP9 cleaves and thereby activates caspase 3 (CASP3) which in turn cleaves a variety of cellular substrates. During apoptosis, cells shrink due to cleavage of cytoskeletal proteins, “blebbing” of the plasma membrane is observed, and genomic DNA is cleaved in a regulated manner by site-specific nucleases. Crucially, phosphatidyl-serine is exposed on the outer leaflet of the cell membrane acting as an “eat me” signal for macrophages which phagocytose the apoptotic cell. This phagocytosis is important because it ensures that fragments of dying cells are not released into the extracellular space. Such fragments, called damage associated molecular patterns (DAMPS), can trigger cell death in neighbouring cells and an inflammatory response. Thus, intrinsic apoptosis, a non-inflammatory mode of cell death, is important for the maintenance of tissue homeostasis.[114]

1.10.2 BCL2 Family Proteins

MOM permeabilisation (MOMP) is regulated by the BCL2, apoptosis regulator (BCL2) protein family. BCL2 proteins are characterised by the presence or absence of four different Bcl-2 homology domains (BH1-4). The presence or absence of different BH domains defines the function of BCL2 family members. For instance, BCL2 family members, BCL2, BCLXL, and MCL1 have all four BH domains and

have an anti-apoptotic function. Conversely, BAD, BID, and PUMA only contain the BH3 domain and promote apoptosis by inhibiting the pro-survival members. BAX and BAK, which oligomerise and form pores in the MOM, thereby triggering apoptosis, contain BH 1, 2, and 3, and a modified version of BH4. The balance between pro-apoptotic and anti-apoptotic BCL2 family members is central in deciding cell fate. UPR signalling can alter this balance and push the cell towards apoptosis[115].

1.11 Physiological Roles of IRE1

IRE1 has multiple physiological roles in cells. Some of these roles occur independently of ER stress, and for others it is presumed that IRE1 becomes active to allow the cell to cope with new stimuli which put strain on the ER.

1.11.1 Development

IRE1 is essential for the development of mammals. IRE1 phosphorylation and splicing of *XBP1* are observed throughout the early stages of embryonic growth and IRE1 deficient mice die at embryonic day 12.5. Defects in the liver and placenta are thought to be responsible for this lethality[116]. XBP1-deficient mice also show lethality starting at embryonic day 12.5[117].

IRE1 and XBP1 also play roles in the different developmental stages of mammary glands. Mammary gland development involves rapid proliferation and invasion of cells in the breast and the production and secretion of large amounts of milk proteins like whey acidic protein (WAP) and casein from specialised cells within the gland. The UPR allows cells to adapt to these changes. Indeed, XBP1 depletion in the mammary epithelium leads to a reduction in proliferation of the mammary gland, and perturbs the differentiation of secretory cells. This leads to a reduction in the production of WAP and caseins which reduces the quality of the milk. As a result, pups fail to thrive and an increase in post-natal mortality is observed[118]. A more specific KO of *XBP1* in the mammary epithelium showed similar effects on the quantity of protein in the milk, and reduced growth of pups[119].

1.11.2 Immunology

As mentioned in a previous section, IRE1 is required for the maturation and function of many immune cell types. XBP1 is required for (1) the differentiation of B cells into plasma cells[120], (2) the differentiation of $CD8^+$ T-cells during infection[121], (3)

the development and function of dendritic cells (DCs) [122-124], (4) the expression cytokines after TLR stimulation in macrophages[59], (5) eosinophil differentiation[125], and (6) the function of intestinal Paneth cells which secrete anti-microbial proteins[99,126]. It has been assumed that these immune cells require XBP1 to adapt and expand their secretory output, and that IRE1 becomes active as a result of increased ER burden. However, IRE1 becomes active during differentiation of plasma cells before Immunoglobulin (Ig) production[99]. RIDD is important for the survival of certain subsets of dendritic cells[127] and has been observed to cleave mRNA encoding immunoglobulin (Ig) heavy chain when XBP1 is depleted from plasma cells, thus reducing IgM secretion[128]. These studies have illustrated that the immune system requires IRE1 RNase activity to function properly.

Immune responses occur in both physiological and pathological circumstances and the immune system plays a crucial role in a variety of diseases, including cancer. The role that IRE1 plays in cancer-associated immune responses has come to prominence over the last few years and is discussed in section 1.12.3[129].

1.11.3 Cell Adhesion & Migration

Two studies have linked IRE1 to cell migration. Dejeans *et al* (2012) showed that glioma-like cells expressing a dominant negative form of IRE1 (DN_IRE1) are more migratory and display increased attachment to collagen and matrigel compared to empty vector (EV) controls. When cells were induced to form neurospheres, the investigators found that DN_IRE1 cells formed smaller, less compact spheres compared to EV, and exhibited a more collective migratory phenotype compared to EV cells which migrated more individually. Furthermore, DN_IRE1 cells exhibited increased focal adhesion and actin stress fibres which are both important for the ability of the cell to migrate. The authors found that in this context, IRE1 cleaves mRNA encoding secreted protein Acidic and Cysteine rich (*SPARC*) which under regular conditions promotes phosphorylation of focal adhesion kinase 2 (FAK2, aka PTK2), and cell migration. Thus IRE1/RIDD activity was shown to control migration of glioma cells[130].

A more recent study by Urra *et al* has demonstrated that IRE1 can control migration of many different cell types in a variety of contexts independently of its RNase and kinase activities, through a physical interaction with filamin A (FLNA). Upon

discovering that IRE1 interacts with FLNA using a yeast two-hybrid system, the researchers examined if depletion of IRE1 could alter cell migration. They found the depletion of IRE1 reduced the migratory capacity of cells and caused disturbances in actin dynamics. Using mutation approaches they found that a C-terminal proline-enriched region, but not the kinase or RNase domain, of IRE1 was important for recruitment, dimerization and phosphorylation of FLNA. They further showed that protein kinase C-α was also recruited to IRE1 and was the likely candidate for FLNA phosphorylation. Lastly, they showed that IRE1-FLNA is important in a variety of physiological contexts, such as development of the cortex in mouse embryos, migration of plasmatocytes in *Drosophila melanogaster*, and in migration-dependent developmental processes in developing zebrafish[131].

1.12 UPR in Disease

Many diseases, such as Alzheimer's disease (AD) and Huntingtins disease (HD), involve a pathological accumulation of misfolded proteins. Additionally, many diseases arise when cells are either unable to engage cell death (cancer), or die too early (neurodegeneration). Since the UPR plays a role in protein folding and in cell fate regulation, it is not surprising that it plays diverse functional roles in many diseases. For instance, in the context of cancer, the UPR can drive tumour growth, but in protein folding diseases, UPR signalling can have a protective effect by helping cells to clear toxic protein aggregates.

1.12.1 Neurodegenerative Diseases

The term neurodegenerative disease covers many diseases which are characterised by perturbation in the normal function of a population of neuronal cells. Such diseases include PD, HD, Alzheimer's disease (AD), and amyotrophic lateral sclerosis (ALS). While each disease manifests a different set of debilitating phenotypes, they share a common molecular characteristic; the accumulation of misfolded protein aggregates[20]. Consequently, markers of UPR activity are commonly upregulated in the diseased tissue of PD, HD, AD and ALS patients. ER stress and chronic UPR signalling have classically been considered as pro-degenerative, promoting the apoptosis of neurons[20]. However, it is becoming increasingly clear that the three arms of the UPR play cell-, stress-, and disease-type specific roles in neurodegeneration. For example, conditional genetic depletion of *Xbp1* in a mouse model of ALS resulted in neuroprotection. This result is surprising,

since XBP1 is generally considered to be a pro-survival transcriptional factor. However, loss of XBP1 in this context led to an increase in autophagy which boosted the clearance of superoxide dismutase 1 aggregates which characterise the disease[79]. Conversely, depletion of Xbp1 in the substantia nigra of mice results in ER stress and neuronal loss.[132] Therapeutic interventions to either activate or suppress UPR signalling are being considered for neurodegenerative diseases. However, targeting such multi-functional pathways as the UPR, in such a highly complex organ as the brain, with a variety of tissue types in which potential therapies may have drastically different effects on cell fate, poses a huge challenge for the UPR-neurodegeneration field[20].

1.12.2 Cancer

The UPR is active in a variety of cancer types and directly impacts many of the hallmarks of cancer[23,133]. The UPR is important at all stages of cancer development, and can be both prerequisite for oncogenesis in some circumstances, by allowing cells to cope with intrinsic stress, such as oncogene-induced increase protein demand, while emerging as a harmful side-effect of extrinsic (microenvironmental) stressors after transformation, such as tumour hypoxia[99].

One of the primary challenges of cancer biology is the heterogeneity of different cancer types and cellular heterogeneity within tumours of a given type. As outlined in section 1.11, the UPR has diverse physiological roles in different cell and tissue types. This paradigm holds true in cancers, where the role of the UPR is tumour cell-type and stress-type specific. The UPR, and in particular IRE1/XBP1, is especially relevant in multiple myeloma[66], glioblastoma[134], and breast cancer (discussed in more detail in section 1.13)[104], though it plays distinct roles in each.

UPR as a Gatekeeper of Tumorigenesis:

The UPR provides mechanisms through which cancer cells overcome transformation associated stress, however, pro-death UPR signalling can mediate apoptosis of transformed cells in certain contexts. Work by Romero-Ramirez *et al* (2004) demonstrated that transformed mouse cells do not form tumours in *vivo* when they lack XBP1 whereas all mice injected with wild-type transformed cells develop tumours[135]. Though far less studied, RIDD has been implicated in the degradation of the mRNA encoding period circadian protein homolog 1 (*PER1*) thus suggesting a

potential role for RIDD in cell cycle disruption and carcinogenesis[136]. Nagy *et al* overexpressed the v-myc avian myelocytomatosis viral oncogene homolog (MYC) in *D. melanogaster* cells and found that the cells were reliant on PERK-induced autophagy for sustained overgrowth[137]. In mammalian cells, both c-myc and n-myc activate PERK/ATF4, which confers the cells with an autophagy-dependent survival advantage[138]. Serine/cysteine protease inhibitor SCCA1 was reported by Shesadri *et al* to drive oncogenesis through mild induction of PERK and ATF6 signalling[139]. Tissue-specific suppression of GRP78 was sufficient to block tumorigenesis in murine prostate and endometrioid adenocarcinoma models[140,141]. Thus, there are a variety of contexts in which UPR proteins allow cancer cells to thrive following transformation.

Conversely, many reports indicate that the UPR triggers the death of transformed cells. In 2006 Denoyelle *et al* demonstrated that ER stress was important for the induction of senescence in a HRas proto-oncogene, GTPase-driven model of melanoma, and prevented tumour progression[142]. In a KRAS proto-oncogene, GTPase–driven model of lung cancer, deletion of *CHOP* led to an increase in tumorigenesis, suggesting that pro-apoptotic CHOP activity acts as a barrier to tumour progression. In this context DNAJ HSP40 member C3 (referred to as p58(IPK) in the paper) was found to repress PERK activity and thus deplete CHOP, conferring tumours with a survival advantage under conditions of low glucose[143]. Given this dual role in cell fate at the early stages of cancer, the UPR has been referred to as a gatekeeper of tumorigenesis.

Surviving and Thriving in the Tumour Microenvironment:

Within solid tumours, cancer cells are exposed to a variety of cell-extrinsic stressors which can activate the UPR, such as hypoxia and hypoglycaemia[99]. Since ER proteostasis requires both oxygen and glucose, it is unsurprising that many tumours display constitutive UPR activation which allows them to adapt to stressful conditions. UPR signalling can also be triggered in cancer cells by chemotherapeutics[144] aneuploidy[145] and high-secretory demand. Chemotherapy-induced UPR can confer tumours with therapy resistance in certain contexts[144].

One mechanism through which tumour cells adapt to hypoxic stress is by upregulating genes which mediate angiogenesis (the sprouting of blood vessels from

pre-existing blood vessels). XBP1, ATF6, and PERK have all been reported to be required for VEGF-induced vascularisation in endothelial cells independently of ER stress[96,60]. XBP1s has been linked to the hypoxic response and induction of angiogenesis in TNBC (see section 1.13)[104]. Angiogenesis not only supplies tumours with key nutrients like oxygen and glucose but also provides tumour cells with a route to metastasise, a process whereby tumour cells d from the primary tumour, travel through the vascular system and colonize secondary sites within the body[146]. PERK signalling may allow cancer cells to survive detachment from the ECM by activating autophagy and preventing detachment-induced death, facilitating the spread of cancer cells[147]. Lysosomal-associated membrane protein 3 (*LAMP3*) is a PERK/ATF4 transcriptional target induced by hypoxia and may also be important in allowing tumour cells to metastasise (discussed in section 1.13)[148]. As mentioned in section 1.11.3, IRE1-mediated degradation of *SPARC* mRNA alters the migration and invasive capacity of glioma cells[130].

1.12.3 Tumour-Associated Immune Responses

Immune cells play diverse roles in cancer. $CD8^+$ T-cells are responsible for recognising and destroying cancer cells as part of their regular function. However, the function of many immune cells is subverted to promote tumour growth. Furthermore, tumour cell signalling can diminish anti-tumour immunity, a process called immune suppression[46]. In the last few years the UPR has received attention for its role in regulating immune cell function in the context of cancer.

A seminal paper from Mahadevan *et al* identified a phenomenon termed transmissible ER stress (TERS), wherein macrophages cultured in media derived from ER-stressed tumour cells launched a stress response and displayed an enhanced pro-inflammatory phenotype[149]. This paper illustrated for the first time that ER stressed tumour cells could impact the function of immune cells. A follow-up paper from the same research group demonstrated that TERS augmented the function of DCs in a way which promoted tumour growth, and immune-suppression[149]. Since then, the effectors molecules of TERS have been avidly sought.

In 2015 Cubillos-Ruiz *et al* found that ovarian tumour-associated DCs displayed higher levels of UPR activation when compared to non-tumour derived DCs. In an elegant study, the team linked increased ROS in DCs to lipid dysregulation and the

production of cellular by-products which perturbed ER function and activated the UPR. Aberrant XBP1 signalling in this context disrupted DC lipid homeostasis, and knockdown of XBP1 reduced tumour progression *in vivo* by promoting anti-tumour T-cell activity[124]. IRE1/XBP1 has also been shown to be important for suppression of anti-tumour neutrophil activity. ER-stressed neutrophils adopt an immunosuppressive phenotype, which can be reversed by treatment with an IRE1 RNase inhibitor[129,150].

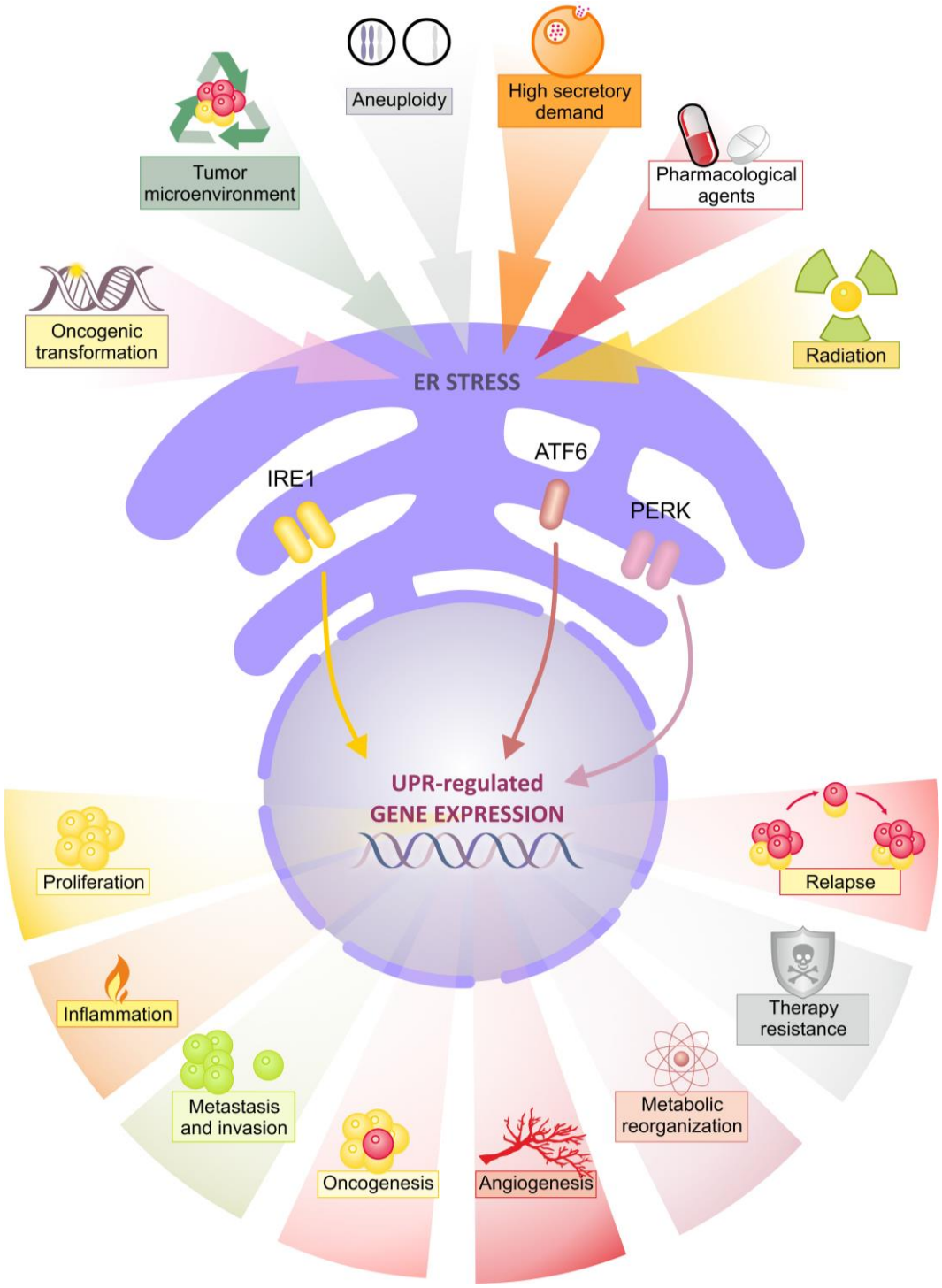

Figure 1.2. Cancer-Associated Stressors Trigger UPR Activity. A variety of cell-intrinsic and –extrinsic stressors lead to UPR activation. In turn the UPR drives multiple pro-tumour processes associated with worse patient outcome. Figure prepared by Katarzyna Mnich.

1.13 Breast Cancer

Breast cancer encompasses a heterogeneous set of diseases with distinct prognoses, physiological and histological characteristics, and treatment options[151]. Different breast cancer subtypes are commonly diagnosed based on the histological expression of three receptor proteins: Estrogen Receptor (ESR1 also known as ERα), Progesterone Receptor (PGR), and human epidermal growth factor receptor 2 (HER2 also known as ERBB2), and often by the differential expression of fifty select genes (PAM50) which infer the "intrinsic" biological subtype. While many other methods of subtyping breast cancers exist, immunohistochemical and PAM50 analyses remain the most prominent. Subtyping of breast cancer helps to inform the course of treatment and has led to great improvements in patient survival. In PAM50 analyses, tumours with a gene expression profile typical of luminal epithelial cells belong to the luminal subtype (of which there are two sub-categories), and are usually hormone receptor positive (ESR1+ PGR+). Most breast tumours are luminal and are often responsive to ESR1 modulators, like tamoxifen, or aromatase inhibitors such as anastrozole. HER2+ cancers overexpress HER2 and are generally treated with antibodies targeting HER2 alone, or in combination with chemotherapeutics. Tumours exhibiting myoepithelial PAM50 profile are referred to as basal-like tumours and are usually ESR-, PGR- and do not have amplified HER2 expression. Such tumours, devoid of ESR1, PGR and lacking HER2 amplification are referred to as triple negative breast cancers (TNBC) and currently lack a targeted therapy[20,152,153]. Though many breast cancer treatments are effective in the short-term, drug resistance commonly develops and patients eventually succumb to the disease[154]. Discovering and targeting mechanisms by which tumours acquire drug resistance is a primary goal for the breast cancer field[146].

1.14 UPR in Breast Cancer

Prolonged and/or intense ER stress is lethal to normal cells, but in cancer UPR signalling is both sustained and non-lethal[99]. In breast cancer, chronic, non-lethal UPR signalling exhibits considerable heterogeneity in signalling output, depending on the breast cancer subtype and the stressors experienced by tumour cells.

1.14.1 ATF6 & PERK

Experimental evidence suggesting a direct role for ATF6 in breast cancer is limited. Nonetheless, ATF6 knockdown was reported to reduce angiogenesis and tumour volume in a breast cancer xenograft model[155]. Estrogen induces ATF6 activation in ESR1+ breast cancer cells, and knockdown of ATF6 significantly decreased estrogen-induced growth[156]. This suggests that ATF6 is at least partly responsible for the proliferation of breast cancer cells challenged with estrogen-induced proliferative stress and for tumour growth and angiogenesis. No molecular mechanism has been reported for these observations but ATF6 may play an indirect role through regulation of *XBP1* and *GRP78*.

In human breast ductal carcinoma *in situ*, p-PERK levels are increased compared with normal breast tissues[147] and p-PERK levels are higher in TNBC cell lines than in luminal cell lines[104].

Breast tumour cells exploit PERK signalling to grow and to survive in harsh microenvironments. PERK ablation in Neu-driven mammary carcinoma cells and PERK knockdown in MDA-MB-468 (TNBC) cells led to smaller tumour volumes when injected into mice[157]. Additionally, animals injected with PERK-deficient cancer cells displayed increased tumour free survival compared to control mice. In a separate experiment the authors observed that aged PERK KO mice spontaneously formed tumours compared to controls, which suggests that PERK has opposing roles in tumorigenesis[157].

PERK/ATF4 mediates hypoxia-induced breast cancer progression via regulation of tribbles homologue 3 (*TRIB3*), unc-51-like autophagy activating kinase 1 (*ULK1*), and lysosomal-associated membrane protein 3 (*LAMP3*). All three genes are induced in hypoxic conditions via PERK/ATF4 and their knockdown, or knockdown of PERK and/or ATF4, reduces cancer cell proliferation (TRIB3 and ULK1), survival (ULK1), and migration (LAMP3) in hypoxia[158]. Furthermore, higher TRIB3 and ULK1 expression is associated with a poor prognosis in breast cancer[159] while higher LAMP3 expression has been associated with lymph node positivity and hormone receptor negative breast cancers[158,160,161].

1.15 IRE1 in Breast Cancer

1.15.1 Activation

A recent comprehensive study of gene expression signatures in primary breast cancer samples has revealed an overexpression of XBP1 in luminal breast cancer, where it is co-expressed with ESR1[162]. Immunohistochemical analysis of 395 breast adenocarcinomas showed that 90% of samples stained strongly for XBP1 total, implying protein overexpression[163]. In a seminal paper, Laurie Glimcher's group identified an XBP1 gene signature using ChIP-Seq which correlated with shorter relapse free survival in two cohorts of TNBC patients, but not in ESR+ breast cancer patients[104]. They also reported increased levels of *XBP1* splicing in primary basal-like tumours compared to ER+/PGR+ tumours. These reports suggest that total XBP1 is overexpressed in luminal cancers while increased XBP1s transcriptional activity is more strongly associated with TNBC. This notion is corroborated in cell lines where basal-like cancers are found to display higher levels of *XBP1* splicing compared to cell lines derived from luminal breast cancers and MCF10A which is a non-tumorigenic breast epithelial cell line[104].

1.15.2 Mutation

Data mining using the Catalogue of Somatic Mutations in Cancer (COSMIC) platform revealed that *IRE1* and *XBP1* are rarely mutated in breast cancer (0.38% and 0.62% respectively). However, *IRE1* has been ranked as the fifth most likely protein kinase gene to harbour a driver mutation across other cancer types[164]. *IRE1* mutations discovered in this study have been characterised *in vitro* and help us to understand why aberrations of IRE1 may benefit tumours. Ghosh *et al* found that enforcing IRE1 oligomerisation and activation through overexpression triggered cell death in the case of WT IRE1, but overexpression of cancer-associated *IRE1* mutants produced little or no lethality. In principle, this demonstrates that cancer cells can acquire mutations which prevent activated IRE1 from mediating cell death.

XBP1 is highly expressed in luminal breast cancers but it is rarely found to be mutated[162]. However, complete genome sequencing of breast cancer and non-neoplastic tissue from 560 individuals revealed four possible exonic driver mutations in *XBP1*. The same study also reported seven mutations in the non-coding region surrounding the *XBP1* gene, at an occurrence significantly higher than that expected

by chance[165]. The *XBP1* mutations identified in the breast cancer samples were of very low incidence, and there was little or no difference between mutation rates in ESR1+ and ESR1- breast cancers[165].

1.15.3 Pro-tumour role

TNBC:

Many *in vivo* and *in vitro* studies directly implicate XBP1 in the pathology of TNBC and luminal breast cancers. Using a transgenic mouse model where splicing of *XBP1* produces a bioluminescent signal, it was found that mammary epithelial tumours displayed splicing of *XBP1* throughout tumorigenesis[166]. In support of this result, patient-derived BCM-2147 (TNBC), MDA-MB-231 (TNBC), NeuT EMTCL2 (mouse breast cancer cell line), and transformed MCF10A cells transplanted into mice form significantly fewer tumours when XBP1 is silenced, versus control cells[104,155] (Ruan *et al* showed a similar effect with IRE1 knockdown[155]). Reciprocally, TNBC patient derived cells exhibiting a non-stem cell-like phenotype (CD44-low/CD24-high) genetically engineered to overexpress XBP1s formed tumours when injected into mice while control cells did not[104].

In vitro, XBP1 interacts directly with Hypoxia Inducible Factor 1α (HIF1α), a key hypoxic stress-responsive transcription factor[104]. The knockdown of XBP1 in TNBC cells caused a significant reduction in the expression of HIF1α target genes, such *VEGFA*) a key mediator of tumour angiogenesis[104]. The role of IRE1/XBP1 in angiogenesis is supported by an *in vivo* experiment in which knockdown of either IRE1 or XBP1 reduced angiogenesis[155]. Together, these studies show that XBP1 is important for TNBC tumour initiation, progression, and adaptation to hypoxic stress.

ESR1+ Breast Cancer:

Estrogen signalling drives many ESR1+ breast cancers and is an enduringly useful therapeutic target; furthermore, estrogen signalling activates all arms of the UPR in breast cancer cells *in vitro* and *in vivo*[156,167]. XBP1 and ESR1 are co-expressed in luminal breast cancers and *in vitro* work has demonstrated the existence of a feed-forward mechanism connecting the proteins[162,168]. Both XBP1 spliced and unspliced isoforms can trigger estrogen-independent ESR1 homodimerization and transcription of ESR1 target genes[168], which include *XBP1* itself[169-173]. This allows ESR1+

tumours to achieve XBP1-dependent, estrogen independent, growth and explains why both XBP1 isoforms can drive ESR1+ cancer, but not TNBC. In support of this conclusion, a human luminal breast cancer cell line overexpressing XBP1s and an unsplicable mutant variant, produced faster growing tumours when injected into mice compared to wild-type cells[172]. XBP1s overexpression in an ESR1+ breast cancer cell line was shown to increase levels of the pro-survival protein BCL-2 and significantly decreased MOMP when cells were challenged with the estrogen antagonists tamoxifen or fulvestrant[174]. Other studies have demonstrated that lowering of XBP1 levels in an ESR1+ cell line significantly reduced estrogen-stimulated growth[175]. Thus, IRE1/XBP1 signalling is intimately linked to ESR1 signalling in luminal breast cancer (see figure 1.3).

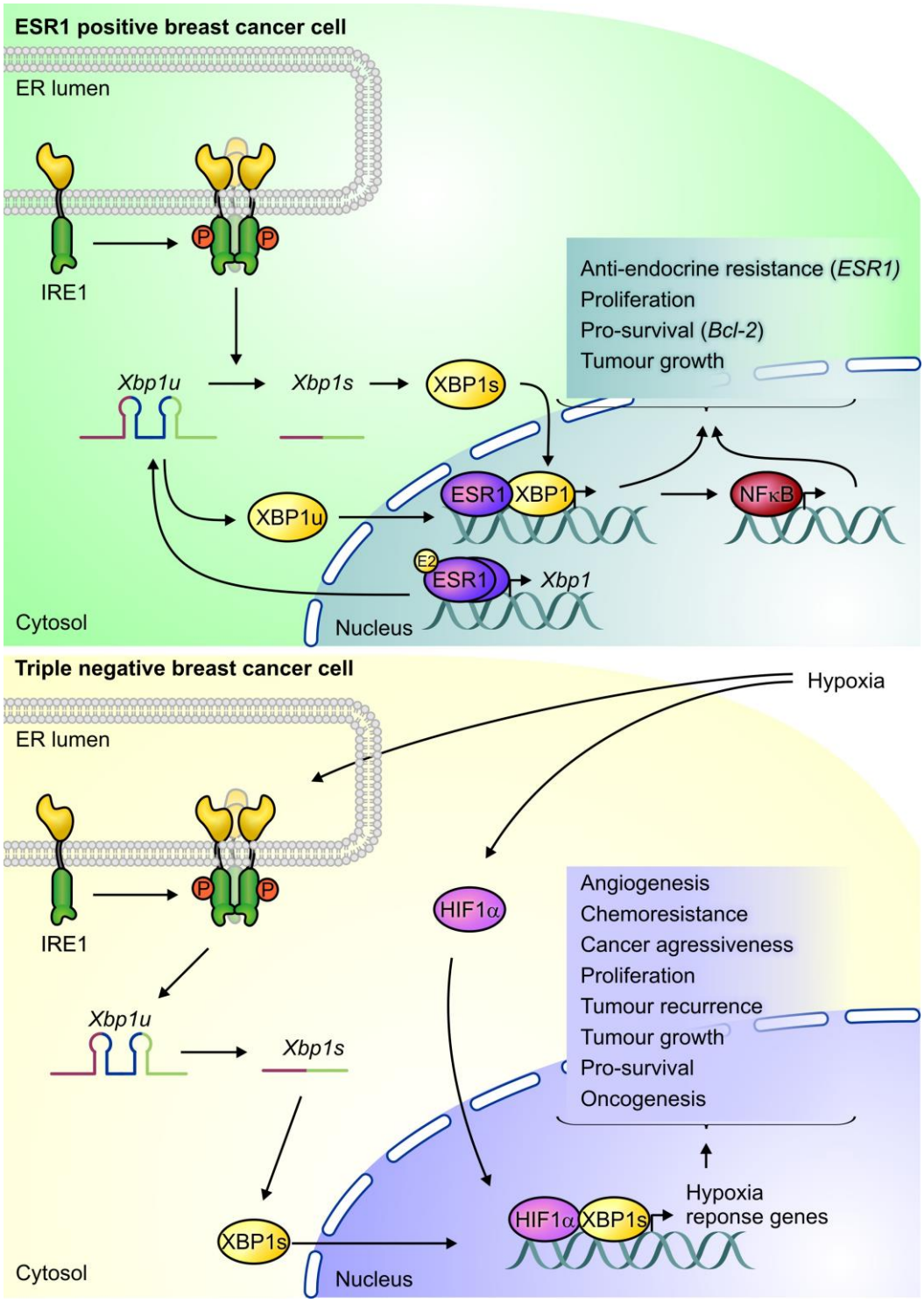

Figure 1.3. IRE1/XBP1s activity in ESR1+ and TNBC cells. Both XBP1 isoforms can activate ESR1 signalling in ESR1+ breast cancer cells and facilitate estrogen-independent tumour survival and proliferation. ESR1 signalling promotes expression of *XBP1*, thus generating a feed-forward mechanism (upper Panel). In TNBC cells, IRE1 exhibits high basal activity and activates XBP1s which dimerises with HIF1α potentiating the expression of hypoxia response genes. This signalling drives tumour growth and angiogenesis (lower panel adapted from Chen *et al* 2014[104]). Figure prepared by Katarzyna Mnich.

1.15.4 Drug Resistance

IRE1/XBP1 confers TNBC cells with resistance to doxorubicin, and paclitaxel, and ESR1+ cancers with resistance to tamoxifen[104,172]. Human TNBC cells injected into mice developed resistance to doxorubicin and paclitaxel treatment over time and knocking down XBP1 was shown to prevent tumour recurrence[104]. In a separate study, overexpression of XBP1s in ESR1+ cells led to tamoxifen resistance in an *in vivo* mouse model. Mice injected with cells bearing a more stable form of XBP1u were also resistant to tamoxifen, but to a lesser extent. *In vitro* work showed that in ESR1+ cells both XBP1 isoforms contribute to tamoxifen resistance via NF-κB[172] (see figure 1.3).

1.16 IRE1-Targeting Drugs

Many compounds are available which target IRE1 proteins, although none are currently approved for use in patients[176,177]. Several IRE1 RNase inhibitors that block *XBP1* splicing and RIDD; MKC-3946, 3-methoxy-6-bromosalicylaldehyde, 4μ8C, STF-083010, and Toyocamycin, have shown promise in multiple myeloma models, where XBP1s is known to be important for tumour progression[178]. Intriguingly, the genotoxic drug doxorubicin was recently identified as a potent inhibitor of the IRE1 RNase[179] which may contribute to its efficacy in breast cancer in some cases. Pharmacologically targeting the UPR in combination with anti-cancer chemotherapeutics has shown a significant synergistic effect in killing breast cancer cells.

1.16.1 MKC8866: IRE1 RNase inhibitor

Through international collaboration our lab has procured a highly specific inhibitor of the IRE1 RNase domain named MKC8866. MKC8866 is a salicyaldehyde derivative (figure 1.4), and is thought to act primarily by forming a Schiff base with a lysine (K907) residue in the RNase domain of IRE1, though it also interacts with other residues within the RNase domain. The reactive nature of aldehydes suggests that MKC8866 may have a milieu of different targets. However, there are a few points which argue in favour of its specificity to the IRE1 RNase domain and there are no reports to the contrary. Firstly, MKC8866 is well tolerated in mice and had no effect on the closest homolog of the IRE1 RNase domain, RNase L of the interferon-γ response, in an *in vitro* assay (though RNase L does not possess a homologous

lysine in its catalytic domain)[180]. Furthermore, previous work from our lab has determined the specificity of MKC8866 to the IRE1 arm of the UPR. Phosphorylation of PERK and cleavage of ATF6 was unaffected by MKC8866 treatment under acute ER stress. Additionally, it was previously shown in our lab that MKC8866 only inhibits proliferation of cells displaying basal *XBP1* splicing[51]. Proliferation of MCF10A cells which do not have basal *XBP1* splicing was unaffected by MKC8866 treatment. Together, these points suggest that MKC8866 is a specific inhibitor of the RNase domain of IRE1.

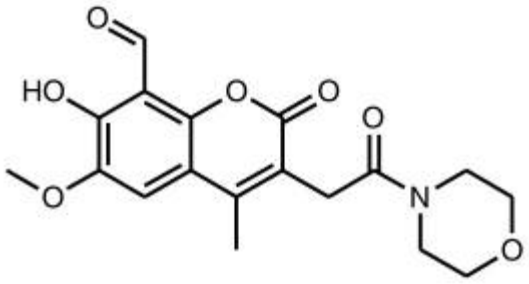

Figure 1.4: Chemical Structure of MKC8866

1.16.2 UPR-targeting drugs in combination therapies

Synergistic anti-breast tumour effects have been observed in the few studies that have investigated the combination of FDA-approved drugs and UPR-specific agents. *In vivo*, the IRE1 RNase inhibitor STF-083010 significantly reduced tamoxifen resistant ESR1+ tumour growth both as a stand-alone therapy and in combination with tamoxifen[181]. Recently Zhao *et al* showed that a combination treatment of MKC8866 and docetaxel eliminated MYC driven tumours in a patient-derived xenograft model. Syngeneic mouse models revealed the same effect on tumour growth in mice with an intact immune system, though only in MYC-driven tumours[182]. *In vitro*, Plumbagin, a compound which lowers GRP78 levels, sensitized breast cancer cells to tamoxifen[94]. The PERK kinase inhibitor GSK2606414 sensitizes de-differentiated HMLEs to paclitaxel and doxorubicin *in vitro*, and to reduce xenograft tumour growth of TNBC cells in the presence of doxorubicin[103]. Since therapy-resistance is a leading cause of tumour recurrence and patient mortality, this handful of studies demonstrate the potential of UPR-targeting drugs in resensitising tumour cells.

1.17 Aims and Objectives

The aim of this thesis was to determine if the IRE1 RNase domain is active in breast cancer, and if so, to elucidate what role it is playing. Specifically, we sought to identify roles in clinically important facets of cancer such as therapy resistance and metastasis.

Chapter II: Materials and Methods

2.1 Mammalian Cell Culture

MDA-MB-231 (a triple negative breast cancer cell line with a mesenchymal-like morphology, isolated from a metastatic site (pleural effusion)) (ATCC HTB-26 (see appendix A for STR-typing) and MCF7 (a luminal breast cancer cell line expressing the estrogen receptor with a epithelial morphology, also isolated from a metastatic site (pleural effusion) (ATCC #HTB-22) cells were maintained in High Glucose DMEM (SIGMA #D6429) supplemented with 10% fetal bovine serum (FBS) and 2 mM L-glutamine (SIGMA #G7513). HCC1806 (a triple negative breast cancer cell line with an epithelial morphology) (ATCC #CRL-2335), T47D (an estrogen receptor positive breast epithelial cell line isolated from pleural effusion) (ECACC #85102201), MDA-MB-468 (a triple negative breast cancer cell line)(HTB-132) and BT-549 (triple negative breast cancer cell line) (ATCC HTB-122) cells were maintained in RPMI media (SIGMA #R0883) supplemented with 10% FBS and 2 mM L-glutamine (SIGMA #G7513). SKBR3 (a HER2+ cell line isolated from a pleural effusion) cells (ECACC) were maintained in McCoys5A media (SIGMA #M9309) supplemented with 10% FBS and 2 mM L-glutamine (SIGMA #G7513). MCF10A (a normal non-transformed breast epithelial cell line) cells (ATCC # CRL-10317) were maintained in DMEM/F12 media (Gibco #11320-074) supplemented with 5% horse serum, 20 ng/mL EGF (Peprotech #AF-100-15), 1 ng/mL cholera toxin (SIGMA #C8052), 10 g/mL Insulin (SIGMA #I1882-100MG), 500 ng/mL Hydrocortisone (SIGMA #H0888-1G)., All cells were cultured at 37 °C and 5% CO_2 in a humidified incubator (unless otherwise stated). Hypoxia experiments were carried out in a in a Coy Laboratory hypoxic glovebox at 37 °C in a humidified 5% CO_2, 1% O_2 atmosphere.

2.2 Drugs used

Tunicamycin (Tm) is a bacteria-derived compound which inhibits transfer of N-acetylglucosamine to dolichol, thereby perturbing N-linked glycosylation (SIGMA #T7765).

Thapsigargin (Tg), is a plant-derived inhibitor of the SERCA pump (SIGMA #T9033).

DTT is a reducing agent which impedes disulphide bond formation (SIGMA #D9779).

Gift from Fosun Orinove (USA). Through international collaboration our lab has procured an inhibitor of the IRE1 RNase domain named MKC8866. See section 1.16.1 for more information.

Actinomycin D (ACTD) is an antibiotic which binds to GC rich regions of DNA and inhibits transcription (SIGMA #A9415).

Paclitaxel is a plant-derived compound which binds to tubulin and prevents microtubule disassembly (SIGMA #T7402).

2.3 siRNA Transfections

For knockdown, MDA-MB-231 cells were transfected with 25 nM of Dharmacon On-Target SMARTpool Plus siRNA targeting XBP1 (L-009552-00), IRE1 (L-004951-02), or non-targeting control (NC) siRNA (D-001810-01-20) using Dharmafect 4 (Dharmacon T-2004-02) according to the manufacturer's instructions.

2.5 RNA Extraction

After harvesting, cells were transferred to an eppendorf tube and centrifuged at 1,500 × g for 4 min at 4 °C. Cell pellets were resuspended in 1 ml TRI Reagent (SIGMA #T9424) and transferred to a 1.5 ml eppendorf tube. The sample was vortexed for 1 min. The sample was incubated at room temperature for 5 min. 200 μL of chloroform (SIGMA #C2432) was added to the samples followed by vortexing for 30 sec and then incubation on ice for 15min. The samples were spun at 17,000 × g for 15 min at 4 °C. The upper aqueous layer of the sample was removed to a new 1.5 mL eppendorf. 1 volume of chilled isopropanol (SIGMA #I9516) was added dropwise to the sample. The sample was inverted ten times and incubated at room temperature for 10 min. The sample was spun at 17,000 × g for 15 min. The supernatant was removed. 1 ml of 85% ethanol (SIGMA #51976) in DEPC (SIGMA #D5758) treated water was added to the pellet. The sample was spun at 17,000 × g for 15 min. The pellet was allowed to air-dry until it there was no excess liquid, but

the pellet still appeared moist. The pellet was resuspended in RNase free water and heated at 65 °C for 15min to remove secondary structures. The sample was centrifuged briefly. RNA was quantified using Thermo Scientific NanoDrop 2000 and stored at -80 °C or processed immediately.

2.5 Reverse Transcription

RNA was reverse transcribed using 0.5-4 μg of RNA (depending on the application) and SuperScript II enzyme (Invitrogen #18064014), with an Oligo DT primer.

2.6 Conventional PCR

RT-PCR products for *XBP1*s were run on 3% gels using UltraPure Agarose (Invitrogen) and 1X Tris Acetate EDTA (TAE) buffer. Gels were run in a 30 cm rig at 120 V. The high percentage gel and large rig was to ensure proper separation of the *XBP1* isoforms which differ by 26 bp. All other PCR products and RNA were run on 1% agarose gels using sodium borate buffer. Gels were imaged using the BioRad Pharos FX^{TM} plus Molecular Imager. Densitometry was carried out using ImageJ software. *XBP1* splicing % was determined using the following formula: (*XBP1*s / *XBP1*s + *XBP1*u) × 100. See table 2.2 for primer sequences.

2.7 qPCR

Specific cDNA and miRNA targets were detected using PrimeTime TaqMan qPCR assays (IDT). miRNA were reverse transcribed using Applied Biosystems™ TaqMan™ MicroRNA reverse transcription Kit (#4366596). Takyon ROX Master Mix (Eurogentec UFRP5XC0501) was used for qPCR reactions. Applied Biosystems 7500 and StepOne Plus qPCR platforms were used for running the experiment. The data was analyzed manually using the ΔΔCt method using the endogenous control stated in the relevant figures.

2.8 Patient Sample Analysis

The Galway University Hospitals Clinical Research Ethics Committee approved the use of human tissue samples following informed patient consent. Patients provided written informed consent for use of samples, and work was performed according to the principles of the Declaration of Helsinki. Breast tissue samples (basal ($n = 5$), luminal ($n = 4$), TAN ($n = 4$)) were harvested in theatre at University Hospital Galway. Primary patient RNA samples were collected following institutional ethical

approval and informed patient consent and stored in RNA*later*® at -80 °C until needed. RNA quality was determined by resolving at least 250 ng of total RNA on a 1% sodium borate agarose gel and samples displaying degradation were excluded from the study. 500 ng of total RNA was reverse transcribed as described above. Total *XBP1* and *XBP1*s transcript levels were normalized to the average Ct of control genes, *PPIA* and *MRPL19* using the ΔΔCt method. A pool of cDNA was used as an inter-plate/run control and as the control sample for ΔΔCt calculations. Results are displayed as: relative *XBP1*s abundance / relative *XBP1* total abundance. See appendix B for patient information.

Levels of *JUP* mRNA were plotted against tumour subtype in the TCGA cohort (n = 595)[162].

2.9 MicroArray and Sample Preparation

MDA-MB-231 cells were seeded at 5×10^5 cells per T25 flask (microarray) or at 3.5×10^6 cells per T175 flask (RNA-seq). Cells were treated with DMSO or MKC8866 (20 μM) at 4 h and 24 h in normoxia and hypoxia (1% O_2). All tubes/tips used in this protocol (when not supplied in a kit) were autoclaved before use. Pipettes were cleaned thoroughly with industrial methylated spirit (IMS) and all tips, tubes, and pipettes were cleaned with RNase inhibiting wipes.

After treatment, harvesting and centrifugation at 1,500 × rpm for 5 min, cell pellets were resuspended in 1 mL TRIZOL and vortexed for 1 min. Sample was incubated at room temperature then stored at -20 °C. Samples were thawed on ice. 200 μL of chloroform was added to the sample. The sample was shaken by hand for 15 sec. Samples were incubated at room temperature for 15 min. Samples were spun at 17,000 × g (Maximum setting) at 4 °C for 15 min. The upper aqueous layer of the sample was removed to a clean labeled 1.5 mL eppendorf tube. 1 volume of 70% ethanol was added to each solution in three equal aliquots, and mixed by inversion. 700 μL of sample was added to a Qiagen RNeasy column. Sample was spun at 8000 × g for 15 sec. The remaining sample was added to the Qiagen RNeasy column and spun at 8000 × g for 15 sec. The flowthrough was discarded. 350 μL RW1 buffer was added to the column. The column was spun at 8000× g for 15 sec. The

flowthrough was discarded. 10 µL of Qiagen DNase was added to 70 µL of RDD buffer and added the solution directly to the column. The samples were incubated at room temperature for 15 min. 350 µL of RW1 buffer was added to the center of the column and spun at 8000 × g for 15 sec. The flowthrough and collection tube were discarded. The column was transferred to a new collection tube. 500 µL RPE buffer was added to the center of the column and spun at 8000 × g for 15 sec; the flowthrough was discarded. This step was repeated. Samples were spun for a further 2 min at 8000 × g. The column was transferred to a clean labeled eppendorf. 30 µL RNase free H_2O was added to the center of the column and incubated for 1min at room temperature. Samples were centrifuged at 8000 × g for 1 min. A further 30 µL RNase free H_2O was added to the center of the column and incubated for 1 min at room temperature. Samples were centrifuged at 8000 × g for 1 min. 25 µL of RNA was taken for downstream processing (Reverse Transcription), the rest was immediately stored at -80 °C.

Inhibition of *XBP1* splicing was confirmed by RT-PCR before the samples were sent to EMBL for analysis. RNA quality was determined by amplifying 5' and 3' ends of the *GAPDH* transcript upon Oligo-dT-primed reverse transcription, and by capillary electrophoresis upon receipt at EMBL. The experiment was performed in triplicate. MicroArray analysis was performed on Affymetrix GeneChip Human Transcriptome Array 2.0 in at the EMBL genetics core facility in Heidlberg, Germany. The data was analysed using *GeneSpring* software. Using the *GeneSpring* software (Agilent technologies) differential expression data genes with p-value below 0.05 and Fold Changes over 1.3 were considered differentially expressed between the conditions. Venny software was accessed at http://bioinfogp.cnb.csic.es/tools/venny/[183]

TaqMan qPCR		
GAPDH	FWD	TGTAGTTGAGGTCAATGAAGGG
	REV	ACATCGCTCAGACACCATG
	Probe	AAGGTCGGAGTCAACGGATTTGGTC
XBP1s	FWD	GGAATGAAGTGAGGCCAGT
	REV	AGAGTCAATACCGCCAGAATC
	Probe	TGAGTCCGCAGCAGGTGCA
XBP1 Total	FWD	TGGATTCTGGCGGTATTGAC
	REV	TCCTTCTGGGTAGACCTCTG
	Probe	TGGGCATTCTGGACAACTTGGACC
PPIA	FWD	CATCCTAAAGCATACGGGTCC
	REV	TCTTTCACTTTGCCAAACACC
	Probe	TGCTTGCCATCCAACCACTCAGTC
MRPL19	FWD	CTTAGGAATGTTATCGAAGGACAAG
	REV	GCTATATTCAGGAAGGGCATCT
	Probe	CTCGGGTCCAGGAGAGATTCAGGTG
CXCL1	FWD	TCTCTCTTTCCTCTTCTGTTCCTA
	REV	CATCCCCCATAGTTAAGAAAATCATC
	Probe	AAGCTCACTGGTGGCTGTTCCT
IL6	FWD	GCAGATGAGTACAAAAGTCCTGA
	REV	TTCTGTGCCTGCAGCTTC
	Probe	CAACCACAAATGCCAGCCTGCT
IL8	FWD	GGGTGGAAAGGTTTGGAGTAT
	REV	TTGGCAGCCTTCCTGATTT
	Probe	CAGCTCTGTGTGAAGGTGCAGTTT
GMCSF	FWD	TGACAAGCAGAAAGTCCTTCAG
	REV	CAGCCTCACCAAGCTCAAG
	Probe	CCAGCCACTACAAGCAGCACTG
TGFβ2	FWD	TGAGTCACAACAGACCAACC
	REV	TCAATGTAAAGTGGACGTAGGC
	Probe	AAAGCAATAGGCCGCATCCAAAGC
IRE1	FWD	GCATAGTCAAAGTAGGTGGCA
	REV	GATAGTCTCTGCCCATCAACC
	Probe	TGTACGACACCAAACCCGAGAGC
JUP	FWD	GAACTCTGTGCGTCTCAACT
	REV	AGATTCCTGATCAAGCCGATG
	Probe	CTTCACGATGGCTGGGATGCC
CDON	FWD	GAAGTGTGACTGTCTCTGCTTT
	REV	GAAGCTGCAAATGAACATGGT
	Probe	CCATGAGAGATGCTTCTGCCTGTGT

CCNG2	FWD	GCTAGGCATTTAGAAACCAACTC
	REV	TGTATTAGCCTTGTGCCTTCTC
	Probe	CCAGTAATTCAACAGATTTCAAAGTTTCCACTTCC
ING4	FWD	CAGGCAAAATGGAACCACTC
	REV	GAAGAAAGCTGCTCGTGCT
	Probe	CCCCAAGACTGCCCAGAAGAACTT
TIMP3	FWD	CGGTACATCTTCATCTGCTTGA
	REV	CCTTCTGCAACTCCGACATC
	Probe	CCTCCTTTACCAGCTTCTTCCCCAC
SNAI2	FWD	CAGATGAGCCCTCAGATTTGAC
	REV	AGGACACATTAGAACTCACACG
	Probe	AGCCTTTTTCTTGCCCTCACTGC
CD59	FWD	AACCCAACTGCTGACTGCAAAACAG
	REV	CAATGCTCAAACTTCCAACACT
	Probe	GCCTGCAGTGCTACAACT

Table 2.1 QPCR Primer and Probe Sequences

Transcript	**FWD 5' - 3'**	**REV 5' - 3'**
GAPDH	ACCACAGTCCATGCCATC	TCCACCACCCTGTTGCTG
***XBP1*s**	TCTGCTGAGTCCGCAGCAGG	CTCTAAGACTAGAGGCTTGG
***XBP1*u**	CAGACTACGTGCGCCTCTGC	CTTCTGGGTAGACTTCTGGG
Conventional *XBP1* Splicing	CCTGGTTGCTGAAGAGGAGG	CCATGGGGAGATGTTCTGGAG
Total *XBP1*	CCTGGTTCTCAACTACAAGGC	AGTAGCAGCTCAGACTGCCA
JUP	GACATACACCTACGACTC	CCTGGTAGTTGATGAGATG
***JUP* Exon 3 Cleavage Site**	ATGTGCCCTGGTGTGTCAG	TCTTCGACAGCTGGTTCACAA
ACTB	CCAGTGGTACGGCCAGAGG	GCGAGAAGATGACCCAGATC
RPL19	TCAGGTACAGGCTGTGATACA	GGGCATAGGTAAGCGGAAGG

Table 2.2 RT-PCR Primer Sequences

2.10 Western Blot

Cells were lysed in Radioimmunoprecipitation Assay (RIPA) buffer or SDS buffer (4% SDS, 120 mM Tris HCl pH 6.8, 10% glycerol, 100 mM DTT, bromophenol blue). Total protein was quantified using a BCA assay (Thermo Scientific). Proteins were separated using SDS-PAGE.

Reagents	**6.5% Resolving gel (mL)**	**8% Resolving gel (mL)**	**10% Resolving gel (mL)**	**3% Stacking gel (mL)**
H_2O	2.55	2.3	1.95	2.265
30% Acrylamide	1.05	1.3	1.65	0.3
1.5M Tris, pH 8.8	1.3	1.3	1.3	
1M Tris, pH 6.8	0	0	0	0.375
10% SDS	0.05	0.05	0.05	0.03
10% APS	0.05	0.05	0.05	0.03
TEMED	0.05	0.003	0.003	0.003
Total Volume	**5**	**5**	**5**	**3**

Table 2.3 SDS PAGE Gel Recipes

Proteins were transferred to a nitrocellulose membrane. After transfer the membrane was blocked for 1 h and probed with an appropriate primary antibody overnight. Blots were washed three times with PBS plus 0.1% Tween-20 and incubated with secondary antibody HRP-conjugated for 1 h at room temperature. Blots were washed again as below and washed in PBS before developing. The membranes were incubated with Western Lightning ECL substrates (Perkin Elmer) for 5 min. The signal was acquired in dark room after the exposure of Agfa Medical X ray film blue 18×24 (Medray CP-BU) on the top of the membrane.

Protein	**Antibody**	**Blocking**	**1° Antibody Conditions**	**2° Antibody Conditions**	**Washes**
XBP1s	Biolegend #647502	5% milk in PBST (0.1% Tween) 1 h at room temperature	1:2,000, 5% milk in PBST (0.1% Tween) 4 °C overnight	1:10,000, 5% milk in PBST (0.1% Tween) 1 h room temperature	3 ×10 min in PBST (0.1% Tween)
ACTB	SIGMA #A2066	5% milk in PBST (0.1% Tween) 1 h at room temperature	1:5,000, 5% milk in PBST (0.1% Tween) 4°C overnight	1:10,000, 5% milk in PBST (0.1% Tween) 1 h room temperature	3 × 10 min in PBST (0.1% Tween)
JUP	Cell Signaling Technology #2309S	5% milk in PBST (0.1% Tween) 1 h at room temperature	1:2,000, 5% milk in PBST (0.1% Tween) 4°C overnight	1:10,000, 5% milk in PBST (0.1% Tween) 1 h room temperature	3 × 10 min in PBST (0.1% Tween)
HIF1α	Novus Biologicals #NB100-479	10% milk in PBST (0.2% Tween) 1 h at room temperature	1:4,000, 10% milk in PBST (0.2% Tween) 4°C overnight	1:10,000 Anti-Rabbit, 10% milk in PBST (0.2% Tween) 1 h room temperature	3 × 10 min PBS (0.2% Triton X100)
HSP90	Santa Cruz #SC-13119	5% milk in PBST (0.1% Tween) 1 h at room temperature	1:5,000, 5% milk in PBST (0.1% Tween) 4°C overnight	1:10,000, 5% milk in PBST (0.1% Tween) 1 h room temperature	3 × 10 min in 1 x PBST (0.1% Tween)
IRE1α	Cell Signalling Technology #14C10	5% milk in PBST (0.1% Tween) 1 h at room temperature	1:2,000, 5% milk in PBST (0.1% Tween) 4°C overnight	1:10,000, 5% milk in PBST (0.1% Tween) 1 h room temperature	3 × 10 min in PBST (0.1% Tween)

Table 2.4 Western Blot Antibodies: Incubation and Washing Conditions

2.11 ELISA

IL-6 (DY206), IL-8 (DY208), CXCL1 (DY275), GM-CSF (DY215) and TGFβ2 (DY302) DUOSET ELISA's were purchased from R&D Systems and carried out as per manufacturer's instructions.

2.12 *In Vitro* RNA Cleavage Assay

5 μg of total RNA from MCF7 cells was incubated with 2.25 μg GST-IRE1 (SinoBiological 11905-H20B,) 2 mM ATP, and 1x *in vitro* RNA cleavage buffer, with DMSO or MKC8866 (20 μM) for 4 h at 37 °C. After cleavage proteinase K was added to the mixture to a final concentration of 100 μg/mL and samples were incubated at 30 °C for 30 min. RNA was precipitated by adding 20 μL of chilled iso-propanol to each sample and centrifugation at 17,000 × g for 15 min at 4 °C. Supernatant was removed and 50 μL of 70 % ethanol was added and samples were centrifuged at17, 000 × g for 10 min at 4 °C. Supernatant was removed again and 50 μL of 70 % ethanol was added and samples were centrifuged again at 17,000 × for 10 min at 4 °C. RNA pellets were allowed to air dry before further processing. Total RNA quality was determined by running at least 250 ng of RNA on a 1% agarose gel.

Preparation of buffer:

5X *in vitro* RNA cleavage buffer: Tris 250 mM, NaCl 3 M, $MgCl_2$ 25 mM, $MnCl_2$ 25 mM, β-mercaptoethanol 25 mM.

5X buffer was prepared as above and then diluted to 2X. pH was adjusted to 7.4 using HCl. Buffer was filter sterilised.

2.13 Mammosphere Formation Assay

MDA-MB-231 cells were treated with 10 nM Paclitaxel (SIGMA #T7402) for 72 h. Cells were washed once with complete growth medium then allowed to recover in complete medium containing DMSO or MKC8866 (20 μM) for a further 72 h. After recovery cell viability was determined using Trypan blue staining. Viable cells from each treatment were seeded in triplicate at 1×10^3 cells/well in 96 well ultra-low attachment surface plates (Corning #10554961) in DMEM/F12 medium (Gibco

#11320-074) supplemented with B27-supplement (ThermoFisher #12587010) and 20 ng/ml epidermal growth factor (Peprotech #AF-100-15). Completely untreated cells were also seeded as a control. Mammospheres measuring >40 μm were quantified in five fields per well, and mammosphere formation efficiency (MFE %) was determined using the following formula: (Number of Mammospheres >40 μm / Number of cells seeded) x 100.

2.14 Scratch/Wound Healing Assay

MDA-MB-231 cells were seeded at 3×10^5 cells in 6-well plates and treated 24h later with DMSO or MKC8866 (20 μM). 48hr post-treatment a P200 tip was used to make two vertical scratches per well through the monolayer of cells. Media was removed from cells and cells were washed with 1 mL media. Conditioned media was spun down at 17,000 × g before adding it back onto the cells. Pictures representing the 0 h time point and further indicated time points were taken using a 4X magnification. ImageJ software was used to measure the distance between each side of the wounds and % scratch closure was calculated using the following formula: ((Average Scratch Width @ time 0 - Average of Scratch Width @ time X) / Average Scratch Width @ time 0) * 100 = % Scratch Closure @ time X.

2.15 Transwell Migration Assay

MDA-MB-231 cells were seeded at 9×10^5 in 10 cm dishes. 24 h post-seeding cells were treated with DMSO or MKC8866 (20 μM) or transfected with siRNA targeting IRE1 for a further 48 h. The underside of boyden chambers (COSTAR #3422) and surface of control wells (no boyden chamber) were coated with fibronectin (SIGMA #0895) (0.5 μg/mL) or laminin (Sigma #11243217001) (1 μg/mL) in sterile H_2O overnight at 4 °C. Cells were trypsinised and the trypsin was quenched with serum-free media. Cells were centrifuged at 120 × g for 5 min. The pellet was resuspended in serum-free media. Cells were spun down again and resuspended in serum-free media. Fibronectin and laminin was removed from the wells and the wells were washed once with 1x PBS. 400 μL of serum-free media was added to the bottom of control wells (no boyden chamber). 500 μL of serum-free media was added to the bottom of wells containing the boyden chambers and 300 μL of serum free media was added into the boyden chamber. Cells were counted and each treatment was seeded in duplicate into fibronectin and laminin coated chambers in 100 μL at a

density of 300,000 cells/mL. Cells were allowed to migrate for 6 h under normal culture conditions. Media was removed from the wells and chambers and crystal violet stain (20% Methanol (SIGMA #34860), 0.05% Crystal Violet was added to wells and chambers and incubate at room temperature for 30 min. After incubation crystal violet stain was removed and chambers were washed with H_2O and cotton swabs. Chambers and wells were allowed to air dry. After chambers were dry five fields/membrane were imaged and total migrated cells were quantified using imageJ software and the CellCounter plugin.

2.16 *In Vivo* Experiments

All animal experiments were performed in accordance with the ethical guidelines of the IACUC committee at Charles River Laboratories, Piedmont, South Carolina approved the study protocol (IACUC ASP #: 980701). Female athymic nude mice (Crl:NU(Ncr)-*Foxn1nu*, Charles River) were implanted subcutaneously in the right flank with 5×10^6 MDA-MB-231 cells (0.1 mL cell suspension in PBS). Mice with tumors measuring between 225 and 250 mm^3 were randomized into six treatment groups consisting of ten mice with individual tumor volumes ranging from 196 to 288 mm^3 and group mean tumor volumes from 225 to 227 mm^3 (considered day 1 of treatment). Change in tumor volume was monitored by calipers 2 times per week with tumor volume calculated as V = (L x S2)/2 by measuring the long (L) and short (S) axes of tumors. Paclitaxel (Lot CP2N10007) was purchased as a dry powder from Phyton Biotech, LLC (Fort Worth, TX). A 10 mg/ml paclitaxel stock solution in 50% ethanol: 50% Cremophor EL was prepared and stored at room temperature protected from light before dosing. On each day of dosing, an aliquot of the paclitaxel stock was diluted with 5% dextrose in water (D5W) to yield a 1.0 mg/ml paclitaxel dosing solution in a vehicle consisting of 5% ethanol: 5% Cremophor EL: 90% D5W (Vehicle 1) which provided the 10 mg/kg dose in a 10 ml/kg dosing volume. Mice were administered 10 mg/kg paclitaxel weekly by intravenous injection. The IRE1 inhibitor, MKC8866, was administered at a dose volume of 10 ml/kg from a 30 mg/mL suspension in 1% microcrystalline cellulose in a simple sugar at 300 mg/kg daily by oral gavage (Vehicle 2). Treatment groups were as follows: For Group 1, the paclitaxel vehicle was administered intravenously weekly and the MKC8866 vehicle was administered orally daily throughout the course of the study. For Groups 2-6, paclitaxel was administered weekly throughout the course of

the study. In combination with paclitaxel, MKC8866 was also administered orally daily from day 1-28 (Group 3), from day 14-60 (Group 4), from day 28-60 (Group 5) and from day 1-60 (Group 6). Treatments in all groups were administered until tumors reached maximal size or day 60, whichever came first.

For the xenograft regrowth post-paclitaxel *in vivo* experiment female athymic nude mice (Crl:NU(Ncr)-*Foxn1nu*, Charles River) were implanted subcutaneously in the right flank as described above. Following establishment of palpable tumors mice were randomized into treatment groups consisting of 10 mice per group with group mean tumor volumes from 227 to 230 mm^3 (considered day 1 of treatment). A 7.5 mg/ml paclitaxel stock solution in 50% ethanol: 50% Cremophor EL was prepared and stored at room temperature protected from light before dosing. On each day of dosing, an aliquot of the paclitaxel stock was diluted with 5% dextrose in water (D5W) to yield a 0.75 mg/ml paclitaxel dosing solution in a vehicle consisting of 5% ethanol: 5% Cremophor EL: 90% D5W (Vehicle 1) which provided the 7.5 mg/kg dose in a 7.5 mg/kg dosing volume. Mice were administered 7.5 mg/kg paclitaxel once every other day for five doses by intravenous injection. MKC8866 was administered daily for 28 days at a dose volume of 10 mg/kg from a 30 mg/kg suspension in 1% microcrystalline cellulose in a simple sugar at 300 mg/kg daily by oral gavage (Vehicle 2). Group 1 received paclitaxel (7.5 mg/kg) alone while group 2 received paclitaxel (7.5 mg/kg) plus 300 mg/kg MKC8866.

If, during the course of the study, tumors became necrotic or if measurement of the tumor in 2 dimensions was not possible using calipers, measurement was stopped. Mice were observed frequently for health and overt signs of any adverse treatment-related side effects, and noteworthy clinical observations were recorded. Individual body weight loss was monitored per protocol, and any animal whose weight exceeded the limits for acceptable body weight loss was euthanized. Acceptable toxicity was defined as a group mean body weight loss of less than 20% during the study and not more than one treatment related death among ten treated animals, or 10%. Any dosing regimen resulting in greater toxicity was considered above the maximum tolerated dose.

2.17 COSMIC Database Interrogation for UPR Mutants

Mutations in *XBP1*, *IRE1*, *PERK*, *ATF6*, and *GRP78* were compiled using COSMIC database (https://cancer.sanger.ac.uk/cosmic). "Breast Cancer" was used as the search term on the home page. "breast, carcinoma" was selected as the disease type. Under the "Genes" heading the "Genes with mutations tab was selected". Searches were performed for XBP1, "ERN1" (IRE1), "EIF2AK3" (PERK), "ATF6" and "HSPA5" (GRP78). The "Variants" tab was clicked and the variants were exported to excel in "CSV" format. The domains in which the variants occurred were manually annotated with reference to UniProt (https://www.uniprot.org/). The final interrogation for this thesis was performed on 28th July 2018. The database may have been updated since then.

2.18 Data availability

Microarray data supporting the findings of this study have been deposited in the Gene Expression Omnibus and are publicly available under the GEO accession number GSE99766 [https://www.ncbi.nlm.nih.gov/geo/query/acc.cgi?acc=GSE99766].

2.19 M-Fold of RNA for IRE1 Cleavage Site Prediction

The m-fold web server was accessed at (http://unafold.rna.albany.edu). The canonical IRE1 cleavage site in exons 3 and 5 of JUP mRNA plus 15 bases upstream and downstream of this site were analysed using default settings.

2.20 Densitometry – ImageJ

ImageJ software was downloaded from (lukemiller.org2013). Levels of target gene expression was normalised to the relevant control gene, and target gene/control gene for each sample was normalised to the relevant control sample.

2.21 miRDB Analysis

miRDB software was accessed at http://mirdb.org/. "JUP" was entered as the gene symbol in the "Search by target gene window". All potential targets identified were used in the analysis.

2.22 TFbind

The 1,000 bp sequence downstream of the transcription start site of miR98/Let7 was obtained from the ensemble database (ensembl.org). TFbind software was accessed at http://tfbind.hgc.jp/.

2.23 JUP mRNA levels in TCGA Cohort

2.24 Statistical Analyses

Patient mRNA expression data, QPCR data, RT-PCR and western blot densitometry data, mammosphere, ELISA, and *in vivo* data are expressed as mean ± SEM. Differences between treatments were determined by student's two-tailed t-test. For patient data, ANOVA tests were used to determine if differences were significant between groups.

Chapter III: Investigating IRE1 RNase activity in breast cancer

3.1 Introduction and Research Rationale

3.1.1 IRE1 in TNBC: The gap in our knowledge

To date, only two studies have reported direct roles for IRE1 in TNBC. IRE1/XBP1s has been reported to be driven by MYC in TNBC and to promote therapy resistance[182]. It has also been shown to promote TNBC growth and therapy resistance through regulation of the hypoxia response[104]. While very informative, these studies provide only small pieces of what is likely a much bigger picture. IRE1 RNase activity may have a large effect on the composition of the transcriptome through XBP1s transcriptional activity and through RIDD, and given the diversity of IRE1 RNase functions in different cell- and stress-contexts, it stands to reason that it may have broader, hitherto unknown, functions in TNBC[73,184]. Since IRE1 has been reported to be active in breast tumours (and specifically in TNBC[104]) but not in healthy tissue, a broad, unbiased investigation of its activity is warranted to identify novel functions.

3.1.2 Physiological and tumour-associated hypoxia

Hypoxia is a physiological condition in which a part of the body does not receive adequate oxygen. Each tissue in the body requires different concentrations of oxygen to function properly, thus oxygen levels that constitute a hypoxic environment are tissue-specific[133].

Different physiological conditions can emerge which trigger localized hypoxia in the body. Local inflammatory responses can cause hypoxia due to the constriction of blood vessels up- and downstream of the site of infection and abundance of immune cells such a neutrophils which consume high quantities of oxygen in processes like oxidative bursts[185]. Hypoxia also occurs in cancer[186]. Tumour cells exhibit uncontrolled growth, and thus have the ability to outgrow local vasculature. Consequently, blood vessels cannot supply all parts of the tumour with nutrients including oxygen. In solid tumours this leads to the formation of harsh tumour microenvironments in which tumour cells are exposed to a variety of physiological stressors including oxygen deprivation[99]. Anoxia (complete lack of oxygen) has been

reported in breast tumours[187], while healthy breast tissue is exposed to approximately 9% oxygen[188]. This suggests that cells within a tumour can be exposed to a gradient of oxygen deprivation, from normoxia (approximately 9%) to anoxia, depending on their proximity to blood vessels.

Given the importance of oxygen to cellular vitality and the global health of the organism, cells possess a rapid hypoxic stress response mechanism. The hypoxic response aims to restore proper oxygen levels to the deprived tissue or cells by upregulating genes involved in erythropoiesis (generation of new red blood cells) and angiogenesis (sprouting of new blood vessels from pre-existing blood vessels)[189]. This response is desirable under normal conditions to prevent tissue damage. However, in the context of cancer the hypoxia response is implicated in tumour progression. In fact, tumours displaying higher levels of hypoxic response markers often have a worse prognosis[190].

The primary molecular player in the hypoxia response is hypoxia inducible factor 1α (HIF1α)[191]. Under normoxic conditions HIF1α is constantly hydroxylated at proline residues by oxygen dependant prolyl-hydroxylases[192]. This hydroxylation causes HIF1α to be recognised by the oxygen-dependant E3 ubiquitin ligase Von Hippel-Lindau factor which ubiquitinates HIF1α, thus tagging it for proteasomal degradation[193]. Under conditions of hypoxia HIF1α is not hydroxylated and accumulates within cells, translocating to the nucleus through the binding of arylhydrocarbon nuclear transporter (ARH aka HIF1β). A heterodimer of HIF1α and HIF1β constitutes the active HIF1 transcritpion factor which is largely responsible for mediating the cellular response to hypoxia[194]. Downstream target genes of HIF1 include *VEGF*, erythropoietin, genes involved in glycolysis, and other genes which contain a hypoxia response element in their promoters[189].

XBP1 has been reported to form a complex with HIF1α, which potentiates the hypoxic response in TNBC[104]. However, the role of XBP1s in potentiating TNBC tumour growth in hypoxia is far from elucidated. To this end, hypoxic stress-specific analysis of IRE1 RNase activity will give us new more clinically relevant insights into the role IRE1 plays in TNBC.

3.1.3 Rationale

To determine if IRE1 RNase is a viable therapeutic target in breast cancer it was important to validate the recent literature and determine its activity in breast cancer. If IRE1 is inactive in breast cancer then there is no sense in targeting its activity. Furthermore, good therapeutic targets should be specifically active in the diseased tissue and not in normal tissue. In breast cancer there is added value in determining whether any target is more prevalent in a given subtype. As mentioned in the introduction, the discovery of targets specifically active in TNBC is important to the field since TNBC currently lacks targeted therapies which have proved vital for treatment of ER+ and HER2+ breast cancers[195]. Given the potential of IRE1 RNase to alter the composition of the transcriptome through XBP1s transcriptional activity and RIDD, a high throughput unbiased approach would allow examination of cellular pathways controlled by IRE1, and the identification of specific target genes for further evaluation.

3.2 TNBC cells exhibit increased XBP1 splicing compared to other subtypes

To determine whether IRE1 RNase is active in breast cancer we determined levels of *XBP1*s mRNA by PCR (table 2.2) and XBP1s protein levels by western blot (table 2.4) in breast cancer cell lines representing the three histological subtypes: ER+ (MCF7, T47D), HER2+ (SKBR3), and TNBC (MDA-MB-468, HCC1806, MDA-MB-231). MCF10A cells are non-transformed breast epithelial cell line which served as a "normal" breast tissue control. We found that the TNBC cells had increased levels of *XBP1*s mRNA relative to *XBP1*u mRNA, indicating increased splicing activity of the IRE1 RNase (Fig 3.1A). TNBC cells also had higher levels of XBP1s protein than the luminal cancers while SKBR3 (HER2) also expressed the XBP1s protein (Fig 3.1B). XBP1s transcript and protein were absent in MCF10A cells, suggesting that IRE1 RNase activity is specific to breast tumours and not to normal breast tissue, and is more prevalent in TNBC than other types.

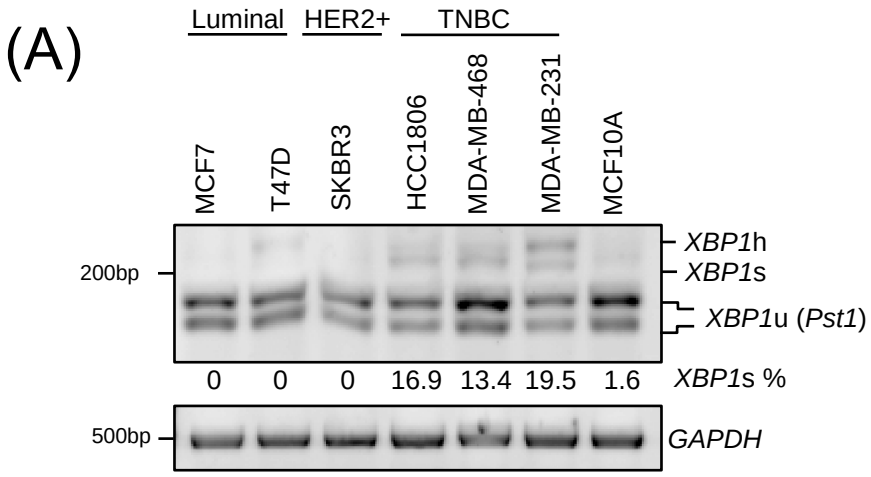
(A)
Luminal
HER2+
TNBC
MCF7
T47D
SKBR3
HCC1806
MDA-MB-468
MDA-MB-231
MCF10A
200bp
XBP1h
XBP1s
XBP1u (Pst1)
0 0 0 16.9 13.4 19.5 1.6
XBP1s %
500bp
GAPDH

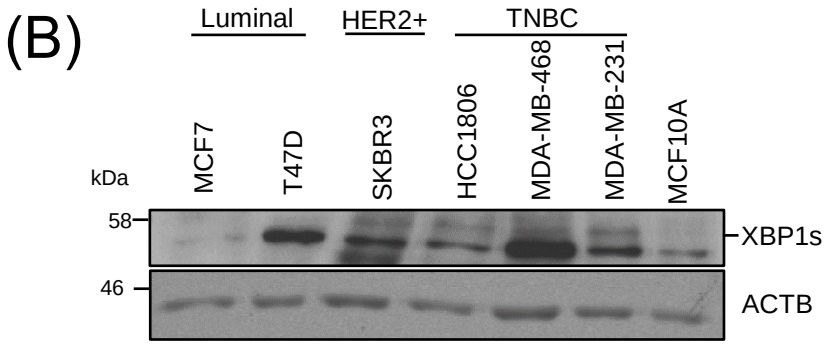
(B)
Luminal
HER2+
TNBC
MCF7
T47D
SKBR3
HCC1806
MDA-MB-468
MDA-MB-231
MCF10A
kDa
58
46
XBP1s
ACTB

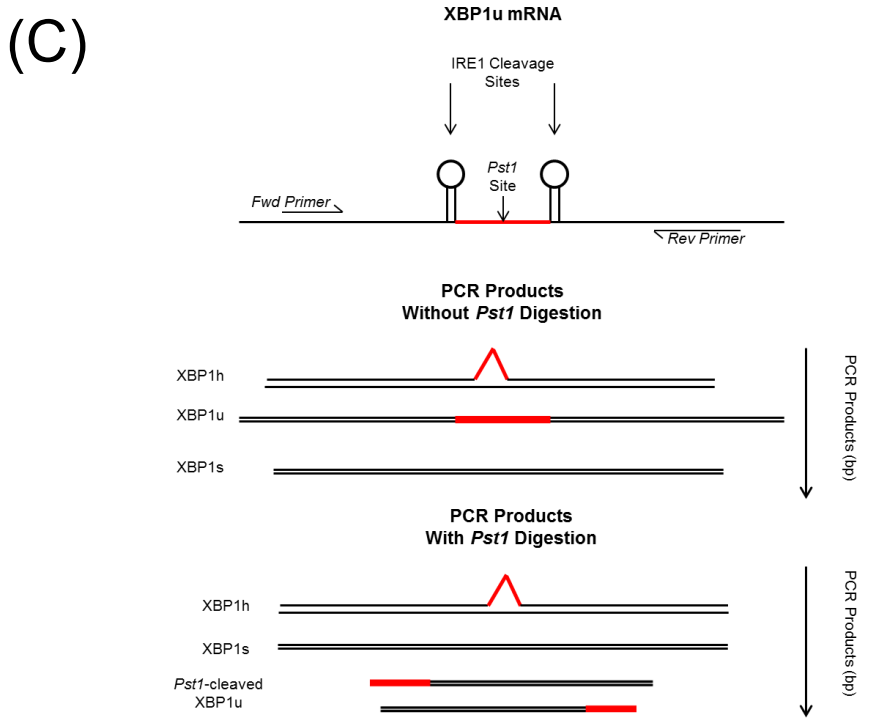
(C)
XBP1u mRNA
IRE1 Cleavage Sites
Pst1 Site
Fwd Primer
Rev Primer
PCR Products Without Pst1 Digestion
XBP1h
XBP1u
XBP1s
PCR Products (bp)
PCR Products With Pst1 Digestion
XBP1h
XBP1s
Pst1-cleaved XBP1u
PCR Products (bp)

Figure 3.1. XBP1 expression levels in breast cancer cell lines. Indicated breast cell lines were grown to 90% confluence over 48 h. After 48 h cells were lysed and protein and RNA was extracted. (A) RNA was reverse transcribed and conventional PCR for *GAPDH* and *XBP1* splicing was performed. *XBP1* splicing PCR products were digested by *Pst1* and all products were resolved on a 1% agarose, sodium borate gel. *XBP1* splicing % was determined by this formula: (*XBP1*s)/(*XBP1*u+*XBP1*s) x 100 (B) Cell lysates were probed for XBP1s and ACTB protein using western blot. (C) Diagrammatic representation of the XBP1u transcript and subsequent PCR products with and without *Pst1* digestion.

3.3 Increased splicing of XBP1 is associated with the TNBC subtype in primary human breast tumours

To gain a more clinically relevant picture of IRE1 RNase activity in breast cancer we obtained RNA from primary breast tumours and tumour adjacent normal (TAN) tissue from collaborators in University Hospital Galway and examined levels of *XBP1* splicing using qPCR (table 2.1). *MRPL19* and *PPIA* were determined to be the most stably expressed potential endogenous control genes, and a combination of both was used. *ACTB* and *GAPDH* were also tested. The patient information received from the hospital allowed us to determine whether there was a correlation between total *XBP1*, *XBP1*s, or the ratio of *XBP1* splicing and different tumour characteristics. Neither total XBP1 nor *XBP1*s differed significantly between tumours and TAN samples. Likewise there were no significant differences in *XBP1* splicing across tumour grades and tumour sizes. However, the luminal subtype tumours had significantly higher total *XBP1* compared to TNBC, but TNBC had significantly higher levels of *XBP1* splicing compared to luminal and TAN tissue, recapitulating our data from cell lines and from the literature (Fig 3.2). The data from cell lines showed that TNBC cell lines have increased levels of *XBP1*s mRNA relative to total *XBP1* mRNA levels (expressed as percentage splicing (Fig. 3.1). The data in Fig 3.2 showed that the small number of basal-like (which in this case are all TNBC) patient samples have higher levels of *XBP1*s relative to *XBP1* total as determined by qPCR (table 2.1) rather than RT-PCR (table 2.2).

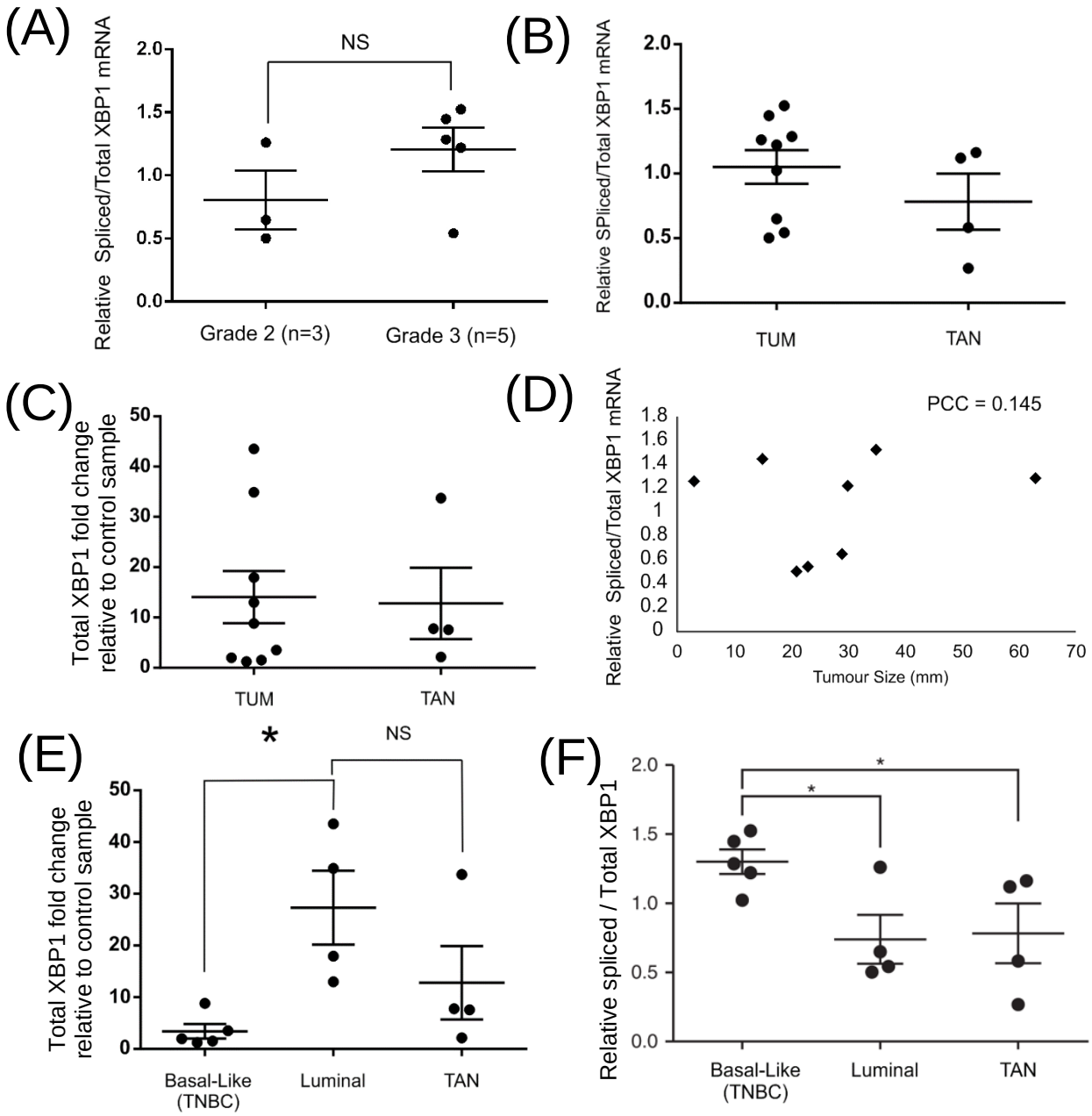

Figure 3.2. Increased splicing of *XBP1* is associated with the TNBC subtype in primary human breast tumours. RNA from primary breast cancer patients was reverse transcribed and qPCR was performed for *XBP1*s, *XBP1* Total, using *MRPL19*, *PPIA* as control genes., (A)(B)(D)(F) Spliced/Total *XBP1* and (C)(E) Total *XBP1* levels were plotted against indicated tumour characteristics. Dots represent individual patients. Units represent fold change in mRNA levels in individual patients vs interrun control pool of cDNA Error bars represent SEM, P* <0.05, ANOVA Single Factor. PCC = Pearson's correlation coefficient. Basal-like (n = 5), luminal (n = 4), TAN (n = 4). See appendix B for patient information.

3.4 Mutations in IRE1 and XBP1in breast cancers

Mutations in *IRE1* and *XBP1* have been reported in other cancers, but none have been reported or characterised in breast cancer. Though characterisation of mutants is beyond the scope of this thesis, datamining of publicly available databases would give an indication of the extent of *IRE1*/*XBP1* mutations in cancer, and perhaps identify variants which might improve our understanding of why this signalling pathway is amplified in TNBC. Datamining using the Catalogue of Somatic Mutations in Cancer (COSMIC) platform revealed that *IRE1* and *XBP1* are rarely mutated in breast cancer (0.38% and 0.62% respectively). However, IRE1 has been ranked as the fifth most likely kinase to harbour a driver mutation across other cancer types[164]. *IRE1* mutations discovered in this study have been characterized *in vitro* and do not induce cell death when over expressed, unlike wildtype IRE1 which does[77]. In principle, this suggests that cancer cells can acquire mutations which prevent IRE1 from mediating cell death. Though no *IRE1* mutations have been functionally characterized in breast cancer, using data from the COSMIC platform, we found six reported base substitution mutations, three of which are located in the kinase domain (Table 3.1). Similarly none of the XBP1 mutations identified have been characterised though most of them occur within a domain with a characterised function (Table 3.1). The biological impact of these mutations is not known, although they do not occur at residues reported to be important for IRE1 kinase activity. See supplementary figure 1 for locations of *XBP1* mRNA and XBP1 protein functional domains.

Gene Symbol	CDS Mutation	AA Mutation	Domain	Incidence
ERN1	c.224C>A	p.P75Q	Luminal	2
ERN1	c.1113G>A	p.A371A	Luminal	1
ERN1	c.1157_1158delAT	p.H386fs*8	Luminal	1
ERN1	c.1362G>A	p.L454L	Transmembrane	1
ERN1	c.1486_1487insAGC	p.Q495_L496insQ	Cytoplasmic	1
ERN1	c.2108G>A	p.G703D	Cytoplasmic/Kinase	1
ERN1	c.2142C>T	p.L714L	Cytoplasmic/Kinase	1
ERN1	c.2300T>C	p.V767A	Cytoplasmic/Kinase	1
ERN1	c.2416C>T	p.R806C	Cytoplasmic/Kinase	1
ERN1	c.2468C>T	p.A823V	Cytoplasmic/Kinase	1
ERN1	c.2811C>T	p.F937F	Cytoplasmic/RNase	1
XBP1	c.24G>A	p.P8P	-	1
XBP1	c.109C>G	p.P37A	-	1
XBP1	c.127C>G	p.Q43E	-	1
XBP1	c.243_244delAG	p.R81fs*16	bZIP/Nuclear Localization Signal	2
XBP1	c.269G>C	p.R90P	bZIP/Nuclear Localization Signal	1
XBP1	c.289_291delGAG	p.E97delE	-	1
XBP1	c.321_323delAGA	p.E108delE	bZIP/ Leucine Zipper	1
XBP1	c.363G>C	p.E121D	bZIP/ Leucine Zipper	1
XBP1	c.560_561delCT	p.S187fs*6	-	2
XBP1	c.569_570delCA	p.S190fs*1	-	1
XBP1	c.635_636ins11	p.P213fs*45	-	1
XBP1	c.693delC	p.L232fs*22	-	2
XBP1	c.706_707insC	p.L236fs*16	Translational Pausing of own mRNA	1
XBP1	c.712_713delCT	p.L238fs*13	Translational Pausing of own mRNA	1
XBP1	c.895_896delGT	p.V299fs*10	Transactivation Domain	1
XBP1	c.936G>A	p.P312P	Transactivation Domain	1
XBP1	c.1007A>T	p.Y336F	Transactivation Domain	2

Table 3.1: Mutations of UPR Proteins in Breast Cancer

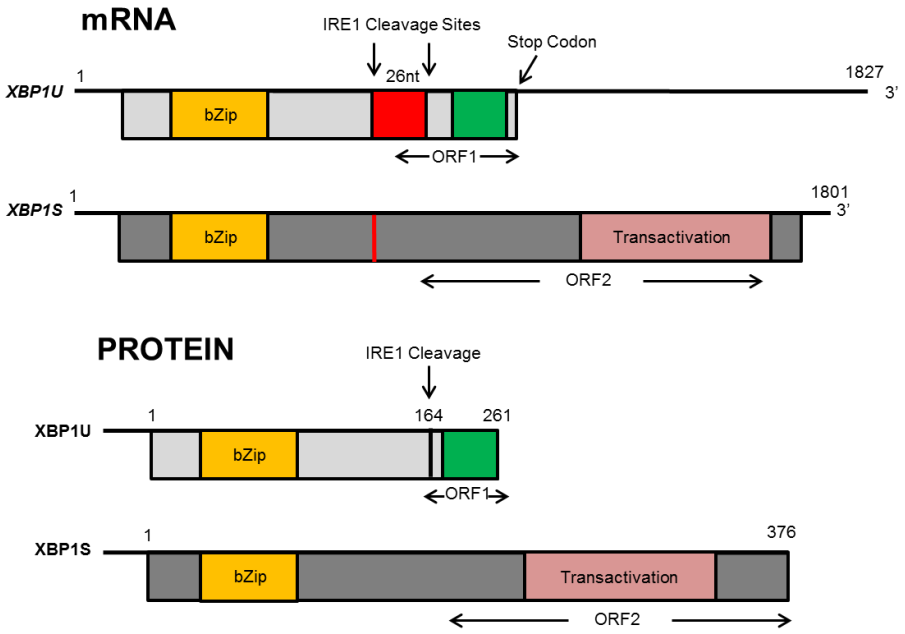

Supplementary Figure for table 3.1 Layout of functional domains in *XBP1*u and *XBP1*s mRNA and protein. Splicing of a 26nt intron (red) from *XBP1*u mRNA leads to a frameshift and translation of an alternate open reading frame (ORF) allowing the shorter spliced transcript to be translated into a longer protein (XBP1s) containing a transactivation domain. *XBP1*u mRNA contains a region reported to be responsible for translational pausing (green) which facilitates the splicing event.

3.5 MKC8866 Inhibits XBP1 Splicing

Having determined that the IRE1 RNase is more active in TNBC than other subtypes of breast cancer, and less active in normal tissue, we sought to determine its target genes in TNBC. For this we employed a small molecule inhibitor of the IRE1 RNase domain, MKC8866. To determine whether MKC8866 could inhibit *XBP1* splicing we treated MDA-MB-231 (human TNBC) cells (the cells which exhibited the highest levels of basal *XBP1* splicing) with a high dose of dithiothreitol (DTT) (2 mM) which rapidly induces ER stress by preventing the formation of disulphide bonds and thus hyperactivates IRE1, with and without MKC8866 (20 μM) and assessed levels of *XBP1* splicing by PCR (table 2.2). MKC8866 reduced DTT-induced *XBP1* splicing to basal levels and ablated basal levels of *XBP1*s when administered alone (Fig 3.3A). To determine whether MKC8866 reduced the accumulation of XBP1s protein under ER stress, MDA-MB-231 cells were treated with Thapsigargin (Tg) (500 ng), which inhibits sarco/endoplasmic reticulum Ca^{2+} ATPase (SERCA), thereby depleting luminal ER calcium stored and triggering ER

stress, with and without MKC8866 (20 μM) and levels of XBP1s protein assessed by western blot (table 2.3, 2.4). Similar to the effect on mRNA levels, MKC8866 reduced ER stress-induced XBP1s levels to basal levels, and inhibited the accumulation of XBP1s protein when administered alone (Fig 3.3B). To determine whether MKC8866 could deplete the levels of XBP1s transcriptional targets, MDA-MB-231 cells were treated with MKC8866 alone and harvested after 4, 8, 12, and 24 h of treatment. A time-dependent decrease was observed in the transcript levels of XBP1s targets *HERP* and *ERDJ4* upon MKC8866 treatment as determined by qPCR (table 2.1) (Fig 3.3C).

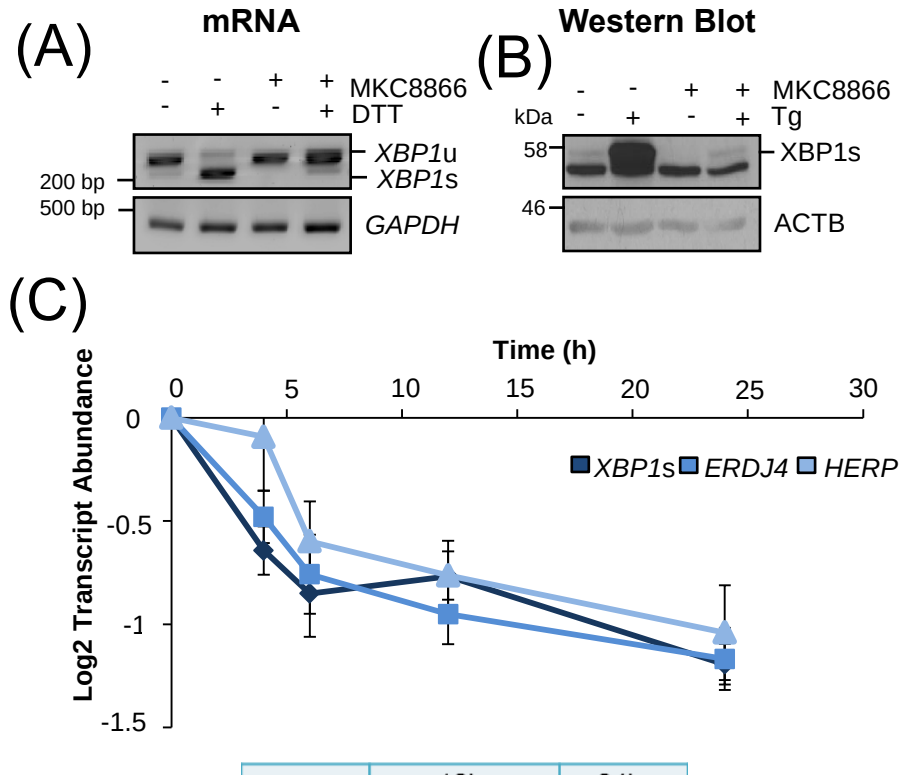

	12hr	24hr
XBP1s	-	*
ERDJ4	*	*
HERP	*	-

Figure 3.3. MKC8866 Inhibits XBP1 Splicing in MDA-MB-231 Cells. (A) MDA-MB-231 Cells were treated with DTT (2 mM) and MKC8866 (20 μM) for 4hr as indicated above. Abundance of *XBP1*s, *XBP1*u, and *GAPDH* were determined using RT-PCR. (B) MDA-MB-231 cells were treated with Tg (500 nM) and MKC8866 (20 μM) for 24hr as indicated above. Abundance of XBP1s and ACTB was determined using Western Blot. (C) MDA-MB-231 cells were treated with MKC8866 (20 μM) at the indicated time points. Relative abundance of *XBP1*s, *ERDJ4*, and *HERP* transcripts were determined via qPCR using *GAPDH* as endogenous control. Values shown represent the mean result of 4 independent repeats ± SEM, P* <0.05.

3.6 MKC8866 Inhibits IRE1/RIDD Activity

Having determined that MKC8866 could effectively inhibit XBP1 splicing it was important to determine whether the less studied RIDD activity of IRE1 was also inhibited. Though there are no reported RIDD substrates in breast cancer it was important for this project that a positive control for RIDD activity in MDA-MB-231 cells be determined. There are RIDD substrates which display some conservation across different cell types. One such substrate is *CD59*, encodes a glycoprotein which acts as an inhibitor of the complement protease cascade in the innate immune system and is reported as a RIDD substrate in HEK-293T and HeLa cells. We wanted to know if *CD59* was a RIDD substrate in MDA-MB-231 cells and whether MKC8866 could prevent its cleavage by IRE1. To answer this question, we pre-treated MDA-MB-231 cells with MKC8866 (20 μM) and Actinomycin D (ACTD) which inhibits transcription by binding to GC rich regions of DNA, for 2h, then treated cells with DTT (2 mM) for a further 4hr before harvesting and analysing *CD59* mRNA using qPCR (table 2.1) (Fig 3.4A). ACTD was used to allow us to determine whether the regulation of *CD59* by IRE1 was independent of transcription (i.e. through RIDD and not XBP1s). To confirm that the ACTD treatment worked we examined levels of *GRP78* which undergoes robust transcriptional upregulation under ER stress. Co-treatment of ACTD and DTT reduced *GRP78* levels to basal levels indicating complete inhibition of ER stress-induced transcription (Fig 3.4B). *XBP1*s was used as positive control for both DTT and MKC8866 treatments (Fig 3.4C). Addition of MKC8866 was able to rescue the DTT-induced depletion of *CD59* under ACTD treatment, suggesting that MKC8866 could block transcription-independent downregulation of *CD59* by IRE1, in addition to inhibiting *XBP1* splicing.

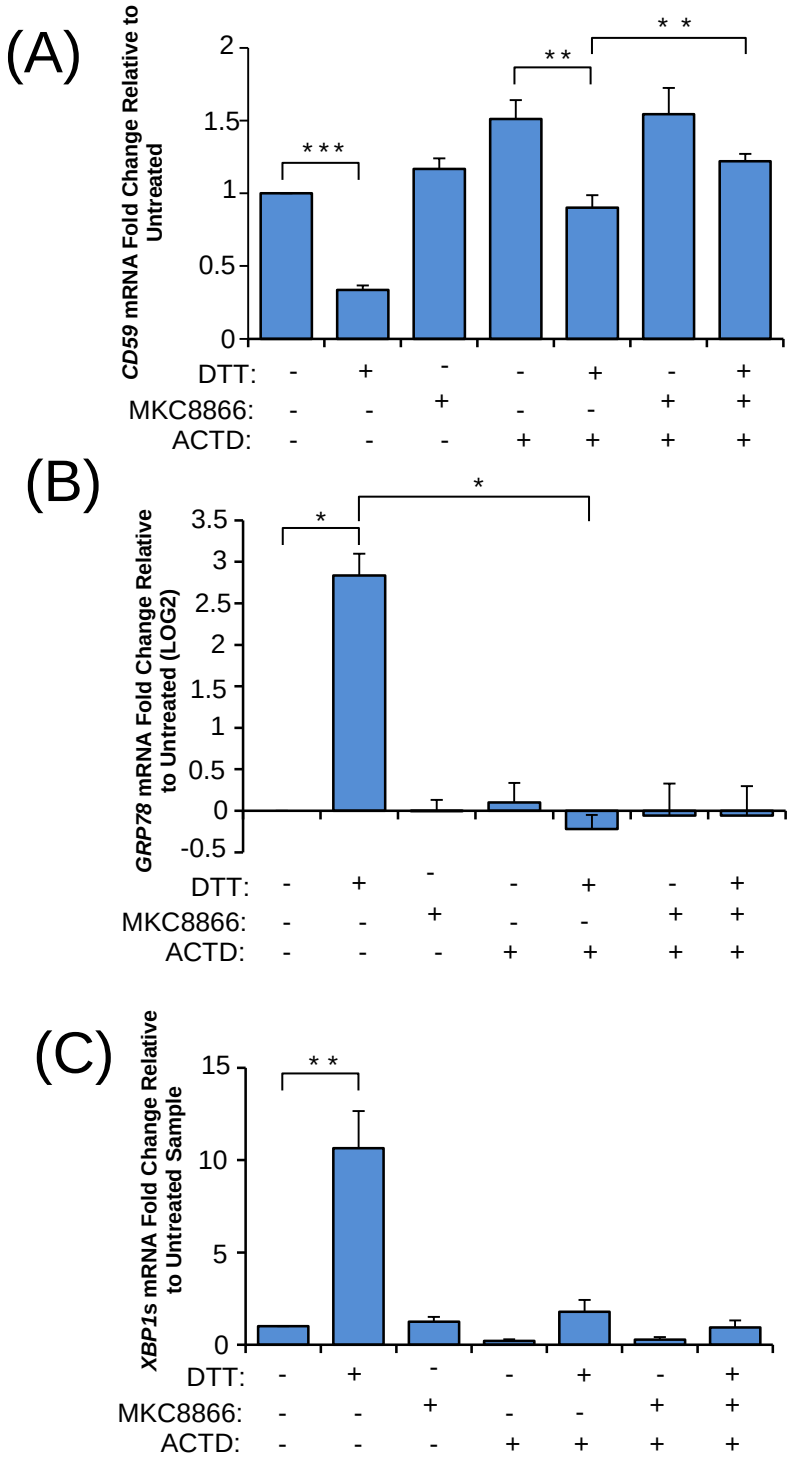

Figure 3.4. MKC8866 inhibits IRE1/RIDD activity. MDA-MB-231 cells were treated with ACTD (2 µg/mL) and MKC8866 (20 µM) for 2h as indicated above. Then cells were treated with DTT (2 mM) for a further 4hr as indicated above. Relative abundance of *CD59* (A), *GRP78* (B), and *XBP1*s (C) transcripts were determined via qPCR using *MRPL19* as endogenous control. Values shown represent the mean result of 4 independent repeats ± SEM, P* <0.05.

3.7 Exploration of IRE1 RNase activity on transcriptome of TNBC cells using Gene MicroArray Approach

Having established that MKC8866 could inhibit both XBP1 splicing and RIDD, we sought to determine IRE1 RNase targets in breast cancer. For this we employed an unbiased microarray-based gene expression approach. MDA-MB-231 cells were treated with MKC8866 (20 μM) for 4 and 24 h in normoxic (21% O_2) and hypoxic (1% O_2) conditions after which cells were harvested and RNA extracted. Depletion of *XBP1*s by MKC8866 was determined by RT-PCR analysis of *XBP1*s mRNA levels by PCR (table 2.2) (Fig 3.5A). To ensure that the hypoxic response had been activated in cells we analysed the accumulation of HIF1A within cells, and found that treatment in 1% O_2, induced HIF1α accumulation via Western blot (table 2.3, 2.4) (Fig 3.5B). Three repeats of the experiment were sent to EMBL, Heidelberg for analysis on Affymetrix Human GeneChip Human 2.0 ST Array. Initial analysis was performed by an EMBL technician using GeneSpring software.

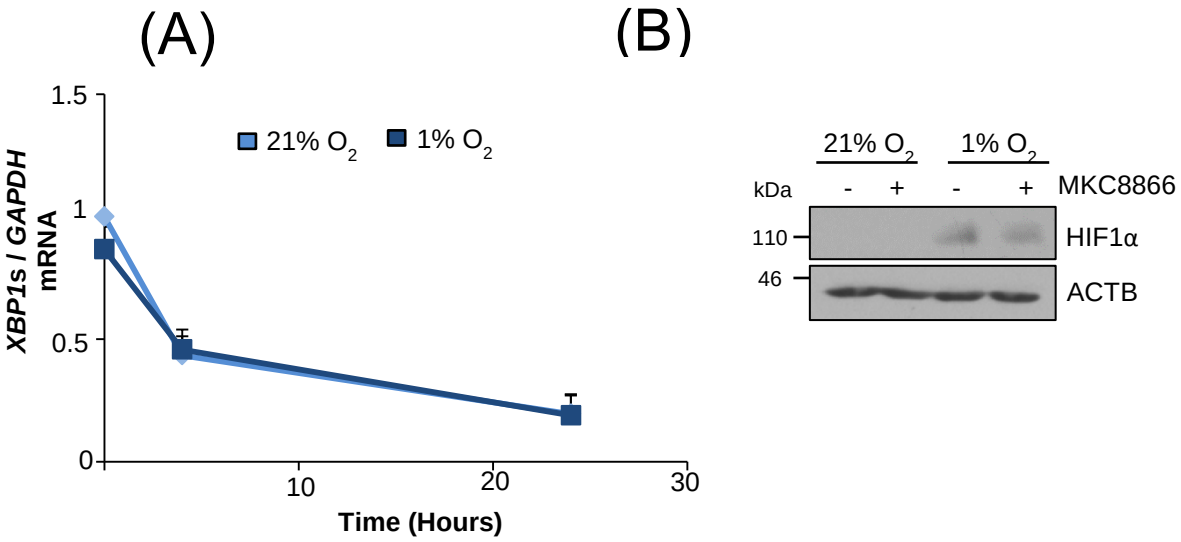

Figure 3.5. Exploration of IRE1 RNase activity on transcriptome of TNBC cells using Gene MicroArray Approach. MDA-MB-231 cells were treated with MKC8866 (20 μM) for indicated times in normoxia (21% O_2) and hypoxia (1% O2). Before sending for analysis (A) inhibition of *XBP1* splicing was confirmed with RT-PCR (graph represents densitometry of the three repeats sent for analysis) and (B) induction of hypoxic response was confirmed using Western blot to detect accumulation of HIF1α using ACTB as loading control. Values shown represent the mean result of 3 independent repeats ± SEM.

3.8 Overview of MKC8866-induced Transcriptome Changes

MKC8866 treatment altered the expression of 768 genes. The composition of the transcriptome and of those genes regulated by MKC8866 changed dramatically under hypoxic conditions. Furthermore the levels of hypoxia used did not induce splicing of *XBP1*, suggesting that the changes of XBP1 target genes come about through mechanisms other than increased XBP1s such as dimerization with other transcription factors such as HIF1α[104] or histone modifications[196]. Furthermore, MKC8866 treatment did not reduce the levels of canonical XBP1s targets typical of UPR responses. Together these observations suggested to us that basal IRE1 RNase activity in TNBC was playing a role outside of its classical role in maintaining ER homeostasis. We prepared volcano plots to better visualise the extent and significance of gene expression changes in normoxia (Fig. 3.6C) and hypoxia (Fig. 3.6D) Precise contributions to other cellular functions identified in this MicroArray experiment are presented in chapters IV and V of this thesis. See appendix C for complete gene lists.

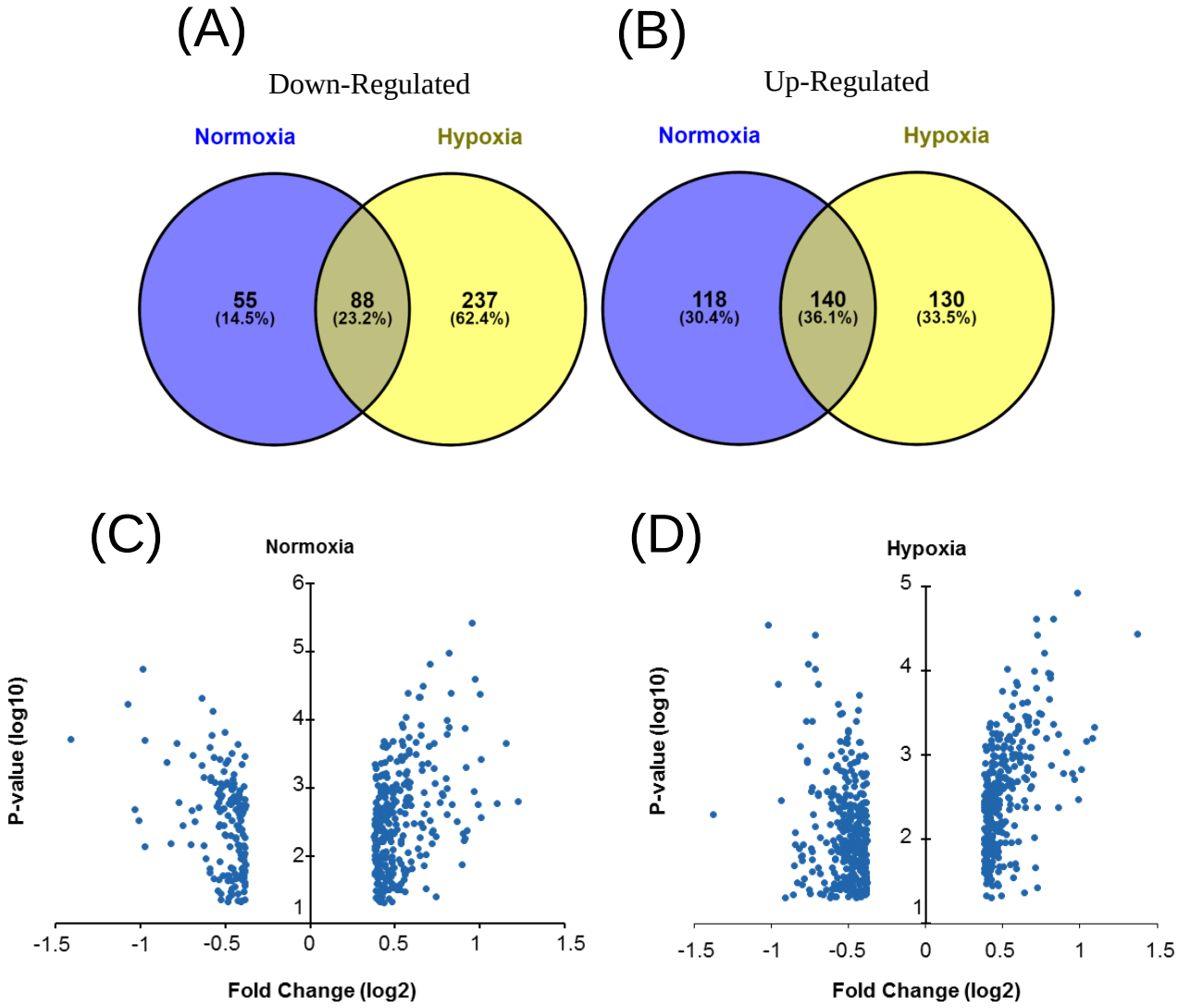

Figure 3.6. Global Changes in Transcriptome in Hypoxia and under MKC8866 treatment. (A) Pie-chart representation of overlap of genes downregulated by MKC8866 in normoxia and hypoxia. (B) Pie-chart representation of overlap of genes upregulated by MKC8866 in normoxia and hypoxia. Volcano plot of gene changes in normoxia (C) and hypoxia (D).

3.9 Discussion

In this study we sought to take a broad look at IRE1 RNase activity in breast cancer. We chose a transcriptomic approach because the immediate effect of IRE1 RNase activity is observed at this level, rather than the protein level. First we validated recent literature by showing that IRE1 RNase is active in breast cancer, as evidenced by increased *XBP1* splicing, but not in normal tissue. As normal tissue control we had at our disposal MCF10A cells, which are non-transformed breast epithelial cells, and primary samples of tumour adjacent breast tissue.

Though our data suggest that TNBC and basal-like tumours have increased IRE1 RNase activity there is a major caveat worth considering. The limited number of cell lines and of patient samples do not provide sufficient evidence to allow us to claim that most (or all) breast cancers of this subtype will display increased IRE1 RNase activity. Furthermore, there is an insufficient number of patient samples to allow for multivariate analyses which would allow us to correct for the tumour stage, which may contribute to increased IRE1 RNase activity, and is often found to be increased in TNBC versus non-TNBC cancers[153]. Thus, the work outlined in this chapter constitutes another small piece of evidence which suggests that IRE1 RNase activity is increased in these subtypes, as reported elsewhere[104].

Increased abundance of ER stress markers are observed across most if not all cancer types. The pervading idea is that tumour cells are experiencing a variety of stressors, such as increased growth, nutrient deprivation, or increased secretory demand, which perturbs protein folding within the ER and thus activates the UPR. The low incidence of mutations to UPR sensors in breast cancer that we observed when we interrogated the COSMIC database supports this notion. In other words, the UPR sensors are active in cancer because of ER stress, and not because of mutations which may render them constitutively active. In fact, mutations in IRE1 found in others cancer when characterised were found to be inactive for RNase activity which runs contrary to the notion that high IRE1 RNase activity drives cancer growth. This conventional idea that tumour associated stressors generate ER stress and thus activate the UPR may not represent the full picture of UPR activation in breast cancer however. ER stress-independent mechanisms may also be playing a role.

Activation of UPR sensors has been observed in a variety of circumstances to occur before any overt stress to the ER folding environment. This pre-emptive activation is observed in B-cells during differentiation in plasma cells before the mass production and secretion of IgM[197], and in ESR1+ breast cancer cells challenged with estrogen [175]. Thus, there are mechanisms within cells which drive UPR activation independently of ER stress. This pre-emptive activation likely serves a physiological role in preparing cells for increased protein before it occurs, providing a buffer to stress rather than relying on the UPR as a purely reactionary mechanism once protein folding homeostasis (and therefore cellular health) is already compromised. It is conceivable that cancer cells may exploit pre-emptive UPR activation to gain a

survival advantage. *XBP1* splicing was observed to occur at all stages of tumorigenesis, presumably before the cancer cells were exposed to a harsh microenvironment-induced ER stress[166]. A very recent study has found that MYC activates IRE1. MYC is an oncogene which induces cell proliferation and protein production and therefore might be thought to drive UPR activation solely through ER stress. However, Zhao *et al* found that MYC directly binds within the *IRE1* promoter region and activates IRE1 activity through IRE1 overexpression[182]. These MYC-driven mechanisms (i.e. proliferative stress and direct regulation of *IRE1*) are not mutually exclusive, and it is likely that both contribute to IRE1 activation in TNBC. Though these studies are few, they serve to diversify the mechanisms through which the UPR becomes active in cancer.

In agreement with the literature, we also found that the TNBC subtypes had increased splicing when compared to the luminal subtype but that luminal subtypes had significantly higher levels of total *XBP1*. A likely explanation for these observations is found in the different mechanisms which drive TNBC and luminal cancers (see figure 1.3). Luminal cancers are usually ESR1+ and are driven in part by estrogen signalling. Both XBP1 isoforms can trigger estrogen independent ESR1+ signalling, and thus play a role in driving ESR1+ cancers. There is an advantage in this case for the tumour cells to have high levels of total XBP1, but not necessarily high levels of IRE1 RNase activity. TNBCs on the other hand, do not express ESR1 and thus cannot take advantage of both XBP1 isoforms. Instead, TNBCs apparently rely on XBP1s transcriptional activity to drive their growth and survive hypoxia by interacting with HIF1α. Therefore, it is favourable for TNBC cells to have increased IRE1 RNase activity and thus increase XBP1s rather than having increased levels of total XBP1. These observations suggest that TNBCs are more likely to respond to IRE1 RNase inhibitors since such drugs should in theory deplete XBP1s. ESR1+ cancers may not respond as well since IRE1 RNase inhibition may not affect total XBP1 levels.

The use of small molecule inhibitors in biomedical research comes with advantages and disadvantages. They provide a useful research tool for quickly dissecting the activity of specific enzymatic activity, while also having the potential for use in the clinic. However, there is always the possibility that the small molecule binds elsewhere in the proteome besides its supposed target, such as when “specific”

PERK kinase inhibitors turn out to have a higher affinity for RIPK1 than PERK[198]. Thus, when choosing a small molecule inhibitor of the IRE1 RNase domain, we needed to be sure first that it did in fact inhibit the IRE1 RNase domain, and second to validate any results we obtained with appropriate genetic approaches. We primarily used small interfering RNA (siRNA) to fulfil the latter in later chapters.

We confirmed that the MKC8866 inhibits the activity of IRE1 RNase in the presence of very high doses of ER stressors and without pre-treatment. While indicating that the inhibitor worked under extreme non-physiological stress, the most important result for us going forward was that MKC8866 could ablate basal XBP1 splicing. Indeed, XBP1s protein or mRNA was undetectable (by conventional PCR and western blot) when MDA-MB-231 cells were treated with MKC8866 alone. Furthermore XBP1 target genes were also depleted following MKC8866 treatment and thus we concluded that MKC8866 fit its purpose as a research tool in dissecting IRE1 RNase activity. Pharmacological screening to define the specificity of MKC8866 for IRE1 is beyond the scope of this thesis. However, we have used genetic approaches to validate our findings.

Determining if MKC8866 could block RIDD activity was somewhat more complicated than the relatively simple process of assaying *XBP1* splicing. Firstly, there have been no RIDD substrates reported in breast cancer. Secondly, treating with high doses of ER stress could cause depletion of a given mRNA through a variety of mechanisms besides IRE1/RIDD, such as XBP1s, ATF4, or ATF6 driving the expression of a miRNA which targets that mRNA, or some other unknown pleiotropic effect of the chemical ER stress inducer. Thus, even if MKC8866 treatment rescued the levels of an mRNA depleted during ER stress, it would not prove that its depletion was through RIDD. Depletion of an mRNA during ER stress could only be attributed to RIDD, if it was IRE1 RNase-dependant but transcription-independent. This necessitated the use of ACTD, and the assaying of a gene transcriptionally induced by ER stress as a control. *GRP78* was selected as the gene whose levels would indicate to us whether ER stress-induced transcription was depleted. As expected, *GRP78* was robustly induced by ER stress, and addition of ACTD reduced *GRP78* levels to basal. This meant that we could have confidence that changes in *CD59* levels were IRE1 RNase-dependent but transcription

independent. MKC8866 rescued IRE1 RNase-mediated depletion of *CD59* indicating that MKC8866 could also inhibit RIDD in addition to *XBP1* splicing.

We prepared samples treated with MKC8866 in both normoxia and hypoxia for microarray analysis. As expected, MKC8866 reduced basal levels of *XBP1*s in a time-dependent manner. We confirmed that a hypoxic stress response had been launched within the cells by assaying HIF1α protein levels using western blot and finding that it accumulated. Theoretically, oxygen depletion should perturb protein folding within the ER and activate the UPR. However, hypoxia did not induce an increase in *XBP1* splicing in our model. Possible explanations for this are that the level of oxygen was still sufficiently high to allow the ER to function normally while still being low enough to induce HIF1α accumulation. Indeed, the study which identified XBP1 and HIF1α as binding partners showed that *XBP1* splicing was induced under both severe hypoxia (0.1%) and glucose deprivation[104]. Since we employed 1% oxygen levels, our cells experienced much less stress and perhaps we should not have expected dramatic changes in *XBP1*s levels. The important thing would be to determine if IRE1 RNase adopted new targets under hypoxic conditions. Indeed, the microarray analysis revealed that IRE1 RNase mediates widely different effects on the transcriptome under hypoxic conditions when compared to normoxic conditions.

These analyses revealed that the IRE1 RNase domain potentially has a wide variety of non-canonical functions in TNBC, many of which could be directly linked to processes which allow for tumour progression. This preliminary study opened the door for future studies into novel IRE1 functions in TNBC, namely in cell migration and metastasis (Chapter IV) and secretome modulation and chemotherapy resistance (Chapter V).

Chapter IV: IRE1 Regulates Migration of Breast Cancer Cells by degrading mRNA encoding *JUP*

4.0 Contributions

Figure 4.1, 4.8B – Aitor Almanza

Figure 4.5 - Brian Leuzzi

4.1 Introduction and Research Rationale

Metastasis is a fatal process in cancer. Indeed, the extent of tumour cell invasion and metastasis are the defining characteristics of higher clinical stages of breast cancer (breastcancer.org). Metastasis is a complicated and multifaceted process in which cancer cells break away from a primary tumour, travel through the circulatory system, and localise at a distant site, and begin to proliferate at the new site. Regulation of cell migration and cell adhesion is crucial to this process, as cells must repress cell adhesion proteins to detach from the tumour mass, and subsequently attach to vessel walls and extravasate into a foreign tissue[199]. It has recently been proposed that cell adhesion proteins are also important in allowing tumour cells to survive the stress associated with traversing the circulatory system. Tumour cells travelling as a cluster rather than single cells are reported to have a survival advantage in this context[200]. Thus, understanding and targeting mechanisms by which cancer cells modulate cell adhesion molecules to facilitate metastasis is a primary goal of the breast cancer field.

To date, the RIDD function of the IRE1 RNase has not been studied in any breast cancer subtype. Since XBP1s plays such an important role in TNBC[104,182] and is activated by the same IRE1 domain that controls RIDD, the absence of RIDD studies in breast cancer constitutes a significant gap in our knowledge.

4.1.1 Cell Adhesion and Migration

Cell adhesion and migration are vital to many facets of biology. Unicellular organisms require these mechanisms for motility in seeking out nutrients and avoiding predators. In mammals, cell adhesion and migration are essential for the structure and function of every organ. Mutations in cell adhesion and migration proteins are the cause of many diseases such as bullous diseases[201], and

cardiomyopathies[202], and their aberrant functions are drivers of other diseases like cancer[203]. The abundance of a specific type of junction in a given cell is dependent on the function of the tissue in which that cell resides.

Cell junctions are commonly divided into three groups; occluding junctions, gap junctions, and anchoring junctions. Occluding junctions, also known as tight junctions, are present between epithelial cells which must act as a barrier preventing molecules from moving across the epithelial layer. The gut epithelium is a classic example of an epithelial layer which prevents non-specific leakage from the intestinal lumen into the extracellular matrix (ECM) and surrounding connective tissue. Gap junctions, also known as communication junctions, are present at almost all cell-cell boundaries, and consist of proteins called connexins which form a channel called a connexon through which ions and small soluble molecules can move between the cytosols of connected cells.[204]

Anchorage Junctions:

Anchorage junctions, as the name suggests, form sturdy connections between cells. These junctions are necessary for maintaining tissue integrity, and are critical in tissues, such as cardiac muscle and skin, that are exposed to mechanical stress. There are four types of anchorage junctions: adherens junctions, focal adhesions, desmosomes, and hemidesmosomes. These four can be divided into two groups; those which mediate cell-cell adhesion (adherens junctions and desmosomes) and those which mediate cell-ECM adhesion (focal adhesion and hemidesmosomes). Though different in their constitutive parts, all anchorage junctions consist of an extracellular component, an intracellular anchoring component, and a cytoskeletal component.

Adherens junctions consist of calcium-dependent molecules called cadherins which are embedded in the plasma membrane and span the extracellular space between cells and bind to the cadherins of neighbouring cells (extracellular component). Inside the cell membrane cadherins can bind to α- and β-catenin (CTNNA/B1), α-actinin (ACTN), vinculin (VCL), and junction plakoglobin (JUP) (aka γ-catenin) (anchoring component), which bind to the actin cytoskeleton (cytoskeleton component). At desmosomes, members of the cadherin family called desmocolin and desmoglein act as the intracellular components, connecting to anchoring

components, JUP and desmoplakin, which connect to intermediate filaments (cytoskeleton component). Focal adhesions consist of membrane-bound proteins called integrins (extracellular component) which bind to ECM proteins outside of the cells and to VCL, ACTN1, talin, and filamin (FLN) (anchoring component) inside the cell. These proteins also bind to the actin cytoskeleton (cytoskeleton component). Like focal adhesions, the extracellular component of hemidesmosomes is an integrin. Plectin and other proteins act as the anchoring components, connecting integrin to the keratin intermediate filament[205].

4.1.2 Junction Plakoglobin

JUP is also known as γ-catenin and is a member of the catenin family. Though it has several functions, the best studied role of JUP is in cell-cell adhesion. JUP localizes to two cell-adhesion complexes, adherens junctions and desmosomes[206]. Adherens junctions are present ubiquitously whereas desmosomes are found only at epithelial layers. At adherens junctions, JUP promotes cellular adhesion by binding to α-catenin which binds to cytoskeletal proteins, and to adhesion molecules like e-cadherin which form homodimers between cells. Desmosomes are structurally distinct from adherens junctions and provide additional rigidity at epithelial junctions which are commonly exposed to mechanical stress.[205] Deleterious mutations of JUP are linked with disorders affecting the heart[207] and skin[208], organs where epithelial layers are exposed to a high degree of mechanical stress. *Jup*$^{-/-}$ mice die at embryonic day 10.5 due to heart defects, associated with weaker and thinner ventricular walls[209]. At desmosomes, JUP provides the link between desmoplakin which binds to the cytoskeleton (analogous to the function of α-catenin at adherens junctions) and desmocolins and desmogleins, which act as adhesion molecules between cells (analogous to the function of e-cadherin at adherens junctions). In cancer JUP has been reported mostly as a tumour suppressor in breast cancer, gastric cancer, and squamous cell carcinoma[206] but as pro-tumour in some cases[200].

The loss of adhesion molecules between cells is closely linked to the migratory capacity of cells, and is part of the EMT process[210]. Since the loss of JUP leads to a reduction in the adhesive strength of epithelial layers, one might predict that loss of JUP promotes cell migration and metastasis. Indeed, loss of JUP has been reported to increase cell migration[211]. There is a consensus in the field that JUP promotes cell-

adhesion and reduces cell migration. However, there are conflicting reports regarding the role of JUP in cancer cell migration and metastasis *in vivo*[200,211].

It has been reported that loss of JUP increases the dissemination of breast cancer cells into the bloodstream of mice and that these cells possess clonogenic properties *in vitro*[211]. However, many studies have focussed on examining the migratory capacity of cells *in vitro* as a readout for their migratory/metastatic potential *in vivo*. Powerful new techniques which have allowed researchers to track cells throughout the metastatic process have revealed this outlook to be somewhat short-sighted. A seminal paper by Aceto *et al* in 2014[200] revealed that cell-adhesion proteins confer tumour cells with an increased ability to form successful metastases. They found that single cells were far more likely to break away from primary tumours and be detected in circulation, but less abundant cell clusters were far more likely to form successful metastases. In particular, they found that JUP levels were essential for the integrity of tumour cell clusters, and that loss of JUP from these clusters greatly reduced their ability to establish metastases. Crucially, JUP was associated with decreased metastasis-free survival in breast cancer patients (a finding which has been more recently bolstered[212]).They found that JUP was heterogeneously expressed in the primary tumour, suggesting in some portions of the tumour cells are tightly adhered to one another, but that the cells at the periphery of these portions are more weakly bound to the rest of the tumour, and thus the clusters are primed to dislodge and enter circulation. JUP was necessary for tumour clusters to survive in circulation and form successful metastases. Cumulatively the literature suggests that low levels of JUP are important for allowing cells to break away from tumours, but that cancer cells require JUP to achieve successful metastasis. Thus, identification of factors which control the abundance of JUP is important. Intriguingly, when Aceto *et al* compared the gene expression profiles of matched single circulating tumour cells and circulating tumour cell clusters from multiple patients, they found that total *XBP1* was the most upregulated gene in clusters vs single cells[200]. This indicates that the UPR is active in the tumour clusters but not in the single cells. It further suggests that a link may exist between the UPR and *JUP* expression.

JUP also plays a non-canonical role in focal adhesion. In keratinocytes it was reported that expression of JUP was important for the deposition of ECM proteins, and that it increased in focal adhesions and reduced cellular migration. JUP was

further shown to promote the stability of fibronectin (*FN1*) mRNA, in addition to FN1 deposition. Cell-matrix feedback was shown to be important in the context as ECM deposited by *Jup*$^{+/-}$ keratinocytes was able to revert *Jup*$^{-/-}$ keratinocytes to a more adhesive, less migratory phenotype[213].

There are also non-adhesion-associated functions for JUP reported in migration suppression. For example, JUP binds to p53 and co-operates in the transcription of p53 target genes including *14-3-3σ*, which reduces tumour proliferation and metastasis. Another example is the apparent dominant-negative effect of JUP on β-catenin signalling. Even though JUP and β-catenin are structurally similar and share many binding partners, they appear to play opposite roles in cancer[206]. In the context of Wnt signalling, β-catenin forms complexes with transcriptional machinery more readily than JUP[206]. Where overexpression of JUP has led to increases in cell proliferation and invasion, it is supposed that increased JUP abundance sequesters cytosolic β-catenin binding partners, allowing β-catenin to translocate to the nucleus and promote cancer[206].

Other work reports that breast tumours more readily regain expression of E-cadherin and α- and β-catenin, but not JUP at metastatic sites[214]. Though conflicting, these reports suggest that some breast cancer cells can manipulate the expression of JUP to facilitate successful growth and metastasis. For instance, JUP may be lost during tumour growth at the primary site during EMT, allowing cells to migrate and invade local tissue[211]. Tumour clusters, with a core of JUP expressing cells and JUP negative cells on the periphery can disseminate together into circulation and have an increased likelihood to achieve metastasis. Associative studies vary in implicating JUP in breast cancer metastasis[215]. These conflicting papers have examined the role of JUP in the metastasis of cells to different organs, thus there may be organ-specific roles for JUP in metastasis.

4.1.3 Rationale

IRE1 RNase inhibitors are likely to enter clinical trials soon. However, the precise function of this enzymatic function is far from being fully defined in any cell-type. In breast cancer cells XBP1 has received attention as a driver of both TNBC and luminal cancers. However, little to no work has been done to characterise the role of RIDD in this context. One very recent study has posited that MYC-driven breast

cancers do not possess basal RIDD activity, but this assertion was based on the inability of MKC8866 treatment to elevate supposedly conserved RIDD substrates in cell lines at a single time point, and thus can hardly be considered conclusive[182]. If IRE1 RNase inhibitors enter the clinic it is crucial that we understand the consequences at a molecular level. If RIDD appears to have a tumour suppressor function, then it may not be desirable to inhibit the RNase activity. Opposing functions for XBP1 and RIDD in cancer is not unprecedented. Recently, RIDD was shown to have an anti-tumour role in Glioma, while XBP1s was pro-tumour.[134] Additionally, if IRE1 cleaves many RNA species in breast cancer cells it is entirely possible that RIDD many play both pro-tumour and anti-tumour roles. Thus the role of RIDD in breast cancer needs to be investigated. As we move towards targeting IRE1 in the clinic, clarifying the role of RIDD will inform treatment decisions and directly impact patients.

Many studies which aimed to identify roles for IRE1 RNase in breast cancer employed methods which do not account for changes in RIDD activity, which can be enhanced when XBP1 is depleted[216]. Thus, studies which have employed genetic ablation or knockdown of XBP1 and observed a phenotypic change may have inadvertently been observing an effect of enhanced RIDD, not just XBP1 depletion.

Lastly, studying RIDD has the potential to increase our understanding of basic cellular biology. IRE1's reputation as a signalling hub, linking multiple diverse molecular processes, is growing. Some RIDD substrates are conserved across diverse cell types which suggests that RIDD may have conserved non-cell specific roles in cell biology. Thus, identifying novel RIDD substrates in any cellular context may have important ramifications for cell biology in general, and is thus worth investigating regardless of disease implication.

To explore this gap in our knowledge and to answer clinically relevant questions, we took an unbiased approach to identify RIDD substrates in breast cancer.

4.2 Pathway analysis reveals a potential role for the IRE1 RNase in the regulation of cell migration in MDA-MB-231 cells

To elucidate what biological processes RIDD might be involved in we employed INGENUITY software and looked at the genes which were upregulated in our MicroArray dataset (QIAGEN). We chose to look only at the genes which were upregulated because IRE1/RIDD substrates should, in theory, be upregulated when IRE1 RNase is inhibited. The analysis revealed that genes regulated by the IRE1 RNase were involved in cell migration (Fig 4.1). Furthermore, the analysis suggested that treatment of MDA-MB-231 cells with MKC8866 could reduce cell migration. This suggested that under basal conditions the IRE1 RNase is causing a downregulation of transcripts encoding genes which promote cellular adhesion and inhibit migration. From this we hypothesised that IRE1 RNase activity leads to a downregulation of transcripts involved in cellular adhesion and may play a role in the detachment and migration of breast cancer cells.

Function	Function Annotation	P-value	Activation Z-score
Cellular Movement	**migration of tumor cell lines**	**2.13E-02**	**-1.747**
Cellular Movement	**cell movement of tumor cell lines**	**5.02E-03**	**-1.386**
Cellular Movement	**migration of cells**	**3.10E-03**	**-0.952**
Cellular Movement	**cell movement**	**1.07E-03**	**-0.765**

Fig 4.1 INGENUITY analysis reveals regulation of cell migration by the IRE1 RNase. Genes alternatively regulated by MKC8866 were applied to INGENUITY pathway analysis software. Activation Z-score represents the predicted effect (+ = upregulation, - = downregulation) and extent (numerical value)) on a biological process based on a change of multiple upstream regulators. In this instance upstream regulators are genes whose expression has changed as a result of IRE1 RNase inhibition. For information on how Z-score is determined see: (http://pages.ingenuity.com/rs/ingenuity/images/0812%20upstream_regulator_analysis_whitepaper.pdf)

4.3 Identifying IRE1/RIDD Targets

Next we aimed to determine what transcripts were being regulated by IRE1/RIDD, and which, if any, might play a role in regulating cell adhesion. To answer these questions we comparted three datasets: 1. The genes which were upregulated with MKC8866 treatment 2. Transcripts containing at least one IRE1 consensus cleavage site[217]. 3. Transcripts which were cleaved by IRE1 in an in vitro assay[134] (Fig 4.2A). There were genes common across the datasets but only one gene was common to all three; *JUP*, which encodes a protein with controversial roles in breast cancer cell migration and metastasis (see section 4.1.2). In addition to *JUP* we selected other genes from the interactions of the datasets with reported roles in migration. We chose to analyse Cyclin G2 (*CCNG2*)[218], TIMP metallopeptidase inhibitor 3 (*TIMP3*)[219], Inhibitor of Growth Family member 4 (*ING4*)[220] and, cell-adhesion associated, oncogene downregulated (*CDON*) (Fig 4.2B). To validate the regulation of these genes by IRE1 and to determine the mechanism of their regulation we knocked down IRE1 and XBP1 in MDA-MB-231 cells and analysed the abundance of these transcripts by qPCR (table 2.1) (Fig 4.2C). *CCNG2* was significantly downregulated by XBP1 KD but not IRE1 KD, suggesting that it is a direct XBP1 target and not an IRE1/RIDD target. In fact, XBP1s has previously been found to bind to the *CCNG2* promoter in MDA-MB-231 cells[104]. Levels of *TIMP3*, *ING4*, and *CDON* did not change significantly under any conditions.

(A)

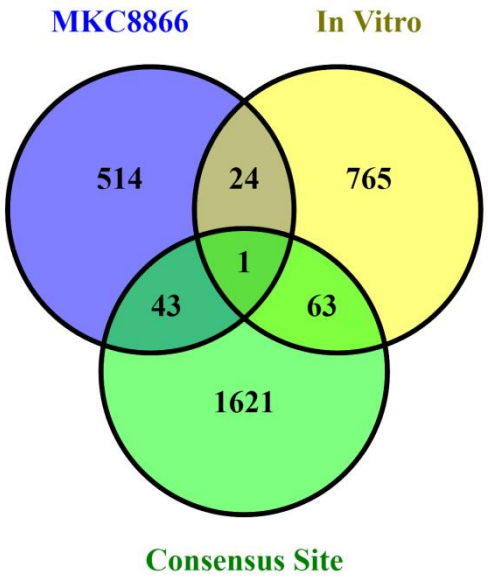

(B)

Gene	Fold Change	Regulation	P-value
JUP	**1.47**	**Up**	**2.413×10^{-3}**
CCNG2	**1.984**	**Up**	**1.767×10^{-3}**
CDON	**1.411**	**Up**	**4.701×10^{-3}**
ING4	**1.374**	**Up**	**3.315×10^{-3}**
TIMP3	**1.324**	**Up**	**9.632×10^{-3}**

(C)

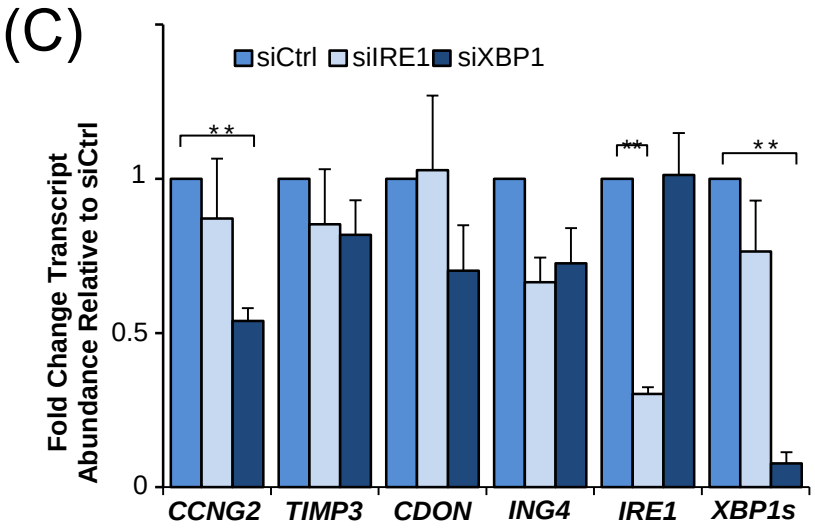

Figure 4.2. Identifying IRE1/RIDD Targets. (A) Pie-chart representation of overlapping genes of MKC8866 treated MDA-MB-231 cells (MKC8866, blue), mRNA cleaved in *in vitro* cleavage assay (In Vitro Cleaved, yellow), transcripts with IRE1 consensus cleavage sites (consensus site, green). (B) Table of potential IRE1 targets identified in microarray. (C) MDA-MB-231 cells were treated for 48 h with siRNA targeting IRE1 and XBP1 and levels of indicated transcripts were analysed by qPCR. Values shown represent the mean result of at least 3 independent repeats ± SEM, P* <0.05, P** <0.001. Student's t-test.

4.4 Identification of JUP as a potential IRE1 Target

JUP levels were significantly upregulated in response to IRE1 KD (Fig 4.3A), and were upregulated to a lesser extent by XBP1 KD as assessed by qPCR (table 2.1) (Fig 4.3B), though not significantly. This suggested that *JUP* may be regulated by both IRE1/RIDD and IRE1/XBP1s. Next we wanted to determine whether KD of IRE1 and XBP1 led to changes in JUP protein level, so we knocked down IRE1 and XBP1 using siRNA and analysed JUP protein levels by western blot (table 2.3, 2.4) (Fig 4.3C,D). We found JUP protein to be upregulated by both IRE1 and XBP1 KD, though only the result with IRE1 KD was significant. KD of XBP1 actually yielded a greater increase in JUP protein levels than IRE1 KD but was insignificant to having a higher variation across repeats. This again suggested that JUP might be regulated by both IRE1/RIDD and IRE1/XBP1.

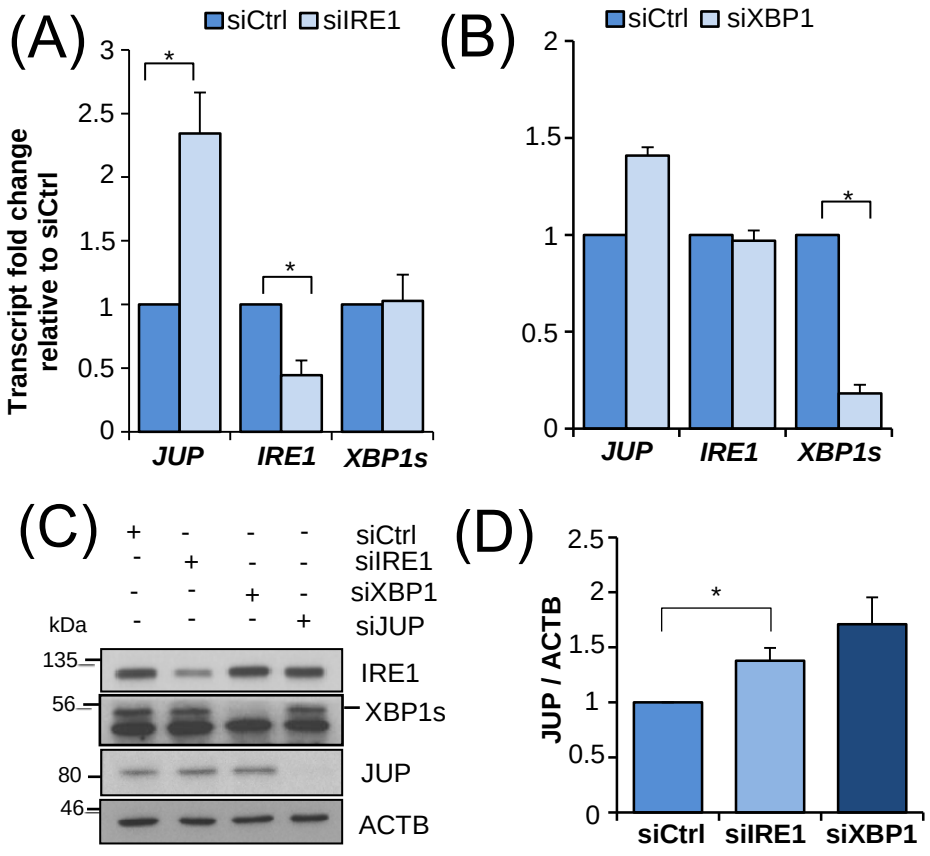

Figure 4.3. Identification of JUP as a potential IRE1 Target. MDA-MB-231 cells were treated with siRNA targeting IRE1 (A) and XBP1 (B) and levels of *JUP* mRNA were analysed by qPCR. (C) MDA-MB-231 cells were treated with siRNA targeting IRE1, XBP1, and JUP, and levels of JUP protein were analysed by western blot and quantified using densitometry (D). Values shown represent the mean result of at least 3 independent repeats ± SEM, P* <0.05, P** <0.001. Student's t-test.

4.5 Investigating XBP1s as a regulator of JUP

Since KD of XBP1 led to an elevation of *JUP* mRNA and protein, we wanted to investigate the mechanism behind this. We thought the most likely explanation would be that XBP1s was driving the expression of a miRNA which represses JUP expression. To explore this possibility we compared three datasets. 1. miRNA predicted to bind to *JUP* mRNA (predicted using miRDB software) 2. miRNA downregulated in our microarray analysis (Chapter III) 3. miRNA potentially regulated by XBP1s (Fig 4.4A). There were no miRNA common to all three datasets and thus no obvious target. However, we did identify miR98/Let7F as a potential XBP1s target that could potentially bind to *JUP* mRNA. Using ProScan software we found three XBP1 binding sites in the promoter miR98/Let7F (Fig 4.4B). Next we knocked down IRE1 and XBP1 and checked levels of miR98/Let7F and miR181 (a target from our MicroArray). miR181 was significantly downregulated by IRE1 KD but not by XBP1 KD as assessed by qPCR (table 2.1) (Fig 4.4C). Levels of miR98/Let7F did not significantly change under either condition as assessed by qPCR (table 2.1) (Fig 4.4D). Since our results did not indicate a clear role for XBP1s in this model we discontinued this line of inquiry.

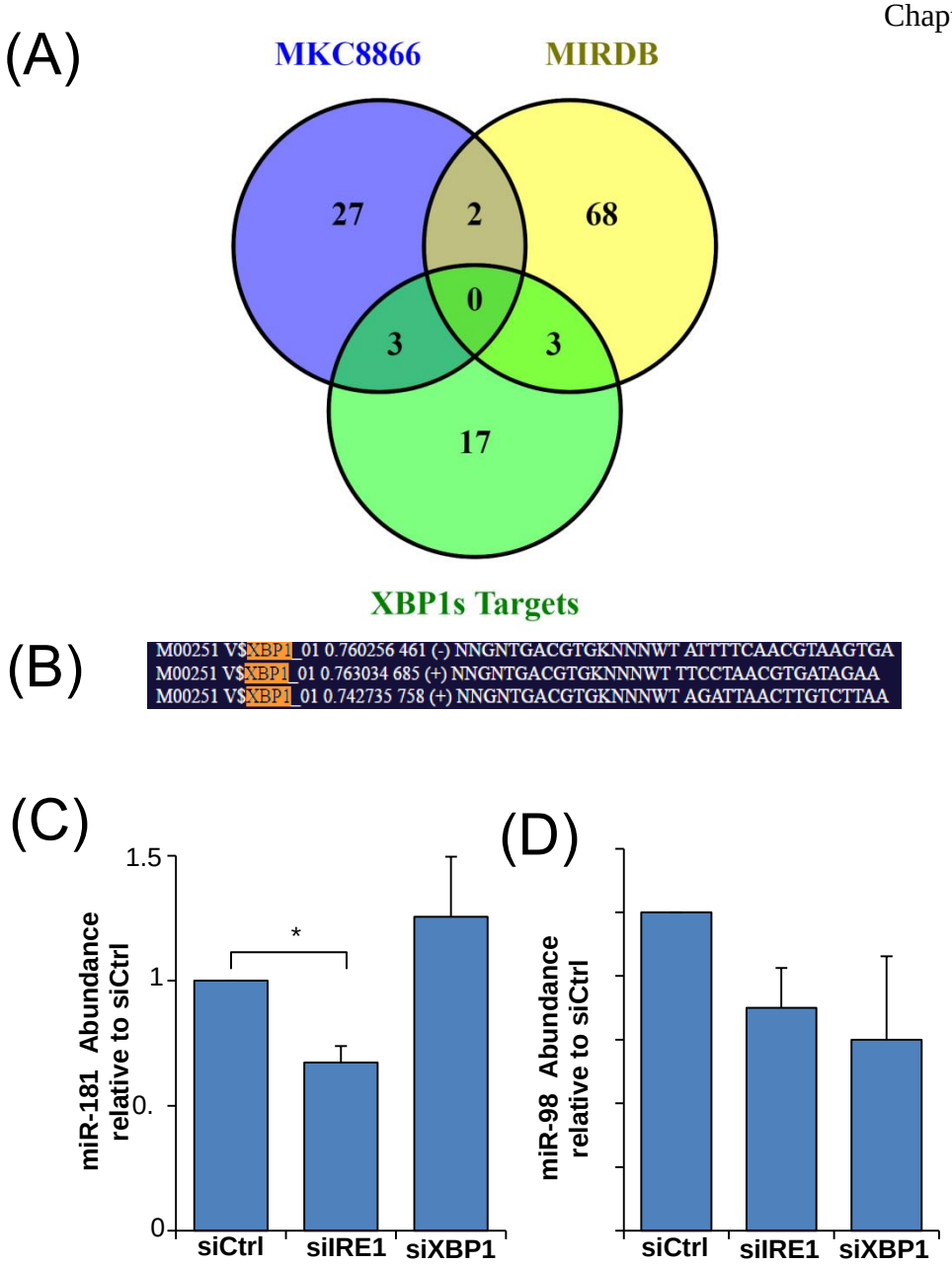

Figure 4.4. Investigating XBP1s as a regulator of JUP. (A) Pie-chart representation of overlapping genes of miRNA predicted to bind to *JUP* mRNA (miRDB, yellow), miRNA promoted by XBP1s (XBP1s Targets, green), miRNA downregulated in microarray analysis (MKC8866), blue). (B) ProScan analysis of XBP1 binding sites in miR98/Let7F promoter. MDA-MB-231 cells were treated with siRNA targeting IRE1 and XBP1 and levels of miR181 (C) and miR98/Let7F (D) were analysed by qPCR. Values shown represent the mean result of at least 2 independent repeats ± SEM, P* <0.05. Student's t-test.

4.6 IRE1 RNase inhibition does not change levels of *JUP* regulator SNAI2

JUP has previously been reported to be repressed by snail family transcriptional repressor 2 (SNAI2) in TNBC cells.[221] To rule out the effect of SNAI2 in our system we treated MDA-MB-231 cells for 24 h with MKC8866 and examined *SNAI2* levels using qPCR (table 2.1) (Fig 4.5). We found that *SNAI2* levels do not change with IRE1 RNase inhibition, suggesting that the regulation of JUP by IRE1 is not through a change in *SNAI2* levels.

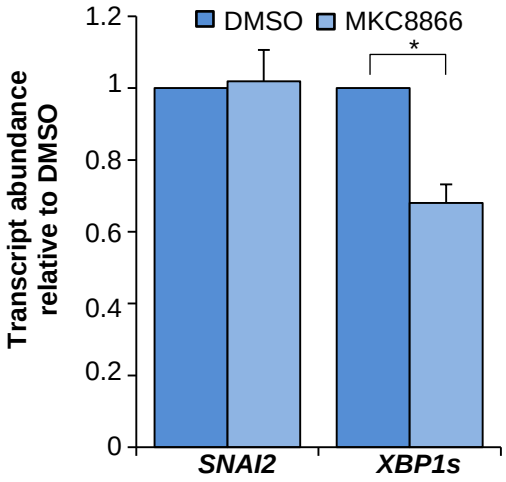

Figure 4.5 IRE1 RNase inhibition does not change levels of JUP regulator *SNAI2*. MDA-MB-231 cells were treated with MKC8866 (20 μM) 24 h and levels of *SNAI2*, *XBP1*s were analysed by qPCR. Values shown represent the mean result of at least 3 independent repeats ± SEM, P* <0.05. Student's t-test.

4.7 *JUP* mRNA is cleaved by IRE1

Since *JUP* had already been reported as a direct target of the IRE1 RNase domain[134] we thought this to be the simplest explanation as to why IRE1 RNase inhibition leads to *JUP* upregulation. It has been reported that IRE1 consensus cleavage sites must exist at stem-loop structures for IRE1 to cleave a given transcript[73]. Prediction analysis of the secondary structure of *JUP* mRNA using m-fold software revealed that two consensus cleavage sites exist on stem loop structures in exon 3 and exon 5 (Fig 4.6A). A high abundance of guanine and cytosine in the stems of these loops added confidence to the prediction. As a positive control, m-fold with the same settings was able to predict the confirmed IRE1 cleavage sites in *XBP1* mRNA. To confirm if *JUP* could be cleaved by IRE1 we performed an *in vitro* cleavage assay in which we incubated total RNA from MCF7 cells with recombinant IRE1 (rIRE1) and then performed RT-PCR using primers flanking the putative cleavage sites (table 2.2 (Fig 4.6B). We found that incubating RNA with rIRE1 led to depletion of *JUP* and that is effect was rescued by adding MKC8866. This suggested that *JUP* could be directly cleaved by IRE1.

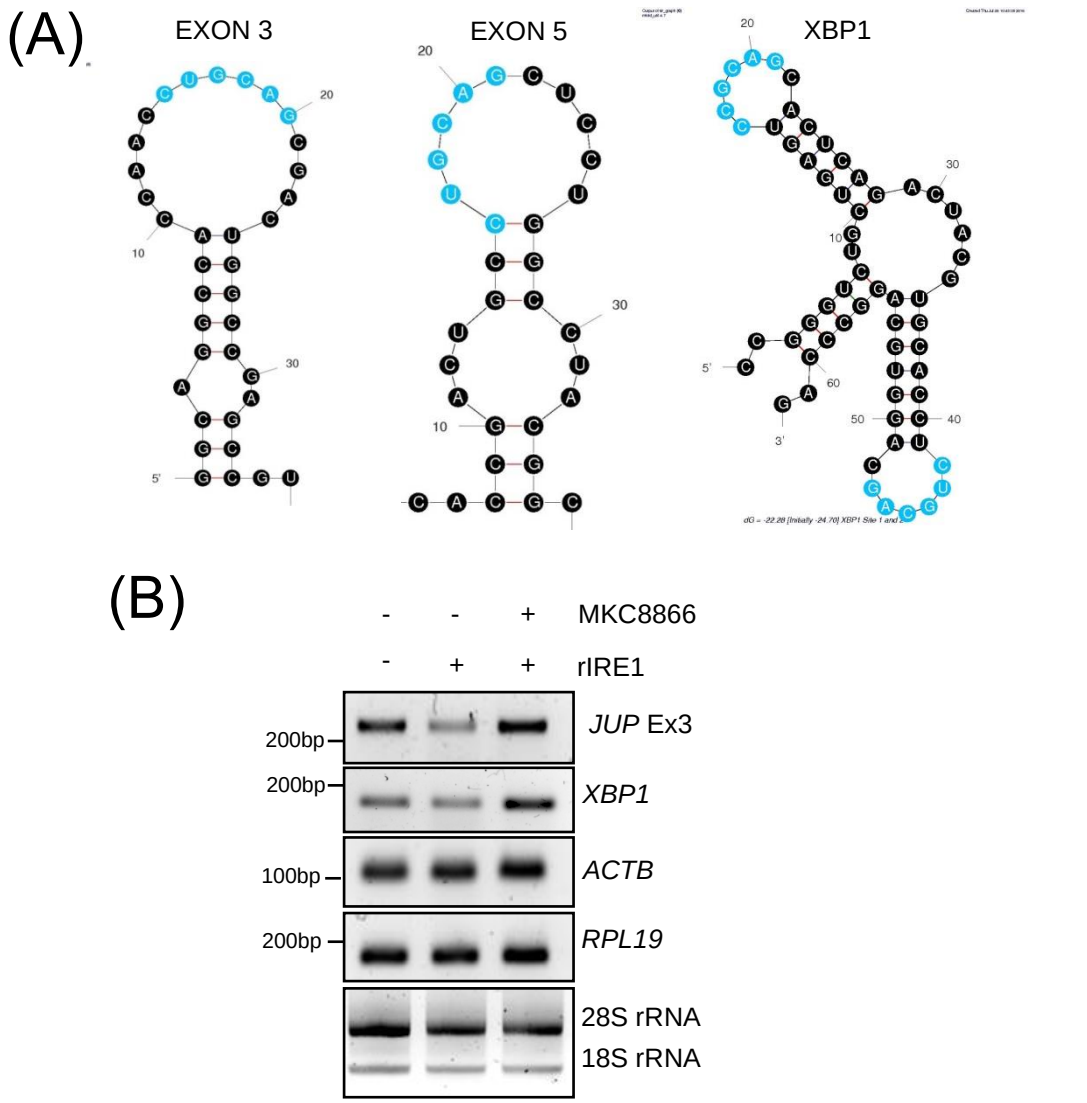

Figure 4.6. *JUP* mRNA is cleaved by IRE1. (A) m-fold software analysis of secondary RNA structure at IRE1 cleavage sites in *JUP* mRNA Exon 3, 5 and *XBP1* splice sites. (B) 5 µg of total RNA from confluent untreated MCF7 cells were incubated with recombinant IRE1 (2.25 µg/mL) with and without MKC8866 (20 µM) for 4 h at 37 °C. RNA was reverse transcribed and levels of indicated transcripts were analysed by RT-PCR (n = 2)

4.8 *JUP* mRNA is downregulated upon ER stress

Having determined that IRE1 can cleave *JUP* in a cell-free system we wanted to determine if IRE1 could cleave *JUP* in cells *in vitro*. To begin addressing this we treated MDA-MB-231 cells with DTT with and without MKC8866 an assessed *JUP* mRNA levels using PCR (table 2.2) (Fig 4.7A). We found that DTT induced depletion of *JUP* mRNA at 4 h and 8 h suggesting that ER stress induced depletion of *JUP*. Moreover, the addition of MKC8866 blocked the depletion of *JUP*, suggesting that the DTT-induced depletion was dependent on IRE1 RNase activity. This suggested that IRE1 can cleave *JUP* in cells. To determine that this was not a DTT-specific effect we treated cells with Tm and found that *JUP* mRNA was depleted using PCR (table 2.2) (Fig 4.7B). See figure 3.1 for explanation of how to interpret *XBP1* PCR results.

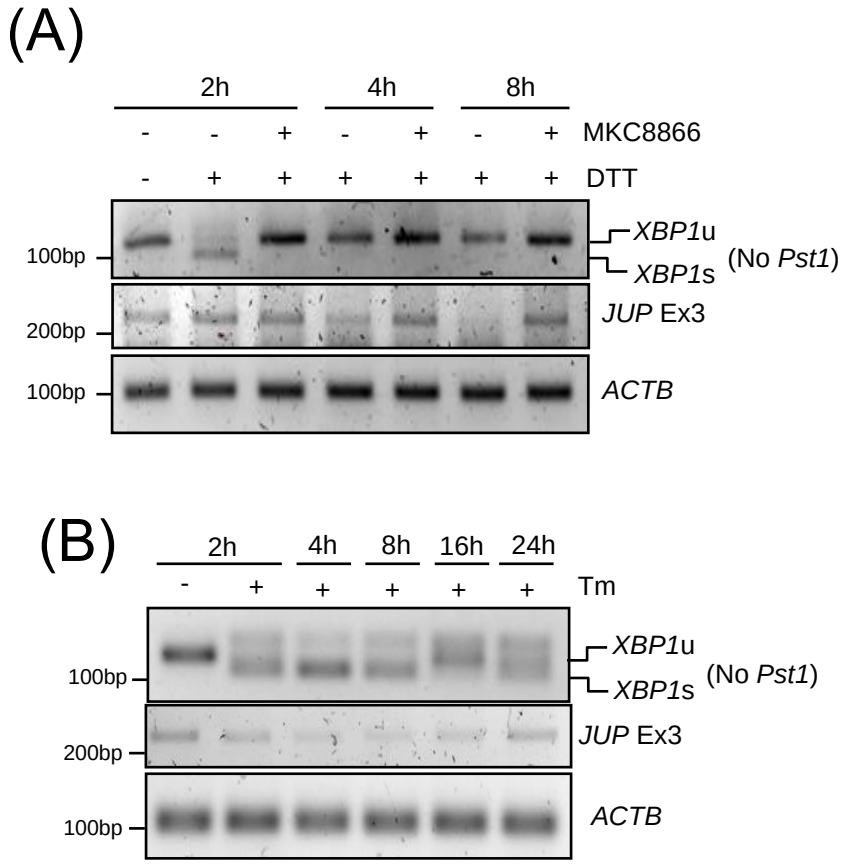

Figure 4.7. *JUP* mRNA is downregulated upon ER stress. MDA-MB-231 cells were treated with (A) DTT (1 mM) ± MKC8866 (20 μM) and (B) Tm (1 μg/mL) for indicated times after which RNA was extracted and levels of indicated transcripts were analysed by RT-PCR. (n = 2)

4.9 *JUP* is downregulated in basal-like breast cancers

To determine if there was an inverse correlation between *XBP1* splicing and *JUP* mRNA levels in breast cancer cells we analysed *JUP* mRNA levels using cDNA from Fig 3.1A and PCR (table 2.2). We found that *JUP* was lowest in TNBC cells where we had previously found that *XBP1*s levels were highest (Fig 4.8A). To determine if the same observation held true in patient samples we analysed *JUP* mRNA levels in 595 breast cancer patients from The Cancer Genome Atlas (TCGA) database. We found that there was significantly lower *JUP* mRNA levels in basal-like cancers when compared to TAN, luminal A, and HER2+ breast cancers (Fig. 4.8B). This suggested that cancers with higher *XBP1* splicing had lower levels of *JUP* mRNA. See figure 3.1C for explanation of *XBP1* PCR products.

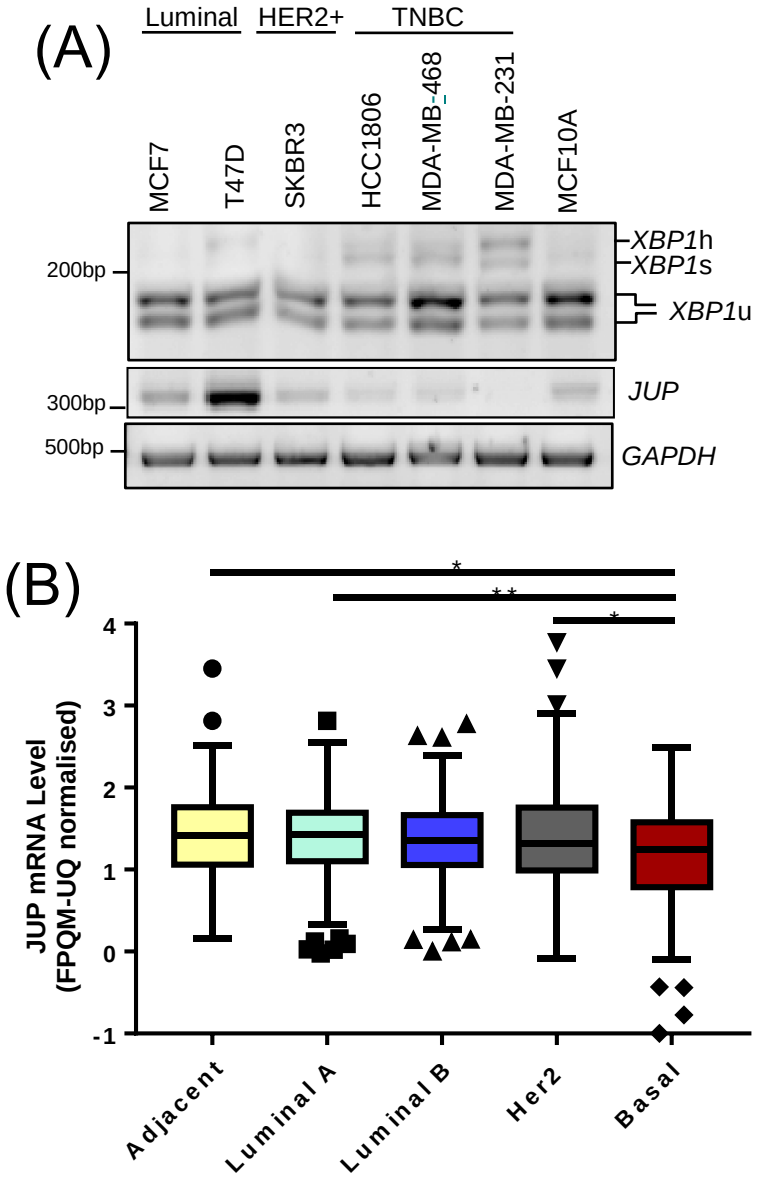

Figure 4.8. *JUP* mRNA is downregulated in basal-like breast cancers. (A) Indicated breast cell lines were allowed to come to 80% confluence over 48h. RNA was extracted from cells and indicated transcripts were amplified via RT-PCR. *XBP1* PCR products were digested using *Pst1* restriction enzyme before electrophoresis. (B) *JUP* mRNA levels plotted against breast cancer subtype in a TCGA cohort of 595 breast cancer patients. Dots represent individual patients. Box plots show the media 25th and 75th percentile. P* <0.05, P** <0.001. ANOVA multiple comparison analysis.

4.10 The IRE1 RNase domain promotes migration of TNBC cells

Having determined that the IRE1 RNase domain was capable of cleaving *JUP* mRNA and that knockdown of IRE1 could increase the levels of *JUP* mRNA and protein, we set about determining whether this had any bearing on cell migration. To answer this question we treated MDA-MB-231 cells with MKC8866 for 48 h and then assayed their migratory capacity using wound healing assays (Fig 4.9A) and transwell migration assays (aka boyden chamber assays) (Fig 4.9C). We found that IRE1 RNase inhibition significantly reduced the migratory capacity of MDA-MB-231 cells in both assays. We counted cells in the wells of the wound healing assay to determine if the effect was due to proliferation and found no significant differences in cell number between the two conditions (Fig 4.9B) After the treatment, but before seeding for transwell migration, we harvested some of the cells and checked *JUP* mRNA (using PCR (table 2.2)) and protein levels (using western blot (table 2.3, 2.4)) in MKC8866 treated and untreated cells. We found that *JUP* levels were increased at both mRNA (Fig 4.9D) and protein (Fig 4.9E) levels in the cells treated with MKC8866. Next we knocked down IRE1 using siRNA and assayed transwell migration (Fig 4.9F). We found that depletion of IRE1 led to a further reduction in the migratory capacity of breast cancer cells compared to MKC8866. Together these results showed that IRE1 RNase inhibition represses the migratory capacity of TNBC cells and causes a correlative increase in *JUP* mRNA and protein levels.

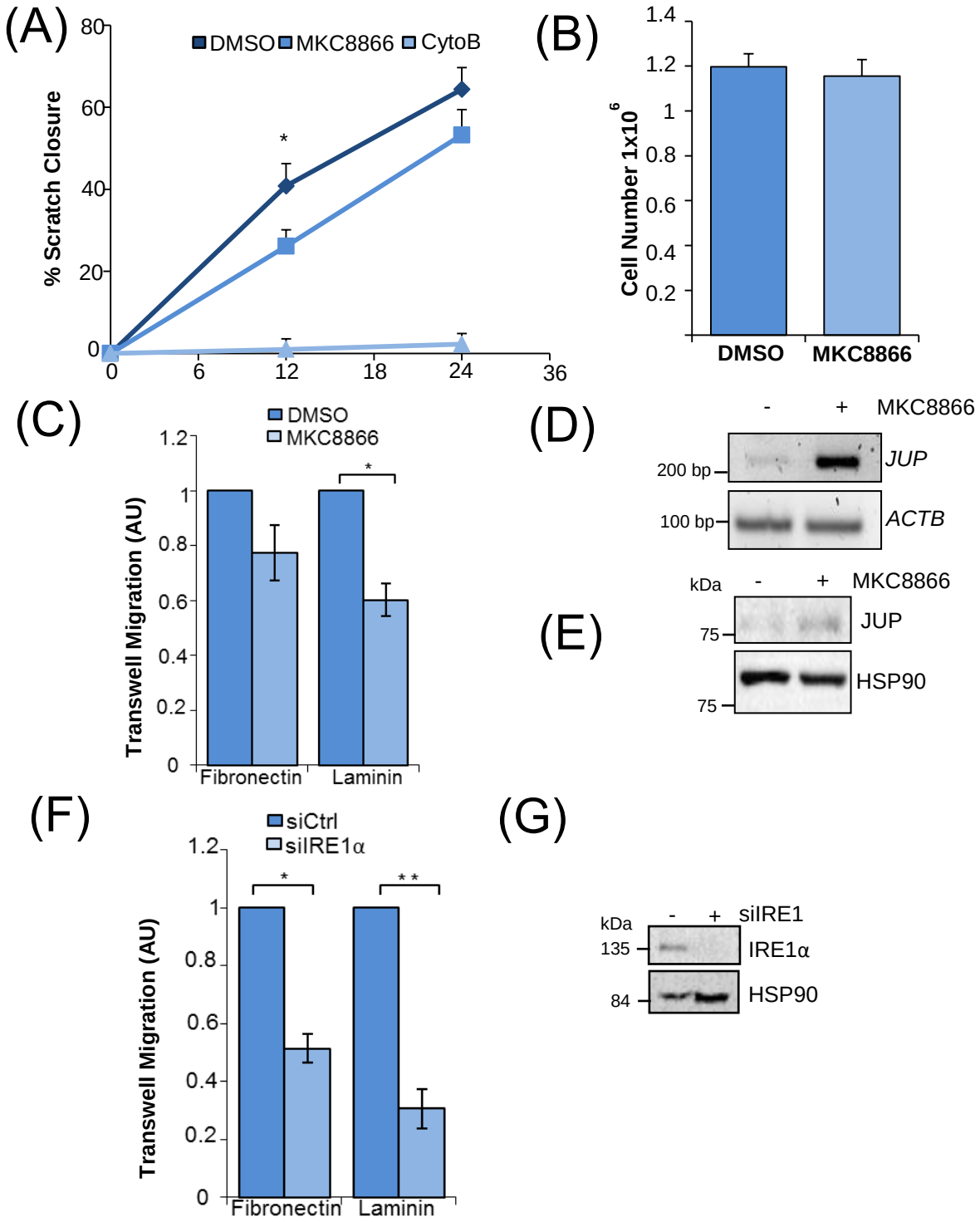

Figure 4.9. IRE1 RNase domain regulates migration in TNBC cells. MDA-MB-231 cells were treated with DMSO or MKC8866 (20 μM) for 48 h and their migratory capacity was analysed by (A-B) wound-healing assay, (C) transwell migration assay. (B) Following the wound-healing assay cell were counted using a haemocytometer. Following treatment but before seeding for migration assays cells were harvested and levels of indicated transcripts were analysed by (D) RT-PCR, and indicated proteins analysed by (E) western blot. (F) MDA-MB-231 cells were treated with siRNA targeting IRE1 for 48 h and migratory capacity was determined by transwell migration assay. (G) KD of IRE1 was confirmed by western blot (table 2.3, 2.4) (n = 3). Values shown represent the mean result of at least 3 independent repeats unless otherwise indicated ± SEM, P* <0.05. Student's t-test.

4.11 Discussion

With the work in this chapter we sought to find a novel function for the IRE1 RNase domain. To address a large gap in our knowledge we investigated a specific role for IRE1/RIDD activity. Using an unbiased microarray approach and INGENUITY software we identified the IRE1 RNase domain as a potential regulator of cell migration in TNBC cells. Since we wanted to identify roles for RIDD, we focussed exclusively on genes which were upregulated in our dataset. We did this because genes which are being basally degraded by IRE1 should be upregulated when IRE1 RNase is inhibited. However, there may be two potential problems with this approach. Firstly, upregulation of a transcript after IRE1 RNase inhibition does not necessarily imply that it is a RIDD substrate. For example, it could be a target of a miRNA which is driven by XBP1s transcriptional activity.

Nevertheless, we identified several targets which were present in our dataset and at least one of the other datasets, including one target which was present in all three (*JUP*). We then sought to validate these targets using a genetic approach. To this end we knocked down IRE1 and XBP1 in MDA-MB-231 cells and found that most of them appeared to be false positives. Indeed, only *JUP* and *CCNG2* changed significantly under any of the conditions. Furthermore, *CCNG2* was downregulated with XBP1 KD while in the MicroArray data it was upregulated. Since XBP1s has been reported to bind to the promoter region of *CCNG2*[104] it seems logical that it should be downregulated with XBP1 KD and perhaps with IRE1 RNase inhibition too. However, there is a possibility that *CCNG2* is also a RIDD substrate since XBP1 depletion has been reported to induce RIDD. These discrepancies between the MicroArray results and the siRNA validation could be attributed to off-target effects of MKC8866. Another possibility is that inhibiting both XBP1 splicing and RIDD with MKC8866 causes effects distinct from those which might be observed if each process was targeted individually. Indeed, XBP1 depletion has been reported to induce RIDD activity[128]. Thus, a RIDD substrate that should be upregulated upon IRE1 RNase inhibition could become downregulated upon XBP1 KD and could be falsely interpreted as an XBP1s target. Furthermore, partial knockdown of proteins does not account for the possibility that the remaining protein which survives the KD may become more active through some compensatory mechanism. Thus, siRNA

mediated KD of XBP1 and IRE1 is not entirely adequate to control for the effects of MKC8866.

Nonetheless, our results appeared to indicate that *JUP* was regulated by IRE1 and perhaps to a lesser extent by XBP1. When we looked at the protein level we found that both IRE1 and XBP1 KD led to an increase of JUP protein, though the increase was only significant with the IRE1 KD. This result seemed logical since depletion of IRE1 and XBP1 had led to increases in *JUP* mRNA levels. However, it did not support the idea that the regulation of JUP was solely through RIDD, since RIDD substrates should become downregulated or perhaps not change at all when XBP1 is depleted.

Since our results indicated that JUP could be regulated through an XBP1 dependent mechanism we investigated if any miRNA driven by XBP1 could potentially target *JUP*. To address this, we compared miRNA predicted to bind to *JUP*, miRNA reported to be regulated by XBP1, and miRNA which were downregulated in our microarray. No miRNA were common to all groups.

JUP is reported to be repressed by SNAI2 in MDA-MB-231 cells[221]. Since SNAI2 promotes EMT it seems logical that it should suppress an epithelial marker such as JUP. To rule out a role for IRE1 in regulating JUP via SNAI2 we treated MDA-MB-231 cells with MKC8866 and found that levels of *SNAI2* did not change, suggesting that SNAI2 is not important in our model.

Next we assessed if *JUP* could be directly cleaved by IRE1. Using *in silico* predictions we found that two consensus IRE1 cleavage sites exist on stem-loop structures in exons 3 and 5 of *JUP* mRNA. The consensus cleavage sequence of IRE1 is CUGCAG. However, this sequence is not completely necessary in order for IRE1 to cleave mRNA. In fact, each of the bases at any position is dispensable[73]. However an exhaustive search for every possible permutation of the cleavage site seemed unnecessarily time-consuming since we directly assayed if *JUP* could be cleaved *in vitro*. Furthermore, only the cleavage site and fifteen bases up- and downstream were entered into the RNA folding software. Thus, allosteric effects of the larger RNA molecule are not taken into account. However, at the very least this result did suggest that IRE1 consensus sites could exist at stem-loop structures in

exons 3 and 5 and suggested that these were possible sites where *JUP* could be cleaved.

RIDD substrates should in theory be down regulated upon ER stress. We had already determined that *CD59* could be depleted by DTT treatment in Chapter III and we found that *JUP* behaved the same way with both DTT treatment and Tm. This downregulation of *JUP* by two different ER stressors, which induce accumulation of misfolded protein in different ways, suggests that the result is dependent on UPR activation. MKC8866 rescued depletion of *JUP* by DTT which suggested the depletion was dependent on IRE1 RNase domain. Moreover, *JUP* levels appeared to have an inverse correlation with *XBP1* splicing, suggesting that while IRE1 RNase is active it splices *XBP1* and depletes *JUP*, but that both of these processes are simultaneously switched off. More work is required to conclusively prove that *JUP* is a RIDD substrate in TNBC cells.

Since we ultimately wanted to show that IRE1 RNase was playing a role in cell migration it was important to determine whether inhibition of IRE1 could produce a change in migratory phenotype. We employed both wound healing assays and transwell migration assays. While both assays measure the ability of cells to move, they are quite different in some respects. The wound healing assay involves disruption of a monolayer of cells with a P200 tip, and is thus inherently more prone to variation than the transwell assay. Furthermore, cells at the boundary of the wound must respond to disturbances in cell-cell adhesion and presumably to damage associated molecular patterns. Furthermore, the wound healing assay can also be a measure of the ability of cells to break cell-cell contacts while the transwell measures only single cell migration. Both assays showed that IRE1 RNase inhibition led to decreased cell migration. Additionally, KD of IRE1 led to a further decrease in transwell migration compared to MKC8866 treatment. This additional decrease could be caused by IRE1 RNase-independent mechanisms. Recently IRE1 was found to be necessary for the phosphorylation of FLNA, a regulator of cell migration. KD of IRE1 could therefore reduce phosphorylation of FLNA and contribute to the reduction in cell migration independently of the RNase domain[131].

In this work we have discovered a new role for the IRE1 RNase in cell migration in TNBC. Since cell migration and metastasis contribute to patient mortality this is a

considerable finding which suggest that targeting the RNase domain could prevent metastasis. We do not know whether this effect is through a novel mechanism (i.e. IRE1/RIDD/*JUP*) or through previously described mechanisms such as regulation of SPARC in glioma[130]. Since SPARC does not appear as a hit in our MicroArray, this would suggest that it is not playing a role in our model. We can be quite confident that the mechanism behind the phenotype we are observing is distinct from the role played by IRE1 in regulating FLNA[131], since the process we describe appears to be RNase dependant. Furthermore when we KD IRE1 we get a further decrease in cell migration compared to MKC8866 alone, suggesting that RNase-dependant and –independent mechanisms are at work. Since SPARC and FLNA do not appear to be playing a role, and we have shown that IRE1 modulates levels of JUP this seems like the most likely mechanism behind the migration phenotype. Modulation of JUP levels has been shown elsewhere to affect migration of cancer cells. Depletion of JUP increases migration[211] and expression of JUP decreases migration[222]. Thus, it seems likely that the IRE1-dependent change we are observing in JUP levels is contributing, at least in part, to the observed migration phenotype.

However, if this observed phenotype is through the regulation of JUP, the results of targeting the IRE1 RNase domain may have undesirable effects on metastasis (see section 6.2).

4.12 Future Perspectives

The results we have obtained so far make us confident that *JUP* is a RIDD substrate in MDA-MB-231 cells. There are multiple reasons for this. Firstly, *JUP* is upregulated with MKC8866 treatment. Secondly, we and others[134] have shown that *JUP* mRNA is cleaved in a cell-free IRE1 RNase assay. Thirdly, *JUP* mRNA contains two consensus IRE1 cleavage sites present on stem-loop structures. Fourthly, *JUP* mRNA is upregulated to a far greater (and more significant) extent with IRE1 KD when compared with XBP1 KD. Fifthly, cells with high *XBP1* splicing have lower *JUP* mRNA. Finally, *JUP* is depleted under ER stress in an IRE1 RNase dependent manner. However, none of these results constitute proof that *JUP* is cleaved under basal conditions by IRE1 in MDA-MB-231 cells.

So far we have made two important findings. Firstly, IRE1 RNase causes basal depletion of *JUP* levels through RIDD. Secondly, IRE1 RNase inhibition reduces

TNBC cells migration and increases *JUP* mRNA and protein levels. The primary question that remains to be answered is; is the depletion of *JUP* by IRE1 *causing* an increased migratory phenotype in TNBC cells? One way this could be answered would be to knock out *JUP* in MDA-MB-231 cells using CRISPR-Cas 9 technology, and then reconstitute the cells with an unsplicable form of *JUP*. This unsplicable form of *JUP* would contain silent mutations at IRE1 consensus cleavage sites, so that protein structure would be identical to the WT JUP. Thus, if cells expressing an uncleavable *JUP* migrated less than cells expressing cleavable *JUP* it would constitute direct proof that IRE1-mediated degradation by *JUP* is responsible for the increased migration of TNBC cells. To bolster this result, the same knockout and reconstitution could be performed in mouse breast cancer cell lines and syngeneic *in vivo* experiments could be performed. Furthermore, the altered cells would be labelled with GFP to allow them to be tracked *in vivo*. This experiment would allow us to answer the question in a more clinically relevant way, since it could illuminate the apparent discrepancies in the role JUP plays in metastasis. It would let us know whether it is desirable to block IRE1-mediated depletion of *JUP* or whether this process should be allowed to persist in breast cancer cells. Thus, this experiment would have a direct bearing on how we think about targeting IRE1 RNase in the clinic (see section 6.2).

This experiment would necessitate the identification of all of the consensus cleavage sites in *JUP* mRNA. To do this *JUP* mRNA would be transcribed *in vitro* and a cleavage assay would be performed and RNA fragments run on a gel. The size of the fragments would give an indication of the location of the cleavage sites which could be cross-checked *in silico.* All cleavage sites would need to be subsequently validated using the *in vitro* cleavage assay before we could proceed with the *in vivo* work.

Since we identify in Chapter V that chemotherapeutics can induce *XBP1* splicing it would be interesting to see if RIDD-mediated degradation of *JUP* is also induced by chemotherapy. The role of JUP in metastasis remains somewhat ambiguous so if it is depleted by chemotherapy it is not clear how this would affect cell migration and metastasis. JUP aside, induction of RIDD by chemotherapies has not been reported elsewhere and would be an important discovery for the field.

Chapter V: IRE1 promotes cytokine production, stem cell maintenance, and therapy resistance in TNBC

5.0 Contributions

The work in this chapter is part of a manuscript published in the journal *Nature Communications* in August 2018.

Susan E Logue, Eoghan P McGrath, Patricia Cleary, Stephanie Greene, Katarzyna Mnich, Aitor Almanza, Eric Chevet, Róisín M Dwyer, Anup Oommen, Patrick Legembre, Florence Godey, Emma C Madden, Brian Leuzzi, Joanna Obacz, Qingping Zeng, John B Patterson, Richard Jäger, Adrienne M Gorman and Afshin Samali . Inhibition of IRE1 RNase activity modulates the tumor cell secretome and enhances response to chemotherapy. *Nature communications* **9**, 3267, doi:10.1038/s41467-018-05763-8 (2018).

The contributions to the experimental results are as follows:

Fig. 5.3 S.L. P.C.

Fig. 5.4 S.L.

Fig. 5.5 S.L.

Fig. 5.6 (E)(F) S.L.

Fig. 5.7 S.G.

5.1 Introduction and Research Rationale

Therapy resistance is a primary clinical challenge faced by the cancer field, and accounts for the dismal survival statistics of recurrent breast cancer patients. Recent reports have indicated that IRE1 RNase activity confers TNBC cells with a survival advantage both under hypoxic conditions and when TNBC cells are challenged with chemotherapeutics[104,182]. The mechanism through which IRE1 RNase promotes resistance to hypoxic environments was well characterised, though not fully elucidated, in 2014[104]. However, the mechanism of resistance to chemotherapeutics downstream of IRE1 was not extensively explored[104]. Given the importance of drug resistance to the clinic, this gap in our knowledge provided fertile ground for further exploration into the role of IRE1 RNase in TNBC.

5.1.1 Cancer Stem Cells & Therapy-induced Secretome

Cancer stem cells (CSCs), as the name suggests, are progenitor cells for tumours. CSCs possess enhanced plasticity, which allows them to acquire resistance to drugs and facilitate tumour recurrence. Since tumour recurrence is usually fatal in breast cancer, understanding the mechanisms which control the stem-cell like phenotype has become a large focus for the cancer field. The UPR and in particular IRE1/XBP1 has previously been implicated in the maintenance of CSC populations. Chen *et al* demonstrated that XBP1 is a regulator of $CD44^{high}/CD24^{low}$ populations within TNBC, though the mechanism was not fully explored[104].

The concept of a treatment-induced secretome which promotes tumour growth and drug resistance was well characterised by Obenauf *et al* in 2015[223]. This paper described how non-resistant tumour cells undergoing treatment can release a plethora of soluble factors which potentiates the growth of resistant cells[223]. Other reports have shown that TNBC cells challenged with paclitaxel produce and secrete IL6, IL8 and TGFβ. Secretion of these factors promoted a stem cell-like phenotype and therapy resistance, but were not linked to the UPR[224,225]. TERS, outlined in the introduction, is a phenomenon first described in 2011 wherein conditioned media from cells challenged with ER stress was able to induce an ER stress response in previously untreated cells. The UPR has been reported to be important for the production and secretion of multiple inflammatory factors such as IL6 and IL8 and for the function and maturation of immune cells which exhibit a high secretory output[197].

5.1.2 Rationale

Taking all of these reports together, there appears to be a link between chemotherapy, the UPR, secretion of soluble factors, CSCs, and therapy resistance. Thus, results from our microarray analysis described in chapter III could reveal IRE1 RNase targets which provide insight into a mechanism which unites these aspects of TNBC biology and shed light on molecular mechanisms of therapy resistance in TNBC.

5.2 Pro-inflammatory Cytokine downregulated upon IRE1 RNase Inhibition

After analysing the microarray results from Chapter III, we found that a subset of pro-inflammatory cytokines, *IL8*, *IL6*, *TGFβ2*, and *GMCSF* were downregulated with IRE1 RNase inhibition (Fig 5.1A). Since *IL8* and *IL6* have been reported elsewhere to be direct transcriptional targets of XBP1s[59], we had confidence in this result, but to confirm the results we treated MDA-MB-231 cells for 48 h with MKC8866 and examined the transcript levels of each gene using qPCR (table 2.1). All genes were significantly downregulated with MKC8866 treatment, confirming the MicroArray result. Another cytokine, *CXCL1*, was identified in a cytokine profiling screen with a similar experimental design (outlined in PhD thesis by Patricia Cleary (Titled: Investigation of IRE1/XBP1s pathway and its potential as a therapeutic target in breast cancer)) and in Logue *et al* 2018[51] and was included as another potentially novel IRE1 RNase target and was also found to be downregulated at the transcriptional level upon MKC8866 treatment (Fig 5.1B).

(A)

Gene	Fold Change	Regulation	p-value
IL8	**2.25**	**Down**	**0.018**
IL6	**1.31**	**Down**	**0.0059**
TGFB2	**1.31**	**Down**	**0.033**
GMCSF	**1.37**	**Down**	**0.034**

(B)

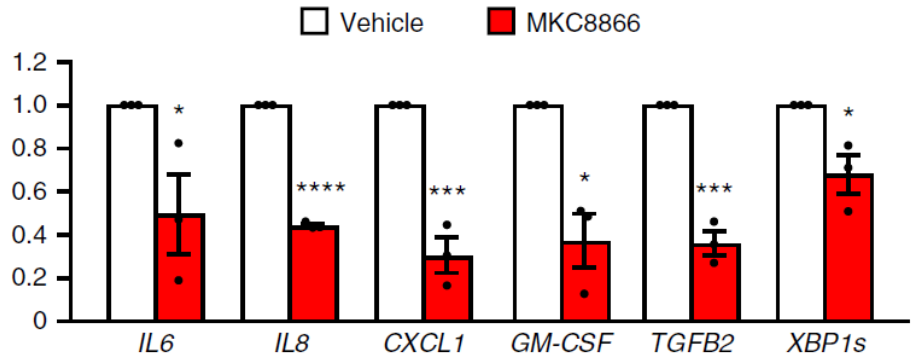

Figure 5.1. Pro-inflammatory Cytokines downregulated upon IRE1 RNase Inhibition. (A) MDA-MB-231 cells were treated as outlined in Chapter III and RNA was sent for MicroArray Analysis and analysed as described in Chapter III. MDA-MB-231 cells were treated for 48 h with MKC8866 (20 μM) after which transcript levels of *IL6*, *IL8*, *CXCL1*, *GMCSF*, *TGFβ2*, and XBP1s were analysed. Values shown represent the mean result of at least 3 independent repeats ± SEM, P* <0.05, P** <0.001, P*** <0.0001, P**** <0.00001 Student's t-test

5.3 siRNA-mediated KD of IRE1 and XBP1 reduce levels of pro-inflammatory cytokines

To determine if the results we saw were due to IRE1 RNase inhibition and not to an off-target effect we knocked down IRE1 and XBP1 and performed qPCR (table 2.1) to check transcript levels. Levels of *IL6*, *IL8*, *CXCL1*, *and GMCSF* mRNA were all reduced upon both IRE1 and XBP1 knockdown whereas *TGFβ2* levels were reduced but not significantly (Fig 5.2). This suggested that *IL6*, *IL8*, *CXCL1*, and *GMCSF* were targets of the IRE1 RNase.

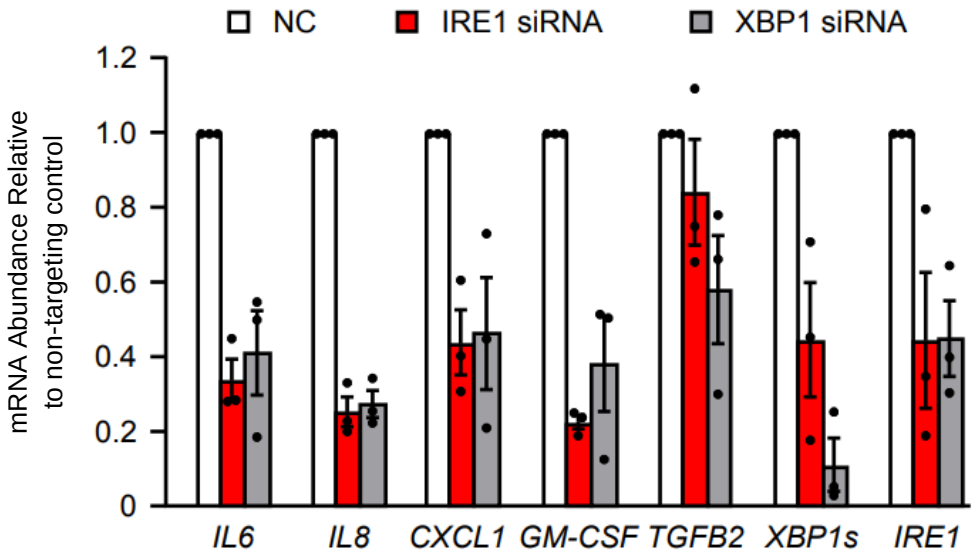

Figure 5.2. siRNA-mediated knockdown of IRE1 and XBP1 reduces levels of pro-inflammatory cytokines (A) MDA-MB-231 cells were transfected with 25 nM Ctrl siRNA, siRNA vs IRE1 and siRNA vs XBP1 for 72 h in medium containing 2% FBS. Transcript abundance of *IL6*, *IL8*, *CXCL1*, *GMCSF*, *TGFB2*, *XBP1*s, and *IRE1* was determined by qPCR. *GAPDH* was used as the endogenous control gene. Values shown represent the mean result of at least 3 independent repeats ± SEM, P* <0.05, P** <0.001, P*** <0.0001, P**** <0.00001 Student's t-test

5.4 IRE1 RNase inhibition decreases the abundance of cytokines in the supernatant of MDA-MB-231 cells

To determine whether regulation at the transcript level yielded changes in the abundance of secreted cytokines, MDA-MB-231 cells were treated with MKC8866 in 2% serum for 48 h after which supernatant was harvested and subjected to ELISA. IRE1 RNase inhibition led to significant decreases in the abundance of IL-6 (Fig 5.3A), IL8 (Fig 5.3B), CXCL1 (Fig 5.3C), GMCSF (Fig 5.3D), and TGFβ2 (Fig 5.3E) in the supernatant of MDA-MB-231 cells. To rule out a cell-type specific effect we tested the ability of IRE1 RNase inhibition to reduce CXCL1 levels in three other TNBC cell lines; HCC1806 (Fig 5.3F), BT549 (Fig 5.3G), and MDA-MB-468 (Fig 5.3H). MKC8866 reduced the abundance of CXCL1 in the media of all three cell lines, suggesting that this phenomenon is not specific to MDA-MB-231 cells.

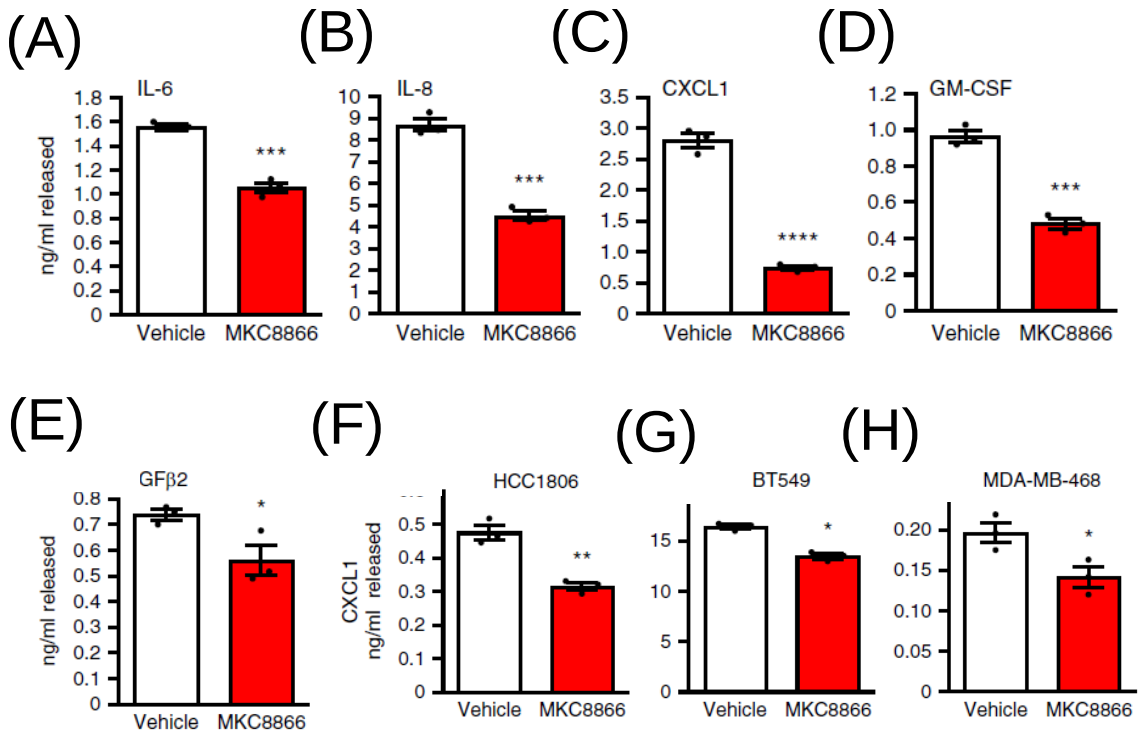

Figure 5.3. IRE1 regulates the abundance of cytokines the in supernatant of breast cancer cells. Cell supernatant was harvested from MDA-MB-231 cells cultured in media containing 2% FBS in the presence of DMSO or 20 μM MKC8866 for 48 h. Cytokine secretion was quantified in cell supernatant using ELISAs selective for IL-6 (A), IL-8 (B), CXCL1 (C) and GM-CSF (D), and TGFβ2 (E). HCC1806 (F), BT549 (G), and MDA-MB-468 (H) cells were cultured as above and levels of CXCL1 in the supernatant was analysed by ELISA. Values shown represent the mean result of at least 3 independent repeats ± SEM, P* <0.05, P** <0.001, P*** <0.0001, P**** <0.00001 Student's t-test.

5.5 siRNA-mediated KD of IRE1 reduces cytokine secretion

To confirm that the reduction in the abundance of cytokines was not an off-target effect of MKC8866 we knocked down IRE1 using siRNA and assessed cytokine levels by qPCR (table 2.1). As expected IRE1 KD reduced levels of IL6 (Fig 5.4A), IL8 (Fig 5.4B), CXCL1 (Fig 5.4C), and GMCSF (Fig 5.4D) in the supernatant of cells, suggesting these factors are genuine IRE1 targets. KD of IRE1 did not deplete TGFβ2 levels to the same extent as MKC8866. To determine whether reduction of TGFβ2 by IRE1 was an off-target effect we co-treated cells with IRE1 KD and MKC8866. When IRE1 was knocked down MKC8866 did not deplete TGFβ2 levels (Fig 5.4E), suggesting that MKC8866 requires IRE1 to downregulate TGFβ2, and thus depletion of TGFβ2 was not an off-target effect. It is possible that depletion of IRE1 triggers a compensatory increase in TGFβ2 levels through an IRE1-independent mechanism. Knockdown of IRE1 was confirmed with western blot (Fig 5.4F).

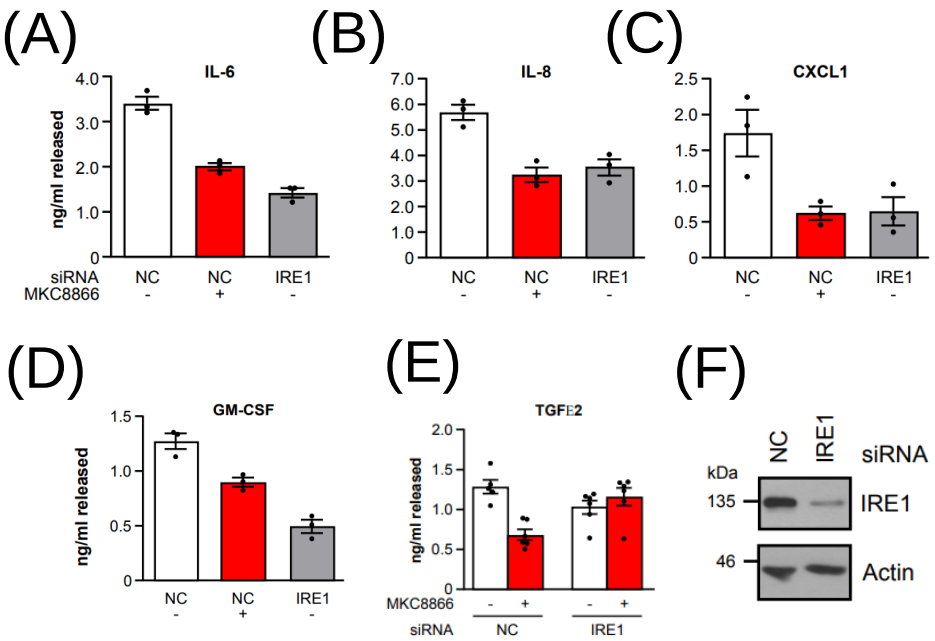

Figure 5.4. siRNA-mediated KD of IRE1 reduces cytokine secretion. (A) MDA-MB-231 cells were transfected with 25 nM non-coding or IRE1 targeting siRNA. Following 72 h knockdown, cell lysates were immunoblotted for IRE1 and Actin. The supernatant was collected from MDA-MB-231 cells following 72 h knockdown with 25 nM non-coding siRNA, 25 nM non-coding siRNA plus 20 μM MKC8866, 25 nM IRE1 targeting siRNA and analysed by ELISA for IL-6 (A), IL-8 (B), CXCL1 (C) and GM-CSF (D) and TGFβ2 (E).IRE1 KD was confirmed by western blot (F). Values shown represent the mean result of at least 3 independent repeats ± SEM, P* <0.05, P** <0.001, P*** <0.0001, P**** <0.00001 Student's t-test.

5.6 Paclitaxel induces IRE1 RNase-dependent cytokine secretion

Since IRE1 RNase seems to regulate pro-inflammatory cytokines which have been linked to CSC maintenance, and XBP1 mediates paclitaxel resistance in TNBC, we wanted to see was there a mechanism through which IRE1 RNase could drive paclitaxel resistance through regulation of cytokine production and secretion. To start, we tested whether paclitaxel could induce IRE1 RNase activity. Treatment of MDA-MB-231 cells with paclitaxel led to a time-dependent increase in the abundance of XBP1s protein (Fig 5.5A) which we could block by co-treatment with MKC8866 (Fig 5.5B) as assessed by western blot (table 2.3,2.4). This suggested that a low, clinically relevant dose[71] of paclitaxel induces IRE1 RNase activity. Next, we checked whether paclitaxel could trigger IRE1 RNase-dependant secretion of IL6 (Fig 5.5C), IL8 (Fig 5.5D), CXCL1 (Fig 5.5E), GMCSF (Fig 5.5F). Paclitaxel increased the secretion of IL8 and CXCL1 in MDA-MB-231 cells. Co-administration of MKC8866 led to a significant reduction in the levels of IL8 and CXCL1, suggesting that paclitaxel-induced cytokine secretion is partly dependant on IRE1 RNase activity, particularly in the case of IL8 and CXCL1.

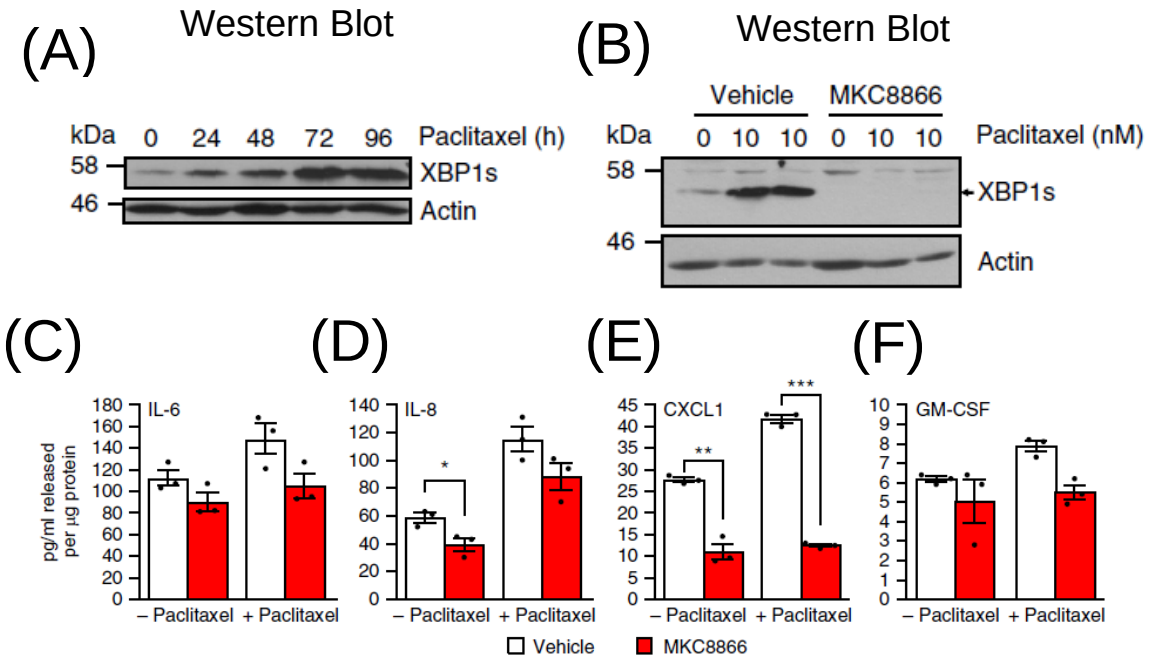

Figure 5.5. Paclitaxel-induced IRE1 RNase–dependent cytokine secretion. (A) MDA-MB-231 cells were treated with 10 nM paclitaxel for the indicated times, cell lysates were immunoblotted for XBP1s and ACTB. (B) MDA-MB-231 cells were treated with 10 nM paclitaxel in the presence of 20 μM MKC8866 or DMSO for 72 h, cell lysates were immunoblotted for XBP1s and ACTB. Results are representative of at least 3 independent experiments. MDA-MB-231 cells were treated with 10 nM paclitaxel in combination with DMSO or 20 μM MKC8866 for 72 h in the presence of Boc.D.fmk (40 μM). Following treatment cells were lysed, protein quantified and the supernatant analysed by ELISA for secretion of IL-6 (C), IL-8 (D), CXCL1 (E) and GM-CSF (F). Values shown represent the mean result of at least 3 independent repeats ± SEM, P* <0.05, P** <0.001, P*** <0.0001, P**** <0.00001

5.7 IRE1 RNase regulates paclitaxel-induced mammosphere formation

Having established that IRE1 RNase activity was activated by paclitaxel and that this led to the secretion of inflammatory factors associated with maintenance of cancer stem cell populations, we wanted to establish if paclitaxel could induce increased mammosphere formation and if IRE1 RNase inhibition could prevent it.

To answer if paclitaxel could trigger and IRE1 RNase-dependent increase in mammosphere formation efficiency, we treated MDA-MB-231 cells for 72 h with 10 nM paclitaxel, washed the cells and added media containing either DMSO or MKC8866, after which cells were allowed to recover for a further 72 h. After this recovery period cells were plated for mammosphere formation over 5 days. We found that paclitaxel robustly induced the formation of mammospheres and that addition of MKC8866 during the recovery phase significantly reduced mammosphere forming efficiency, though the inhibition was not complete (Fig 5.6A).

To determine whether the production and secretion of cytokines was linked to this phenotype we harvested conditioned media after the recovery period and performed ELISA for CXCL1, IL8, IL6, TGFβ2, and GM-CSF (Fig 5.6B). We found that only CXCL1 and IL8 levels were significantly reduced in the supernatant of cells which received MKC8866 during the recovery period. To determine whether CXCL1 and IL8 were playing a functional role in the maintenance of mammosphere forming efficiency we added neutralizing antibodies against CXCL1 and IL8 during the

recovery period (Fig 5.6C). Neutralisation of CXCL1 or IL8 significantly reduced the mammosphere forming efficiency of MDA-MB-231 cells, to roughly the same levels of MKC8866. Depletion of CXCL1 (Fig 5.6E) and IL8 (Fig 5.6F) from the media was confirmed by ELISA.

To confirm the link between the IRE1 RNase and the regulation of mammosphere forming efficiency via modulation of CXCL1 and IL8 levels we added recombinant exogenous CXCL1 and IL8 in addition to MKC8866 during the recovery phase of the experiment. Both CXCL1 and IL8 modestly increased the mammosphere forming efficiency of MDA-MB-231 cells, bolstering our previous findings (Fig 5.6D).

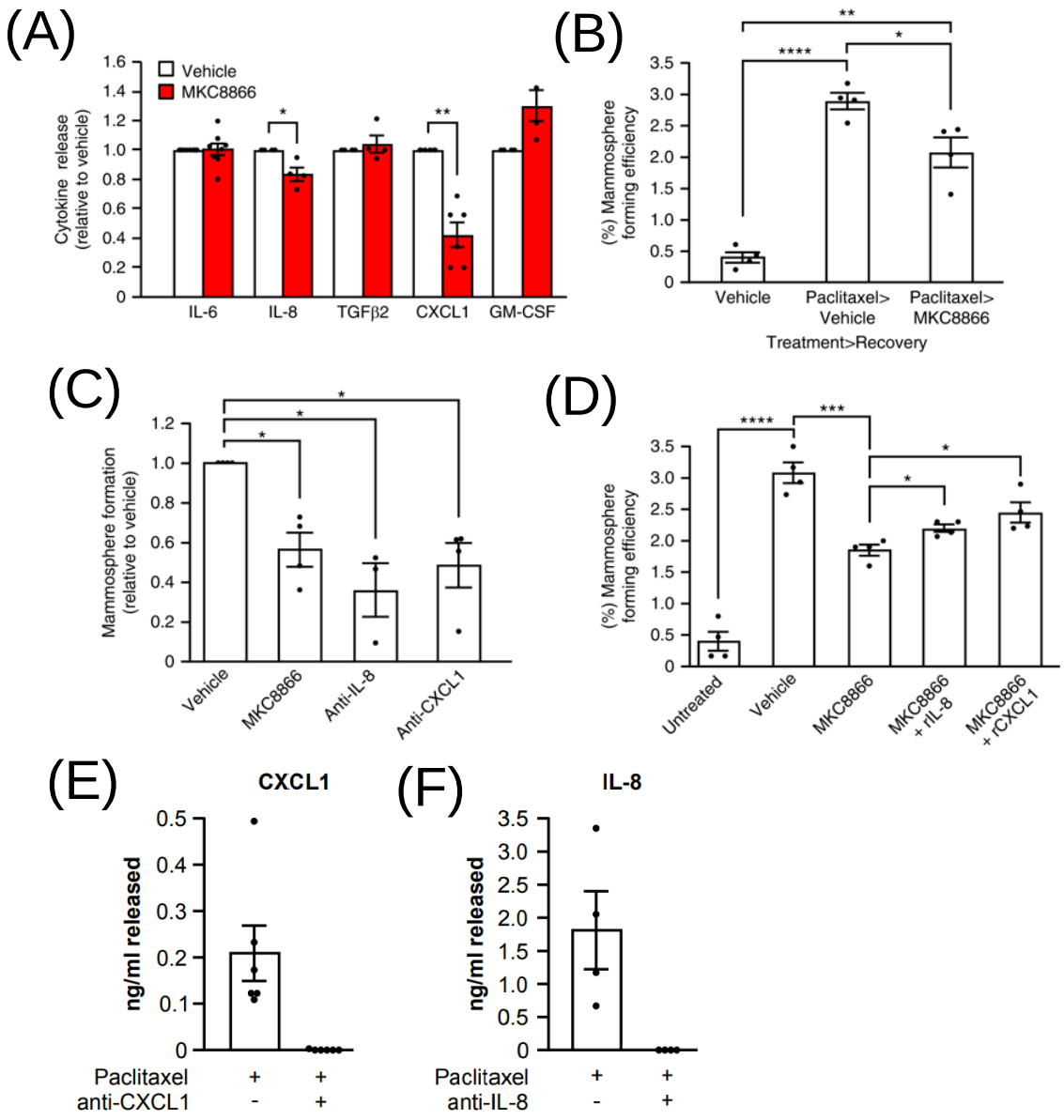

Figure 5.6. IRE1 RNase Regulated Paclitaxel-Induced Mammosphere Formation. MDA-MB-231 cells were treated with paclitaxel (10 nM) for 72 h, after which paclitaxel containing medium was removed and cells were washed. Cells were incubated for a further 72 h in fresh medium containing either DMSO or MKC8866 (20 μM) (A) or neutralizing antibodies against CXCL1 or IL8 (C) or MKC8866 (20 μM) and recombinant CXCL1 or IL8 (D). After treatment, cells were seeded at equal densities onto low-adherence plates and mammospheres were quantified after 5 days. After treatment with MKC8866 during the recovery phase supernatant was harvested and levels of IL6, IL8, CXCL1, and GMCSF were analysed by ELISA (B)(E)(F). Values shown represent the mean result of at least 3 independent repeats ± SEM, P* <0.05, P** <0.001, P*** <0.0001, P**** <0.00001.

5.8 IRE1 RNase Inhibitor MKC8866 Enhances the Effectiveness of Paclitaxel in vivo.

Since CSCs are implicated in therapy resistance in cancer, and we had found that IRE1 could control CSC populations in vitro. We wanted to see if we could recapitulate the results in vivo. To determine the efficacy of MKC8866 treatment in vivo, MDA-MB-231 tumor xenografts were established in athymic nude mice. Once tumors had reached a palpable size (225-250 mm3), animals were randomized into treatment groups and treated with vehicle alone, 300 mg/kg MKC8866 alone, 10 mg/kg paclitaxel alone or a combination of paclitaxel and MKC8866. Treatments in all groups were administered until tumors reached maximal size (2,000 mm^3) or day 60, whichever came first. MKC8866 was well tolerated after 60 consecutive oral doses and, based on pharmacokinetic allometric scaling, systemic exposures were well above anticipated clinical therapeutic levels. Treatment with MKC8866 alone did not attenuate tumor growth compared to vehicle-only controls (Fig. 5.7A). Analysis of percentage *XBP1* mRNA splicing in those tumors treated with MKC8866 confirmed a reduction in IRE1 RNase activity verifying on-target effect (Fig. 5.7B). While paclitaxel treatment reduced tumor growth, combination withMKC8866 markedly enhanced the efficacy of paclitaxel. Significantly reduced tumor growth ($P \leq 0.0001$) was observed throughout the 60 day experiment in animals receiving a paclitaxel-MKC8866 combination compared to paclitaxel alone (Fig 5.7C). A similar synergistic effect was observed following a paclitaxel-MKC8866 combination starting on day 14 (or ~700 mm^3 tumor volume) ($P \leq 0.001$) or on day 28 (or ~1300 mm^3 tumor volume) ($P \leq 0.05$) when compared to paclitaxel alone (Fig 5.7C). The decrease in tumor volume observed following combination of paclitaxel and MKC8866 also translated to an increase in survival.

Mice receiving daily MKC8866 administration in combination with paclitaxel from day 1-60, day 14-60 and day 28-60 displayed significantly longer survival compared to those treated with paclitaxel alone (Fig 5.7E).

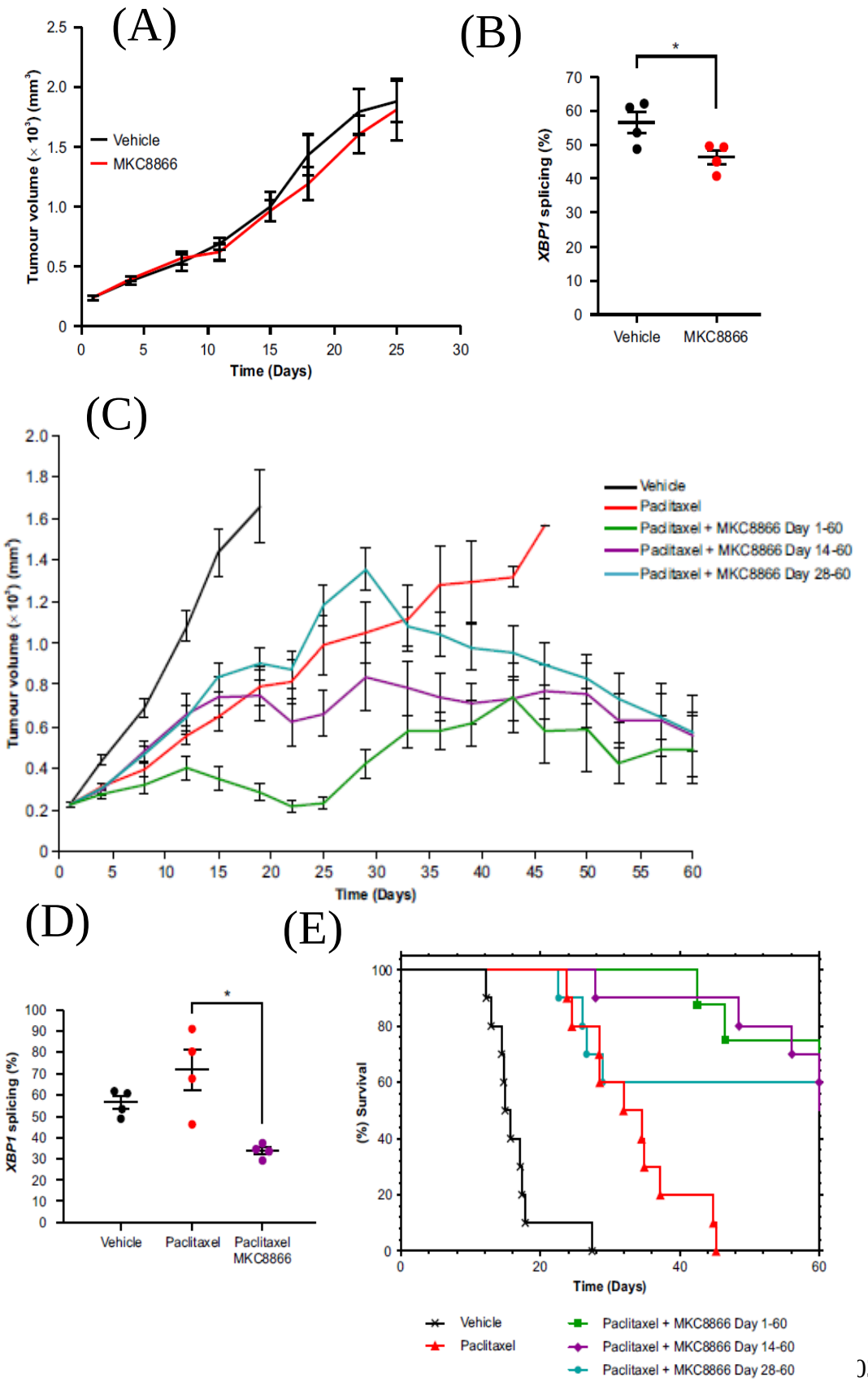

Figure 5.7. MKC8866 Enhances Effectiveness of MKC8866 *in vivo.* Xenografts were established by subcutaneously injecting $5x10^6$ MDA-MB-231 cells into the right flank of female athymic nude mice (Crl:NU(Ncr)-*Foxn1nu*, Charles River). When tumors were palpable (250 mm^3) mice were randomized into groups and treatments initiated. (A) Vehicle-only versus MKC8866 (300 mg kg^{-1}) daily via oral gavage. Tumor size was assessed every 2-3 days via caliper measurement and tumor volume calculated. By day 25, all tumors had reached their maximum permitted size (*n* = 10 mice per group). (B) Percentage *XBP1* mRNA splicing was determined in vehicle-only versus MKC8866 treated xenografts (*n* = 4 per treatment group). (C) Paclitaxel was administered weekly at 10 mg kg^{-1} by intravenous injection alone and in combination with MKC8866 administered daily at 300 mg kg^{-1} by oral gavage from day 14-60, from day 28-60 and from day 1-60. Tumor size was assessed every 2-3 days via caliper measurement and tumor volume calculated (*n* = 10 mice per group). (D) Percentage *XBP1* mRNA splicing was determined in vehicle-only, MKC8866-treated and paclitaxel plus MKC8866-treated xenografts (*n* = 4 per treatment group).

5.9 IRE1 RNase Inhibitor MKC8866 reduces tumour growth post-paclitaxel withdrawal

Since our *in vitro* studies indicated that IRE1 RNase inhibition by MKC8866 reduced mammosphere formation post-paclitaxel treatment, we tested the outcome of maintaining IRE1 inhibition following paclitaxel withdrawal *in vivo*. Following MDA-MB-231 tumor formation, mice were treated with paclitaxel alone (7.5 mg/kg) for days 1-10, or a combination of paclitaxel (days 1-10) and MKC8866 (300 mg/kg, days 1-28). After withdrawal of paclitaxel treatment on day 10, an initial reduction in tumor volume was apparent in both treatment groups (Fig. 5.8A). Tumor regrowth, evident post day 18 in those animals receiving no further treatment, was repressed in the treatment group still receiving MKC8866. Tumor regrowth was only apparent in this group following cessation of MKC8866 on day 28 (Fig 5.8A). Tumor volume measurements revealed 8 out of 10 animals displayed partial tumor regression and 1 animal showed complete tumor regression in the paclitaxel-MKC8866 combination group (Fig 5.8B) This compared favourably to paclitaxel alone, which had just 3 partial regressions, 1 complete regression and 1 tumor-free survival observed (Fig 5.8B). Additional studies are required to fully evaluate tumor growth after treatment is discontinued. Examination of XBP1 splicing in tumors revealed paclitaxel treatment increased IRE1 RNase activity, which was reduced upon combination with MKC8866 (Fig 5.8C, Fig 5.8D).

(A)

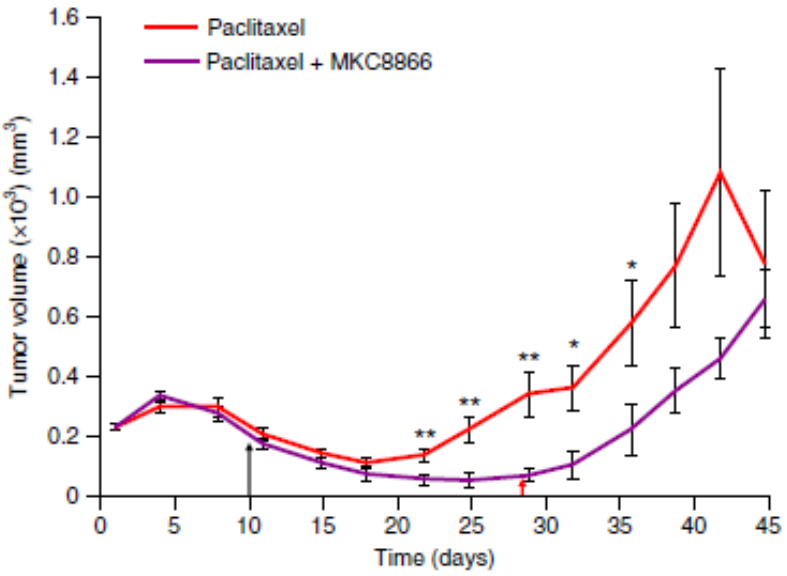

(B)

Group	N	PR	CR	TFS
Paclitaxel	**10**	**3**	**1**	**1**
Paclitaxel + MKC8866	**10**	**8**	**1**	**0**

N = Number of animals per group

PR = Partial Regression

CR = Complete Regression

PR = Tumour Free Survival

(C)

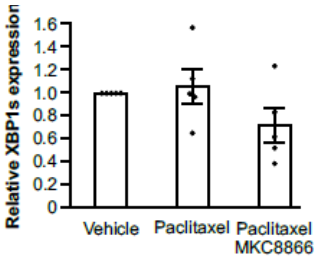

(D)

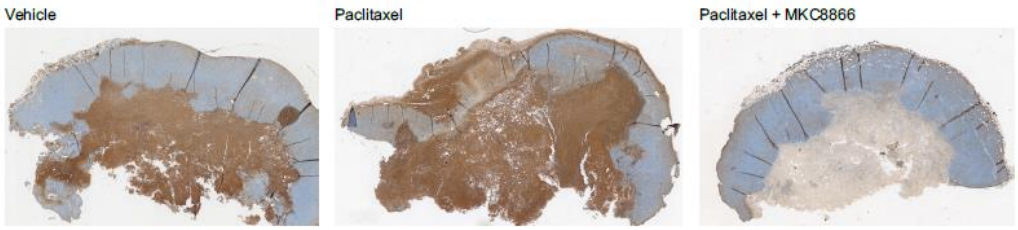

5.8 IRE1 RNase Inhibitor MKC8866 reduces tumour growth post-paclitaxel withdrawal. (A) Tumours were sectioned, fixed and immunostained using anti-XBP1s antibody. (B) Quantification of immuno-staining (n = 5). Error bars represent s.d. (E) Kaplan Meier plot showing survival in animals administered with MKC8866 in combination with paclitaxel (for indicated times) compared to paclitaxel alone or vehicle alone. (C) After tumour formation as outlined above paclitaxel (7.5 mg kg-1 by intravenous injection) was administered every second day until day 10 (last dose indicated by the black arrow) as a single agent or in combination with MKC8866 (300 mg kg-1 by oral gavage). MKC8866 treatment was administered daily from day 1–28 (last dose indicated by the red arrow). Tumor size was assessed every 2-3 days via caliper measurement and tumor volume calculated (n = 10 mice per group). *P<0.05, based on a Student's t-test. Error bars represent ± SEM.

5.10 Discussion

The IRE1/XBP1 axis of the UPR is important for the production and secretion of different factors. This phenomenon is especially well characterised in the context of the immune system, where XBP1 is important for the function of many immune cells (See section 1.10.2). Other cell types classically associated with having a high secretory output, like pancreatic beta cells, also require IRE1 to function properly. More recently, non-canonical roles for IRE1 and XBP1 in secretion have been found in other cells types whose primary functions are not linked to secretion.

This study began with the discovery that IRE1 regulates the secretome of TNBC cells. We have validated recent literature and shown that IRE1 regulates the expression and secretion of IL6 and IL8[125]. However we have also identified novel IRE1 targets in *CXCL1*, *GMCSF*, and *TGFB2*. Importantly we found that this phenomenon is occurring basally in TNBC cells. It is not obvious why these cells should secrete pro-inflammatory factors. However, all of these factors have been shown to have pro-tumour roles[226-229] so perhaps their expression and secretion is a product of selective pressure on these cells since it gives them a survival advantage. This discovery constitutes a further non-canonical role of IRE1 outside of its normal role in mediating the UPR.

We found that paclitaxel induces *XBP1* splicing in breast cancer cells. Since we found that IRE1 drives the expression of pro-tumour secretory factors this is an important result. Additionally we found that paclitaxel promotes enhanced

expression of *IL8* and *CXCL1* in an IRE1-dependent manner. The mechanism through which paclitaxel induces *XBP1* splicing is not known. Since paclitaxel stabilises microtubules[230] it is conceivable that transport of proteins between the ER and the Golgi is disrupted and triggering ER stress through a mechanism similar to BFA. Another possibility that paclitaxel is induces ROS production which in turn perturbs protein folding within the ER[225].

Since therapy resistance is a primary barrier to the long term survival of breast cancer patients, and secreted factors have already been identified as regulators of therapy resistance, we investigated the ability of IRE1 to modulate therapy resistance. CSCs are thought to be primary players in therapy resistance, so we sought to evaluate their abundance upon paclitaxel treatment with and without IRE1 RNase inhibition. High ALDH activity and high expression of CD44 and a low expression of CD24 ($CD44^{high}/CD24^{low}$)[69], are commonly used to identify cancer stem cell populations but they are not functional readouts of stem cell activity. To this end we performed the mammosphere formation assay which tests the ability of single cells to form breast cancer cell spheroids (mammospheres) in a serum-free, reduced-adhesion environment. This is a well-established assay based on findings that cells within mammospheres have increased tumour forming ability *in vivo* compared cancer cells cultured under normal conditions[231]. We found that paclitaxel induced robust mammosphere formation and that MKC8866 significantly reduced this effect. We used a combination of recombinant cytokines and neutralising antibodies against the cytokines to show that this phenotype was in part modulated by IRE1-dependant regulation of cytokines. We found that addition of recombinant CXCL1 or IL8 was able to partially rescue the ability of paclitaxel treated MDA-MB-231 cells to form mammospheres. Perhaps we would have seem a more complete reversion of the phenotype had we combined recombinant CXCL1 and IL8. However, the results we obtained clearly demonstrate that the IRE1 RNase domain controls the production of secreted factors, which is enhanced upon paclitaxel treatment, and that this processes has a direct bearing on CSC populations which are responsible for therapy resistance and tumour recurrence.

Having achieved such a strong effect *in vitro* we wanted to see if we could observe similar effects *in vivo*. To this end we performed xenograft experiments in which mice received MKC8866 alone or in combination with paclitaxel. MKC8866

treatment alone had no effect on the growth of tumour cells *in vivo* which suggests that the IRE1 RNase is not responsible for regulating tumour cell growth under basal conditions. However, when cells were treated with paclitaxel, MKC8866 did have the ability to prevent tumour growth. This suggests that under basal conditions tumour cells have other mechanisms in place, besides IRE1 RNase, which allows them to grow. However, when tumour cells are challenged with paclitaxel they switch to becoming reliant on the IRE1 RNase for survival. It is not clear why this switch occurs. It is possible that the production of inflammatory cytokines which promote the CSC phenotype, and thus therapy resistance, is blocked by MKC8866 addition. Another possibility is that tumour cells are experiencing severe ER stress upon paclitaxel treatment and that pro-survival XBP1s signalling is facilitating their survival. Thus, when XBP1s is removed the tumour cells die. Whatever the mechanism it is clear that the IRE1 RNase domain promotes therapy resistance in TNBC and that blocking this activity reduces tumour growth and lengthens the lifespan of the mice in this study.

This work bolsters recent findings in the field that XBP1s can promote therapy resistance in TNBC. Chen *et al* found that knockdown of XBP1 sensitised TNBC cells to certain therapies and reduced the CSC population[104]. More recently Zhao *et al* employed MKC8866 in vivo and showed that it sensitized breast tumour cells to docetaxel[182].

In conclusion this work provides a strong rational for the use of IRE1 RNase inhibitors in combination therapies to treat breast cancer patients. This prospect is especially exciting for TNBC which currently lacks a targeted therapy.

5.11 Future Perspectives

This work has firmly established that the IRE1 RNase regulates the production and secretion of pro-tumour secreted factors. The promoter regions of *IL6* and *IL8* have previously been reported to be directly bound by XBP1s[59]. However, the mechanisms though which *CXCL1*, *GMCSF* and *TGFβ2* are regulated remain to be elucidated. All of these factors were downregulated upon IRE1 RNase inhibition and upon knockdown of IRE1 and XBP1. This would suggest that they are direct targets of XBP1s transcriptional activity. Chromatin immunoprecipitation or luciferase promoter based assays could be used to determine if this is the case. If these

approached yield negative results, RIDD-dependent mechanisms would need to be considered.

One important implication of this work is the potential for TNBC cells to modulate the immune system via secretion of IL6, IL8, CXCL1, GMCSF, and TGFβ2. Immune cells have the ability to detect and eliminate tumour cells, however this anti-tumour function can be subverted by tumour cells to promote tumour growth. IL6, IL8, and CXCL1 all have pro-tumour roles[232], however it has been reported that GMCSF can re-educate macrophages to destroy tumour cells [233]. Going forward it will be important to establish the effect of MKC8866 inhibition on the infiltration of immune cells to the tumour. It will also be important to determine the types of immune cells (and their activation mode) which are recruited. The diversity of function of the cytokines we have identified makes predicting the outcome of the effect of IRE1 RNase inhibition on immune cells challenging. See section 6.2.5 for further discussion.

Chapter VI: General Discussion & Future Directions

6.1 What is the function of IRE1?

IRE1 was initially discovered within the context of ER stress and how cells mediate the response to a dysregulation of protein homeostasis within the ER[35]. While this is undoubtedly an important function of IRE1, it is becoming increasingly clear that many of IRE1's activities are ER stress-independent. While it might be argued that ER stress-independent IRE1 activation acts as a pre-emptive buffer against impending stress in some cases, as is the case during B-cell differentiation and MYC-driven proliferation, the same cannot be said for all IRE1-dependent mechanisms. For instance, the recent discovery that IRE1 acts as a scaffold for the recruitment and phosphorylation of FLNA and that this interaction is a highly conserved mechanism through which IRE1 controls cellular movement in a wide variety of contexts[131], has no direct link to the accumulation of misfolded proteins within the ER. In this thesis we have shown that in the context of TNBC, IRE1 is basally active and controls the production and secretion of a variety of soluble factors which enhances the CSC phenotype and leads to therapy resistance. Furthermore we have identified the first RIDD substrate in breast cancer, and have provided data which suggests that by cleaving this substrate IRE1 can control the migration and metastasis of breast cancer cells. To date, this last discovery constitutes the third distinct mechanism through which IRE1 controls cellular movement[130,131]. So the answer to the question of "what is the function of IRE1 in TNBC?" must now touch upon elements that are distinct from ER stress and encompass previous discoveries in the field as well as those discovered in this thesis. So, in addition to mediating the UPR in response to accumulation of misfolded proteins within the lumen of the ER, IRE1 is a regulator of the hypoxia response[104], a regulator of pro-inflammatory cytokines (Chapter V), and a regulator of cell migration (Chapter IV) in TNBC. Neither of the functions discovered in this thesis have any logical bearing on the resolution of ER stress (i.e. the accumulation of misfolded proteins within the ER). In fact, other work from our laboratory ((outlined in PhD thesis by Patricia Cleary (Title: Investigation of IRE1/XBP1s pathway and its potential as a therapeutic target in breast cancer) and in Logue *et al* 2018[51])) has shown that in promoting the production of cytokines, IRE1 promotes the proliferation of TNBC cells, which presumably necessitates an increase in ER

output. It could be argued that IRE1 is only "meant" to be transiently activated and that chronic IRE1 activation in TNBC is representative of a pathological state. In chapter III we showed that IRE1 basally promotes its canonical targets *HERP* and *ERDJ4* in TNBC cells, suggesting that chronic IRE1 activation is causing a prolonged canonical ER stress response, but how should we interpret the acquisition of new ER stress-independent functions by IRE1 in TNBC? One possibility is that these are not new functions gained as a result of a pathological state but rather constitute part of a canonical ER stress response that has been hitherto unnoticed. Perhaps activated IRE1 triggers the secretion of cytokines to alert nearby immune cells to a cell undergoing chronic ER stress, and should therefore be preparing to undergo apoptosis, upon which it should be phagocytosed by the immune cells. Perhaps IRE1 cleaves *JUP* mRNA as an aide to the apoptotic process where cell-cell and cell-ECM contacts are lost. Such processes would drive the death of healthy cells, but could be beneficial to cancer cells which undergo apoptosis less readily.

Whatever the explanation, the ever-growing list of IRE1 functions is something we should consider when approaching the idea of targeting IRE1 in TNBC.

6.2 Targeting IRE1 RNase in TNBC

The treatment of breast cancer has improved dramatically over the past decades. This is due to the identification of drugable targets like ESR1 and HER2, which have revolutionised treatment of ESR1+ and HER2+ cancers respectively and extended the lives of many. Of the histological subtypes TNBC remains the only one without a targeted therapy. Today, TNBC patients are commonly treated with standard systemic cytotoxic chemotherapeutics, with therapy-resistance often occurring. Thus, there is a need to develop targeted therapies for TNBC. With this thesis we have built on previous work suggesting that IRE1 RNase is a good candidate as a target in TNBC. In IRE1 we and others have identified a target which is specifically active in breast cancer and not in non-cancerous breast tissue. Furthermore, we have shown that IRE1 RNase inhibition prevents cell migration *in vitro* and therapy resistance in TNBC cells *in vivo*. Since metastatic capacity and tumour resistance are perhaps the most lethal characteristics a tumour can acquire, the results reported in this thesis provide strong support for the use of IRE1 inhibitors to treat TNBC as an accompanying therapy to standard chemotherapeutics.

6.2.1 IRE1 inhibition and standard chemotherapeutics

Our work and that of others[182] has focussed solely on combining MKC8866 with taxane based therapies (paclitaxel and docetaxel respectively). Another study found that depletion of XBP1 produced similar effects to MKC8866, when mice bearing MDA-MB-231 cell xenografts received the anthracycline doxorubicin or paclitaxel[104]. Platinum based drugs are another class of standard chemotherapeutics, but have not been tested in combination either with IRE1 RNase inhibitors or genetic depletion of the IRE1/XBP1 axis in breast cancer. However, combination of an IRE1 RNase inhibitor with cisplatin was able to trigger cell death in cervical cancer stem cells *in vitro*[234]. This suggests that combination of IRE1 RNase inhibitors with other chemotherapeutics may prove equally useful as the combination with taxanes and anthracyclines.

It is not clear what mechanism is behind the effectiveness of the combination of IRE1 RNase inhibition and standard chemotherapeutics. As mentioned in the introduction, hypoxia is a driver of tumour progression and markers of hypoxia are associated with worse prognosis. Indeed, the VEGF monoclonal antibody bevacizumab is often used in combination with standard chemotherapeutics in the treatment of TNBC[235] to prevent tumour angiogenesis which is driven by hypoxia. IRE1/XBP1s can drive the response to hypoxia and lead to the induction of VEGF[104]. This suggests that IRE1 RNase inhibitors may be an alternative to bevacizumab in supressing VEGF signalling in instances where tumour cell have become resistant to anti-VEGF therapies[236]. Furthermore, the new mechanisms discovered in this thesis suggest that in addition to blocking hypoxia-driven signalling, IRE1 inhibitors may block the secretion of pro-inflammatory cytokines which drive tumour growth.

6.2.2 Novel mechanisms for IRE1 as a therapeutic target

Poly (ADP-ribose) polymerase (PARP) enzymes repair single strand breaks in DNA and contribute to cancer survival. PARP inhibitors are coming to prominence as potential treatments for TNBC. Recent evidence suggests that inhibiting IRE1 may be another viable method to block DNA repair mechanisms in cancer. XBP1 was found to regulate a cluster of DNA damage repair genes in human cells[72] and in yeast IRE1 is required for chromosome maintenance under basal conditions and upon UV exposure[237]. The mechanism(s) behind this phenomenon is not known but

IRE1 appears to have a role in promoting the DNA damage response. We found IRE1 to be particularly active in TNBC, thus, targeting IRE1 may promote cell death in TNBC through furthering DNA damage, and offers an alternative to therapies which mediate their effect through inhibiting DNA repair enzymes such as PARP.

Glycoprotein NMB (gpNMB) is another potential clinical target for a subset of TNBC in which it is overexpressed[235]. gpNMB promotes pro-tumour cell-intrinsic and cell-extrinsic signalling[238]. Intriguingly, gpNMB was found to be robustly induced under ER stress[239]. This suggests that cancer cells which exhibit basal UPR activation (such as TNBC) actively promote expression of gpNMB. The mechanism by which ER stress promotes gpNMB expression is not known. However, these reports indicate that targeting the UPR may provide another method to target gpNMB in cancer.

6.2.3 IRE1 in immunotherapies

As outlined in the introduction (section 1.12.3), IRE1 plays a role in controlling the function of immune cells within the tumour microenvironment. Tumour-associated immune cells can either promote tumour cell destruction or promote tumour growth. UPR signalling is responsible for driving the latter, pro-tumour phenotype. Indeed, treatment of tumour-bearing mice with Tg promotes immunosuppression while combination with a chemical chaperone was able to reverse this phenotype[240]. Therapies which promote tumour cell killing by immune cells, and block the immunosuppressive activity of tumour cells are being developed and some, such as programmed death ligand 1 (PD-L1) inhibitors, have recently been approved by the FDA. Under normal conditions PD-L1 is used by normal cells to curtail immune responses, but is also a route through which tumour cells supress the immune system. Recently IL6 blockade in a mouse model of colorectal cancer was found to sensitise cancer cells to PD-L1-targeting therapies. High IL6 expression in tumour cells was associated with high PD-L1 expression[241]. Since we have shown that IRE1 controls expression and secretion of IL6, IRE1 RNase inhibitors may reduce expression of PD-L1 in tumour cells. IL8, another cytokine we identified as an IRE1 target in TNBC, was recently found to promote PD-L1 expression in gastric cancer, suggesting another through which IRE1 RNase inhibition may help to deplete PD-L1[242].

Cytotoxic T-lymphocyte-associated protein 4 (CTLA-4) is another immune checkpoint protein which is being targeted in cancer. GMCSF, another cytokine we identified in this thesis has been reported as immune-stimulatory, and synergises with anti-CTLA-4 therapy in a mouse model of melanoma[243]. Since MKC8866 depletes GMCSF levels, this observation serves as an example of a potential pitfall to targeting IRE1 in the clinic.

6.2.4 IRE1 in cell-based therapies

Chimeric antigen receptor (CAR) T-cell therapy is a promising new therapeutic approach where immune cells are withdrawn from patient and genetically altered to recognise a tumour cell-specific antigen. However, this therapy can cause complications such as cytokine release syndrome (CRS) which causes fever and breathing problems. It was recently reported that this unwanted side effect could be controlled with blockade of IL6[244]. This suggests that co-administration with and IRE1 RNase inhibitor could prevent cytokine release syndrome (CRS). This approach could also lead to further complications however, since T-cells require XBP1 to function properly[121].

6.2.5 Potential pitfalls of targeting IRE1 in the clinic

Throughout this thesis we have highlighted the scale and diversity of IRE1 RNase targets. The diversity of targets is a direct reflection of the diversity of IRE1 functions. This means that inhibiting the IRE1 RNase domain in humans may have hitherto unsuspected and undesirable effects. Animal work described in this thesis has found that the inhibitor MKC8866 has bypassed the common pitfalls of UPR targeting compounds when applied *in vivo*. However, even if MKC8866 has no unwanted effects on normal tissue, it is still not clear exactly how it will affect the different cells within a tumour mass, with diverse functions, and experiencing diverse stressors. For example, we could consider JUP.

JUP is heterogeneously expressed in primary breast tumours, and has controversial roles in metastasis. Many studies report that loss of JUP promotes cellular migration and dissemination of cancer cells into the bloodstream[211], and if this is true it would be desirable to inhibit IRE1 and thereby rescue levels of JUP and reduce cellular migration. However, another report indicates that JUP is important in allowing tumour cells to survive in circulation and ultimately to form successful metastases[200]. In this case IRE1 RNase inhibition presumably would have no effect on these

circulating tumours with regards to JUP levels, and may in fact increase the metastatic capacity of tumour cells which still reside at the primary tumour site. It may be that targeting the IRE1 RNase domain is too broad a treatment to guarantee an acceptable specificity and predictability of outcome in the clinic. As such, approaches that block XBP1s, while maintaining RIDD, like targeting RNA 2',3'-Cyclic Phosphate And 5'-OH Ligase (the enzyme which ligates spliced *XBP1*)[61] for example, may prove more effective than IRE1 RNase inhibition in some circumstances.

JUP aside, inhibiting RTCB may be preferable to IRE1 RNase inhibition in luminal breasts cancers since in addition to reducing XBP1s levels, total XBP1 levels should, in theory, also be reduced upon RTCB inhibition. Defining the molecular determinants which govern whether IRE1 RNase engages *XBP1* splicing or RIDD activity is an active area of research for the UPR field[245], and is likely to yield insights which may eventually allow both activities to be individually modulated in patients.

Side-effects:

Targeting the UPR in the clinic poses several challenges, including the possibly of unwanted side-effects. Given the diversity of UPR functions, how confident can we be that UPR inhibition will not create more problems than it solves? In section 1.11.2 we outlined the importance of IRE1 signalling in regulating the function of many immune cell types. This makes predicting the outcome of UPR inhibition difficult. However, using a syngeneic model of breast cancer Zhao *et al* have recently demonstrated that MKC8866 can reduce tumour growth when administered with docetaxel to mice with a competent immune system. Furthermore, the authors observed increased $CD4^+$ and $CD8^+$ immune cell infiltration in tumours that received MKC8866 and docetaxel[182]. This suggests, at least in this context, that whatever effect IRE1 RNase inhibition is having on cell types throughout the organism, the net result is a reduction in tumour burden and enhanced anti-tumour immune cell activity. Furthermore, long-term administration of MKC8866 did not cause any damage to the pancreas of the animals, an organ which relies on the UPR for its secretory function. This promising report suggests that IRE1 RNase inhibition may promote immune infiltration and tumour cell destruction without any apparent side-

effect, but will this finding hold true when UPR inhibition is investigated in other cancer types? In a model of ovarian cancer, XBP1 was found to drive a pro-tumour mechanism in dendritic cells, suggesting that targeting this branch of the UPR may promote increased tumour cell killing by dendritic cells[124]. Despite these reports, more studies are required to rule out the potential for unwanted side-effects when targeting the UPR.

A crucial question the field faces is: how can we determine when patients will benefit from UPR-targeting drugs and when should such drugs be avoided? This would appear to necessitate biopsy of the tumour and determination of which UPR arms are active in the tumour cells. Addition of UPR markers to routine assays used to subtype breast tumours could be a useful way to obtain this information.

6.3 Future Directions

6.3.1 Single Cell UPR Analysis

One aspect of UPR in breast cancer which has not been addressed to date is the notion of heterogeneous UPR cascades within the same tumour or tissue type. Since we know that single breast tumours exhibit high levels of heterogeneity in cellular content and gene expression, and that different sections of tumour can be exposed to different levels of stressor (like anoxic tumour cores), and that the UPR is differentially regulated depending on the nature and duration of stress, it stands to reason that a given tumour will experience multiple simultaneous UPRs with distinct outputs. In such a case "*The*" UPR being active is a misnomer, and we should consider multiple UPRs as distinct signalling hubs, some promoting death, others life, some pro-tumour, some anti-tumour. The revolutionary changes in technology which have given us single cell resolution microdissection, and single cell 'omics, mean that we are now poised to adequately dissect tumour heterogeneity. If it is discovered that different regions of the same tumour exhibit different UPR outputs it will revolutionise how we think about the UPR in cancer.

6.3.2 Transmissible ER stress

One well accepted revolution in the UPR field is the notion of transmissible ER stress (TERS). As mentioned in the introduction (section 1.12.5) TERS is a recently observed phenomenon wherein cells challenged with ER stress secrete unknown factors which elicit a stress response in recipient cells. The discovery of this

phenomenon has given rise to the notion that disease specific markers are released into the bloodstream during ER stress and could be used as relatively non-invasive diagnostic markers. TERS also necessitates a shift in how we think about UPR within a given tissue, and raises several questions: Since UPRs are diverse, are TERS also diverse? Do tumour cells transmit ER stress to each other? Does TERS have a role in tumorigenesis? Does TERS have a role in the subjugation of normal stromal cells by tumour cells within the tumour mass? How does TERS affect different tissues and organ which are removed from the disease site? Can TERS prime foreign tissues for metastasis? All of these questions remain to be answered, and their resolution could greatly improve our understanding of the UPR and cancer.

Concluding Remarks

The primary goal of this thesis has been achieved. We have shown that IRE1 RNase is active in TNBC and discovered two novel functions of this domain in TNBC.

1. IRE1 promotes the production and secretion of soluble factors which drive a stem cell-like phenotype and promote therapy resistance.
2. IRE1 promotes the degradation of *JUP* mRNA and facilitates cancer cell migration.

Crucially, we have shown that a small molecule inhibitor of the IRE1 RNase domain can block these pro-tumour processes.

Cumulatively, this thesis has broadened our knowledge of the role that IRE1 plays in breast cancer, and acts as supporting evidence for IRE1 RNase inhibitors to enter the clinic which may prolong and improve the lives of breast cancer patients

References

1 Porter, K. R., Claude, A. & Fullam, E. F. A STUDY OF TISSUE CULTURE CELLS BY ELECTRON MICROSCOPY : METHODS AND PRELIMINARY OBSERVATIONS. The Journal of experimental medicine 81, 233-246 (1945).

2 Palade, G. E. A small particulate component of the cytoplasm. The Journal of Biophysical and Biochemical Cytology 1, 59-68 (1955).

3 Palade, G. E. & Siekevitz, P. LIVER MICROSOMES : AN INTEGRATED MORPHOLOGICAL AND BIOCHEMICAL STUDY. The Journal of Biophysical and Biochemical Cytology 2, 171-200 (1956).

4 Siekevitz, P. Uptake of radioactive alanine in vitro into the proteins of rat liver fractions. The Journal of biological chemistry 195, 549-565 (1952).

5 Smuckler, E. A., Iseri, O. A. & Benditt, E. P. AN INTRACELLULAR DEFECT IN PROTEIN SYNTHESIS INDUCED BY CARBON TETRACHLORIDE. The Journal of experimental medicine 116, 55-72 (1962).

6 Siekevitz, P. & Zamecnik, P. C. Ribosomes and protein synthesis. The Journal of cell biology 91, 53s-65s (1981).

7 Agostinis, P. & Afshin, S. Endoplasmic Reticulum Stress in Health and Disease. (Springer, 2012).

8 Feige, M. J. & Hendershot, L. M. Disulfide bonds in ER protein folding and homeostasis. Current opinion in cell biology 23, 167-175 (2011).

9 Alberts, B. et al. Molecular Biology of the Cell. 4 edn, (Garland Sciences, 2002).

10 Braakman, I. & Bulleid, N. J. Protein folding and modification in the mammalian endoplasmic reticulum. Annual review of biochemistry 80, 71-99, doi:10.1146/annurev-biochem-062209-093836 (2011).

11 Amin-Wetzel, N. et al. A J-Protein Co-chaperone Recruits BiP to Monomerize IRE1 and Repress the Unfolded Protein Response. Cell 171, 1625-1637 e1613, doi:10.1016/j.cell.2017.10.040 (2017).

12 Kelleher, D. J. & Gilmore, R. An evolving view of the eukaryotic oligosaccharyltransferase. Glycobiology 16, 47R-62R, doi:10.1093/glycob/cwj066 (2006).

13 Xu, C. & Ng, D. T. Glycosylation-directed quality control of protein folding. Nature reviews. Molecular cell biology 16, 742-752, doi:10.1038/nrm4073 (2015).

14 Appenzeller-Herzog, C. Glutathione- and non-glutathione-based oxidant control in the endoplasmic reticulum. Journal of cell science 124, 847-855, doi:10.1242/jcs.080895 (2011).

15 Csala, M., Margittai, E. & Banhegyi, G. Redox control of endoplasmic reticulum function. Antioxidants & redox signaling 13, 77-108, doi:10.1089/ars.2009.2529 (2010).

16 Kaufman, R. J. & Malhotra, J. D. Calcium trafficking integrates endoplasmic reticulum function with mitochondrial bioenergetics. Biochimica et biophysica acta 1843, 2233-2239, doi:10.1016/j.bbamcr.2014.03.022 (2014).

17 Qi, L., Tsai, B. & Arvan, P. New Insights into the Physiological Role of Endoplasmic Reticulum-Associated Degradation. Trends in cell biology 27, 430-440, doi:10.1016/j.tcb.2016.12.002 (2017).

18 Bento, C. F. et al. Mammalian Autophagy: How Does It Work? Annual review of biochemistry 85, 685-713, doi:10.1146/annurev-biochem-060815-014556 (2016).
19 Dikic, I. & Elazar, Z. Mechanism and medical implications of mammalian autophagy. Nature reviews. Molecular cell biology, doi:10.1038/s41580-018-0003-4 (2018).
20 Hetz, C. & Saxena, S. ER stress and the unfolded protein response in neurodegeneration. Nature reviews. Neurology 13, 477-491, doi:10.1038/nrneurol.2017.99 (2017).
21 Eizirik, D. L., Cardozo, A. K. & Cnop, M. The role for endoplasmic reticulum stress in diabetes mellitus. Endocrine reviews 29, 42-61, doi:10.1210/er.2007-0015 (2008).
22 Ribeiro, C. M. & Boucher, R. C. Role of endoplasmic reticulum stress in cystic fibrosis-related airway inflammatory responses. Proceedings of the American Thoracic Society 7, 387-394, doi:10.1513/pats.201001-017AW (2010).
23 Urra, H., Dufey, E., Avril, T., Chevet, E. & Hetz, C. Endoplasmic Reticulum Stress and the Hallmarks of Cancer. Trends in cancer 2, 252-262, doi:10.1016/j.trecan.2016.03.007 (2016).
24 Bergmann, T. J. et al. Chemical stresses fail to mimic the unfolded protein response resulting from luminal load with unfolded polypeptides. The Journal of biological chemistry 293, 5600-5612, doi:10.1074/jbc.RA117.001484 (2018).
25 Hetz, C. The unfolded protein response: controlling cell fate decisions under ER stress and beyond. Nature reviews. Molecular cell biology 13, 89-102, doi:10.1038/nrm3270 (2012).
26 Jager, R., Bertrand, M. J., Gorman, A. M., Vandenabeele, P. & Samali, A. The unfolded protein response at the crossroads of cellular life and death during endoplasmic reticulum stress. Biology of the cell / under the auspices of the European Cell Biology Organization 104, 259-270, doi:10.1111/boc.201100055 (2012).
27 Shiu, R. P., Pouyssegur, J. & Pastan, I. Glucose depletion accounts for the induction of two transformation-sensitive membrane proteinsin Rous sarcoma virus-transformed chick embryo fibroblasts. Proceedings of the National Academy of Sciences of the United States of America 74, 3840-3844 (1977).
28 Kozutsumi, Y., Segal, M., Normington, K., Gething, M. J. & Sambrook, J. The presence of malfolded proteins in the endoplasmic reticulum signals the induction of glucose-regulated proteins. Nature 332, 462-464, doi:10.1038/332462a0 (1988).
29 Mori, K., Ma, W., Gething, M. J. & Sambrook, J. A transmembrane protein with a cdc2+/CDC28-related kinase activity is required for signaling from the ER to the nucleus. Cell 74, 743-756 (1993).
30 Cox, J. S., Shamu, C. E. & Walter, P. Transcriptional induction of genes encoding endoplasmic reticulum resident proteins requires a transmembrane protein kinase. Cell 73, 1197-1206 (1993).
31 Nikawa, J. & Yamashita, S. IRE1 encodes a putative protein kinase containing a membrane-spanning domain and is required for inositol phototrophy in Saccharomyces cerevisiae. Molecular microbiology 6, 1441-1446 (1992).

32 Mori, K., Kawahara, T., Yoshida, H., Yanagi, H. & Yura, T. Signalling from endoplasmic reticulum to nucleus: transcription factor with a basic-leucine zipper motif is required for the unfolded protein-response pathway. Genes to cells : devoted to molecular & cellular mechanisms 1, 803-817 (1996).
33 Cox, J. S. & Walter, P. A novel mechanism for regulating activity of a transcription factor that controls the unfolded protein response. Cell 87, 391-404 (1996).
34 Sidrauski, C. & Walter, P. The transmembrane kinase Ire1p is a site-specific endonuclease that initiates mRNA splicing in the unfolded protein response. Cell 90, 1031-1039 (1997).
35 Mori, K. The unfolded protein response: the dawn of a new field. Proceedings of the Japan Academy. Series B, Physical and biological sciences 91, 469-480, doi:10.2183/pjab.91.469 (2015).
36 Tirasophon, W., Welihinda, A. A. & Kaufman, R. J. A stress response pathway from the endoplasmic reticulum to the nucleus requires a novel bifunctional protein kinase/endoribonuclease (Ire1p) in mammalian cells. Genes & development 12, 1812-1824 (1998).
37 Yoshida, H., Matsui, T., Yamamoto, A., Okada, T. & Mori, K. XBP1 mRNA is induced by ATF6 and spliced by IRE1 in response to ER stress to produce a highly active transcription factor. Cell 107, 881-891 (2001).
38 Wang, X. Z. et al. Cloning of mammalian Ire1 reveals diversity in the ER stress responses. The EMBO journal 17, 5708-5717, doi:10.1093/emboj/17.19.5708 (1998).
39 Haze, K., Yoshida, H., Yanagi, H., Yura, T. & Mori, K. Mammalian transcription factor ATF6 is synthesized as a transmembrane protein and activated by proteolysis in response to endoplasmic reticulum stress. Molecular biology of the cell 10, 3787-3799 (1999).
40 Haze, K. et al. Identification of the G13 (cAMP-response-element-binding protein-related protein) gene product related to activating transcription factor 6 as a transcriptional activator of the mammalian unfolded protein response. Biochem J 355, 19-28 (2001).
41 Harding, H. P., Zhang, Y. & Ron, D. Protein translation and folding are coupled by an endoplasmic-reticulum-resident kinase. Nature 397, 271-274, doi:10.1038/16729 (1999).
42 Korennykh, A. V. et al. Structural and functional basis for RNA cleavage by Ire1. BMC biology 9, 47, doi:10.1186/1741-7007-9-47 (2011).
43 Kopp, M. C., Nowak, P. R., Larburu, N., Adams, C. J. & Ali, M. M. In vitro FRET analysis of IRE1 and BiP association and dissociation upon endoplasmic reticulum stress. eLife 7, doi:10.7554/eLife.30257 (2018).
44 Korennykh, A. & Walter, P. Structural basis of the unfolded protein response. Annual review of cell and developmental biology 28, 251-277, doi:10.1146/annurev-cellbio-101011-155826 (2012).
45 Karagoz, G. E. et al. An unfolded protein-induced conformational switch activates mammalian IRE1. eLife 6, doi:10.7554/eLife.30700 (2017).
46 Schreiber, R. D., Old, L. J. & Smyth, M. J. Cancer immunoediting: integrating immunity's roles in cancer suppression and promotion. Science 331, 1565-1570, doi:10.1126/science.1203486 (2011).
47 Yamamoto, K., Yoshida, H., Kokame, K., Kaufman, R. J. & Mori, K. Differential contributions of ATF6 and XBP1 to the activation of endoplasmic reticulum stress-responsive cis-acting elements ERSE, UPRE

and ERSE-II. Journal of biochemistry 136, 343-350, doi:10.1093/jb/mvh122 (2004).

48 Shen, J., Chen, X., Hendershot, L. & Prywes, R. ER stress regulation of ATF6 localization by dissociation of BiP/GRP78 binding and unmasking of Golgi localization signals. Developmental cell 3, 99-111 (2002).

49 Shoulders, M. D. et al. Stress-Independent Activation of XBP1s and/or ATF6 Reveals Three Functionally Diverse ER Proteostasis Environments. Cell reports 3, 1279-1292 (2013).

50 Morishima, N., Nakanishi, K. & Nakano, A. Activating transcription factor-6 (ATF6) mediates apoptosis with reduction of myeloid cell leukemia sequence 1 (Mcl-1) protein via induction of WW domain binding protein 1. The Journal of biological chemistry 286, 35227-35235, doi:10.1074/jbc.M111.233502 (2011).

51 Logue, S. E. et al. Inhibition of IRE1 RNase activity modulates the tumor cell secretome and enhances response to chemotherapy. Nature communications 9, 3267, doi:10.1038/s41467-018-05763-8 (2018).

52 Szegezdi, E., Logue, S. E., Gorman, A. M. & Samali, A. Mediators of endoplasmic reticulum stress-induced apoptosis. EMBO reports 7, 880-885, doi:10.1038/sj.embor.7400779 (2006).

53 Zhang, W. et al. ER stress potentiates insulin resistance through PERK-mediated FOXO phosphorylation. Genes & development 27, 441-449, doi:10.1101/gad.201731.112 (2013).

54 Bobrovnikova-Marjon, E. et al. PERK utilizes intrinsic lipid kinase activity to generate phosphatidic acid, mediate Akt activation, and promote adipocyte differentiation. Mol Cell Biol 32, 2268-2278, doi:10.1128/mcb.00063-12 (2012).

55 Zhu, X. et al. Ubiquitination of inositol-requiring enzyme 1 (IRE1) by the E3 ligase CHIP mediates the IRE1/TRAF2/JNK pathway. The Journal of biological chemistry 289, 30567-30577, doi:10.1074/jbc.M114.562868 (2014).

56 Martino, M. et al. The ER stress transducer IRE1β is required for airway epithelial mucin production. Mucosal immunology 6, 639-654 (2013).

57 Ali, M. M. et al. Structure of the Ire1 autophosphorylation complex and implications for the unfolded protein response. The EMBO journal 30, 894-905, doi:10.1038/emboj.2011.18 (2011).

58 Korennykh, A. V. et al. The unfolded protein response signals through high-order assembly of Ire1. Nature 457, 687-693, doi:10.1038/nature07661 (2009).

59 Martinon, F., Chen, X., Lee, A. H. & Glimcher, L. H. TLR activation of the transcription factor XBP1 regulates innate immune responses in macrophages. Nature immunology 11, 411-418, doi:10.1038/ni.1857 (2010).

60 Karali, E. et al. VEGF Signals through ATF6 and PERK to promote endothelial cell survival and angiogenesis in the absence of ER stress. Molecular cell 54, 559-572, doi:10.1016/j.molcel.2014.03.022 (2014).

61 Lu, Y., Liang, F. X. & Wang, X. A Synthetic Biology Approach Identifies the Mammalian UPR RNA Ligase RtcB. Molecular cell, doi:10.1016/j.molcel.2014.06.032 (2014).

62 Yoshida, H., Oku, M., Suzuki, M. & Mori, K. pXBP1(U) encoded in XBP1 pre-mRNA negatively regulates unfolded protein response activator

pXBP1(S) in mammalian ER stress response. The Journal of cell biology 172, 565-575, doi:10.1083/jcb.200508145 (2006).

63 Yoshida, H., Uemura, A. & Mori, K. pXBP1(U), a negative regulator of the unfolded protein response activator pXBP1(S), targets ATF6 but not ATF4 in proteasome-mediated degradation. Cell structure and function 34, 1-10 (2009).

64 Yanagitani, K., Kimata, Y., Kadokura, H. & Kohno, K. Translational pausing ensures membrane targeting and cytoplasmic splicing of XBP1u mRNA. Science 331, 586-589, doi:10.1126/science.1197142 (2011).

65 Kurata, M. et al. Anti-apoptotic function of Xbp1 as an IL-3 signaling molecule in hematopoietic cells. Cell death & disease 2, e118, doi:10.1038/cddis.2011.1 (2011).

66 Mimura, N. et al. Blockade of XBP1 splicing by inhibition of IRE1alpha is a promising therapeutic option in multiple myeloma. Blood 119, 5772-5781, doi:10.1182/blood-2011-07-366633 (2012).

67 Fujimoto, T. et al. Upregulation and overexpression of human X-box binding protein 1 (hXBP-1) gene in primary breast cancers. Breast cancer (Tokyo, Japan) 10, 301-306 (2003).

68 Lee, A. H., Iwakoshi, N. N. & Glimcher, L. H. XBP-1 regulates a subset of endoplasmic reticulum resident chaperone genes in the unfolded protein response. Mol Cell Biol 23, 7448-7459 (2003).

69 Lombardo, Y., de Giorgio, A., Coombes, C. R., Stebbing, J. & Castellano, L. Mammosphere formation assay from human breast cancer tissues and cell lines. Journal of visualized experiments : JoVE, doi:10.3791/52671 (2015).

70 Sriburi, R., Jackowski, S., Mori, K. & Brewer, J. W. XBP1: a link between the unfolded protein response, lipid biosynthesis, and biogenesis of the endoplasmic reticulum. The Journal of cell biology 167, 35-41, doi:10.1083/jcb.200406136 (2004).

71 Zasadil, L. M. et al. Cytotoxicity of paclitaxel in breast cancer is due to chromosome missegregation on multipolar spindles. Science translational medicine 6, 229ra243, doi:10.1126/scitranslmed.3007965 (2014).

72 Acosta-Alvear, D. et al. XBP1 controls diverse cell type- and condition-specific transcriptional regulatory networks. Molecular cell 27, 53-66, doi:10.1016/j.molcel.2007.06.011 (2007).

73 Maurel, M., Chevet, E., Tavernier, J. & Gerlo, S. Getting RIDD of RNA: IRE1 in cell fate regulation. Trends in biochemical sciences 39, 245-254, doi:10.1016/j.tibs.2014.02.008 (2014).

74 Hollien, J. & Weissman, J. S. Decay of endoplasmic reticulum-localized mRNAs during the unfolded protein response. Science 313, 104-107, doi:10.1126/science.1129631 (2006).

75 Lipson, K. L. et al. Regulation of insulin biosynthesis in pancreatic beta cells by an endoplasmic reticulum-resident protein kinase IRE1. Cell metabolism 4, 245-254, doi:10.1016/j.cmet.2006.07.007 (2006).

76 Upton, J. P. et al. IRE1alpha cleaves select microRNAs during ER stress to derepress translation of proapoptotic Caspase-2. Science 338, 818-822, doi:10.1126/science.1226191 (2012).

77 Ghosh, R. et al. Allosteric Inhibition of the IRE1alpha RNase Preserves Cell Viability and Function during Endoplasmic Reticulum Stress. Cell 158, 534-548, doi:10.1016/j.cell.2014.07.002 (2014).

78 Tam, A. B., Koong, A. C. & Niwa, M. Ire1 Has Distinct Catalytic Mechanisms for XBP1/HAC1 Splicing and RIDD. Cell reports 9, 850-858 (2014).
79 Hetz, C. & Glimcher, L. H. Fine-tuning of the unfolded protein response: Assembling the IRE1alpha interactome. Molecular cell 35, 551-561, doi:10.1016/j.molcel.2009.08.021 (2009).
80 Nguyên, D. T. et al. Nck-dependent Activation of Extracellular Signal-regulated Kinase-1 and Regulation of Cell Survival during Endoplasmic Reticulum Stress. Molecular biology of the cell 15, 4248-4260 (2004).
81 Tam, A. B., Mercado, E. L., Hoffmann, A. & Niwa, M. ER stress activates NF-kappaB by integrating functions of basal IKK activity, IRE1 and PERK. PLoS One 7, e45078, doi:10.1371/journal.pone.0045078 (2012).
82 Liu, Y. et al. Role for the endoplasmic reticulum stress sensor IRE1alpha in liver regenerative responses. Journal of hepatology 62, 590-598, doi:10.1016/j.jhep.2014.10.022 (2015).
83 Jwa, M. & Chang, P. PARP16 is a tail-anchored endoplasmic reticulum protein required for the PERK and IRE1α-mediated unfolded protein response. Nature cell biology 14, 1223-1230 (2012).
84 He, Y. et al. Nonmuscle Myosin IIB Links Cytoskeleton to IRE1α Signaling during ER Stress. Developmental cell 23, 1141-1152 (2012).
85 Mao, T. et al. PKA phosphorylation couples hepatic inositol-requiring enzyme 1α to glucagon signaling in glucose metabolism. Proceedings of the National Academy of Sciences of the United States of America 108, 15852-15857 (2011).
86 Morita, S. et al. Targeting ABL-IRE1alpha Signaling Spares ER-Stressed Pancreatic beta Cells to Reverse Autoimmune Diabetes. Cell metabolism 25, 883-897 e888, doi:10.1016/j.cmet.2017.03.018 (2017).
87 Brozzi, F. et al. A combined "omics" approach identifies N-Myc interactor as a novel cytokine-induced regulator of IRE1 protein and c-Jun N-terminal kinase in pancreatic beta cells. The Journal of biological chemistry 289, 20677-20693, doi:10.1074/jbc.M114.568808 (2014).
88 Plumb, R., Zhang, Z. R., Appathurai, S. & Mariappan, M. A functional link between the co-translational protein translocation pathway and the UPR. eLife 4, doi:10.7554/eLife.07426 (2015).
89 Sundaram, A., Plumb, R., Appathurai, S. & Mariappan, M. The Sec61 translocon limits IRE1α signaling during the unfolded protein response. eLife 6 (2017).
90 Lu, G. et al. PPM1l encodes an inositol requiring-protein 1 (IRE1) specific phosphatase that regulates the functional outcome of the ER stress response(). Molecular Metabolism 2, 405-416 (2013).
91 Lisbona, F. et al. BAX Inhibitor-1 is a negative regulator of the ER stress sensor IRE1α. Molecular cell 33, 679-691 (2009).
92 Eletto, D., Eletto, D., Dersh, D., Gidalevitz, T. & Argon, Y. Protein disulfide isomerase A6 controls the decay of IRE1alpha signaling via disulfide-dependent association. Molecular cell 53, 562-576, doi:10.1016/j.molcel.2014.01.004 (2014).
93 Pinkaew, D. et al. Fortilin binds IRE1alpha and prevents ER stress from signaling apoptotic cell death. Nature communications 8, 18, doi:10.1038/s41467-017-00029-1 (2017).

94 Tschurtschenthaler, M. et al. Defective ATG16L1-mediated removal of IRE1alpha drives Crohn's disease-like ileitis. The Journal of experimental medicine 214, 401-422, doi:10.1084/jem.20160791 (2017).
95 Sun, S. et al. IRE1alpha is an endogenous substrate of endoplasmic-reticulum-associated degradation. Nature cell biology 17, 1546-1555, doi:10.1038/ncb3266 (2015).
96 Zeng, L. et al. Vascular endothelial cell growth-activated XBP1 splicing in endothelial cells is crucial for angiogenesis. Circulation 127, 1712-1722, doi:10.1161/circulationaha.112.001337 (2013).
97 Kitai, Y. et al. Membrane lipid saturation activates IRE1alpha without inducing clustering. Genes to cells : devoted to molecular & cellular mechanisms 18, 798-809, doi:10.1111/gtc.12074 (2013).
98 van Anken, E. et al. Sequential waves of functionally related proteins are expressed when B cells prepare for antibody secretion. Immunity 18, 243-253 (2003).
99 Chevet, E., Hetz, C. & Samali, A. Endoplasmic reticulum stress-activated cell reprogramming in oncogenesis. Cancer discovery 5, 586-597, doi:10.1158/2159-8290.cd-14-1490 (2015).
100 Hur, K. Y. et al. IRE1alpha activation protects mice against acetaminophen-induced hepatotoxicity. The Journal of experimental medicine 209, 307-318, doi:10.1084/jem.20111298 (2012).
101 Ron, D. & Walter, P. Signal integration in the endoplasmic reticulum unfolded protein response. Nature reviews. Molecular cell biology 8, 519-529, doi:10.1038/nrm2199 (2007).
102 Pakos-Zebrucka, K. et al. The integrated stress response. EMBO reports 17, 1374-1395, doi:10.15252/embr.201642195 (2016).
103 Del Vecchio, C. A. et al. De-differentiation confers multidrug resistance via noncanonical PERK-Nrf2 signaling. PLoS Biol 12, e1001945, doi:10.1371/journal.pbio.1001945
PBIOLOGY-D-14-00485 [pii] (2014).
104 Chen, X. et al. XBP1 promotes triple-negative breast cancer by controlling the HIF1alpha pathway. Nature, doi:10.1038/nature13119 (2014).
105 Luo, S., Baumeister, P., Yang, S., Abcouwer, S. F. & Lee, A. S. Induction of Grp78/BiP by translational block: activation of the Grp78 promoter by ATF4 through and upstream ATF/CRE site independent of the endoplasmic reticulum stress elements. The Journal of biological chemistry 278, 37375-37385, doi:10.1074/jbc.M303619200 (2003).
106 Han, D. et al. IRE1alpha kinase activation modes control alternate endoribonuclease outputs to determine divergent cell fates. Cell 138, 562-575, doi:10.1016/j.cell.2009.07.017 (2009).
107 Mao, C., Tai, W. C., Bai, Y., Poizat, C. & Lee, A. S. In vivo regulation of Grp78/BiP transcription in the embryonic heart: role of the endoplasmic reticulum stress response element and GATA-4. The Journal of biological chemistry 281, 8877-8887, doi:10.1074/jbc.M505784200 (2006).
108 Kamagate, A. et al. FoxO1 links hepatic insulin action to endoplasmic reticulum stress. Endocrinology 151, 3521-3535, doi:10.1210/en.2009-1306 (2010).
109 Misra, U. K., Wang, F. & Pizzo, S. V. Transcription factor TFII-I causes transcriptional upregulation of GRP78 synthesis in prostate cancer cells. Journal of cellular biochemistry 106, 381-389, doi:10.1002/jcb.22016 (2009).

110 Ramsay, R. G., Ciznadija, D., Mantamadiotis, T., Anderson, R. & Pearson, R. Expression of stress response protein glucose regulated protein-78 mediated by c-Myb. The international journal of biochemistry & cell biology 37, 1254-1268, doi:10.1016/j.biocel.2004.12.011 (2005).
111 Song, M. S., Park, Y. K., Lee, J. H. & Park, K. Induction of glucose-regulated protein 78 by chronic hypoxia in human gastric tumor cells through a protein kinase C-epsilon/ERK/AP-1 signaling cascade. Cancer research 61, 8322-8330 (2001).
112 Odani, N. et al. Regulation of BiP gene expression by cyclopentenone prostaglandins through unfolded protein response element. The Journal of biological chemistry 271, 16609-16613 (1996).
113 Deegan, S. et al. Deficiency in the mitochondrial apoptotic pathway reveals the toxic potential of autophagy under ER stress conditions. Autophagy 10, 1921-1936, doi:10.4161/15548627.2014.981790 (2014).
114 Elmore, S. Apoptosis: A Review of Programmed Cell Death. Toxicologic pathology 35, 495-516 (2007).
115 Szegezdi, E., Macdonald, D. C., Ni Chonghaile, T., Gupta, S. & Samali, A. Bcl-2 family on guard at the ER. American journal of physiology. Cell physiology 296, C941-953, doi:10.1152/ajpcell.00612.2008 (2009).
116 Iwawaki, T., Akai, R., Yamanaka, S. & Kohno, K. Function of IRE1 alpha in the placenta is essential for placental development and embryonic viability. Proceedings of the National Academy of Sciences of the United States of America 106, 16657-16662, doi:10.1073/pnas.0903775106 (2009).
117 Reimold, A. M. et al. An essential role in liver development for transcription factor XBP-1. Genes & development 14, 152-157 (2000).
118 Hasegawa, D. et al. Epithelial Xbp1 is Required for Cellular Proliferation and Differentiation During Mammary Gland Development. Mol Cell Biol, doi:10.1128/mcb.00136-15 (2015).
119 Davis, K. R. et al. XBP1 Regulates the Biosynthetic Capacity of the Mammary Gland During Lactation by Controlling Epithelial Expansion and Endoplasmic Reticulum Formation. Endocrinology 157, 417-428, doi:10.1210/en.2015-1676 (2016).
120 Reimold, A. M. et al. Plasma cell differentiation requires the transcription factor XBP-1. Nature 412, 300-307, doi:10.1038/35085509 (2001).
121 Kamimura, D. & Bevan, M. J. Endoplasmic reticulum stress regulator XBP-1 contributes to effector CD8+ T cell differentiation during acute infection. Journal of immunology (Baltimore, Md. : 1950) 181, 5433-5441 (2008).
122 Iwakoshi, N. N., Pypaert, M. & Glimcher, L. H. The transcription factor XBP-1 is essential for the development and survival of dendritic cells. The Journal of experimental medicine 204, 2267-2275, doi:10.1084/jem.20070525 (2007).
123 Osorio, F. et al. The unfolded-protein-response sensor IRE-1alpha regulates the function of CD8alpha+ dendritic cells. Nature immunology 15, 248-257, doi:10.1038/ni.2808 (2014).
124 Cubillos-Ruiz, J. R. et al. ER Stress Sensor XBP1 Controls Anti-tumor Immunity by Disrupting Dendritic Cell Homeostasis. Cell 161, 1527-1538, doi:10.1016/j.cell.2015.05.025 (2015).
125 Bettigole, S. E. et al. The transcription factor XBP1 is selectively required for eosinophil differentiation. Nature immunology 16, 829-837, doi:10.1038/ni.3225 (2015).

126 Kaser, A. et al. XBP1 links ER stress to intestinal inflammation and confers genetic risk for human inflammatory bowel disease. Cell 134, 743-756, doi:10.1016/j.cell.2008.07.021 (2008).
127 Tavernier, S. J. et al. Regulated IRE1-dependent mRNA decay sets the threshold for dendritic cell survival. Nature cell biology 19, 698-710, doi:10.1038/ncb3518 (2017).
128 Benhamron, S. et al. Regulated IRE1-dependent decay participates in curtailing immunoglobulin secretion from plasma cells. European journal of immunology 44, 867-876, doi:10.1002/eji.201343953 (2014).
129 Cubillos-Ruiz, J. R., Bettigole, S. E. & Glimcher, L. H. Tumorigenic and Immunosuppressive Effects of Endoplasmic Reticulum Stress in Cancer. Cell 168, 692-706, doi:10.1016/j.cell.2016.12.004 (2017).
130 Dejeans, N. et al. Autocrine control of glioma cells adhesion and migration through IRE1alpha-mediated cleavage of SPARC mRNA. Journal of cell science 125, 4278-4287, doi:10.1242/jcs.099291 (2012).
131 Urra, H. et al. IRE1alpha governs cytoskeleton remodelling and cell migration through a direct interaction with filamin A. Nature cell biology 20, 942-953, doi:10.1038/s41556-018-0141-0 (2018).
132 Valdes, P. et al. Control of dopaminergic neuron survival by the unfolded protein response transcription factor XBP1. Proceedings of the National Academy of Sciences of the United States of America 111, 6804-6809, doi:10.1073/pnas.1321845111 (2014).
133 Semenza, G. L. Hypoxia-inducible factors in physiology and medicine. Cell 148, 399-408, doi:10.1016/j.cell.2012.01.021 (2012).
134 Lhomond, S. et al. Dual IRE1 RNase functions dictate glioblastoma development. EMBO molecular medicine, doi:10.15252/emmm.201707929 (2018).
135 Romero-Ramirez, L. et al. XBP1 is essential for survival under hypoxic conditions and is required for tumor growth. Cancer research 64, 5943-5947, doi:10.1158/0008-5472.can-04-1606 (2004).
136 Pluquet, O. et al. Posttranscriptional regulation of PER1 underlies the oncogenic function of IREalpha. Cancer research 73, 4732-4743, doi:10.1158/0008-5472.can-12-3989 (2013).
137 Nagy, P., Varga, A., Pircs, K., Hegedus, K. & Juhasz, G. Myc-driven overgrowth requires unfolded protein response-mediated induction of autophagy and antioxidant responses in Drosophila melanogaster. PLoS genetics 9, e1003664, doi:10.1371/journal.pgen.1003664 (2013).
138 Hart, L. S. et al. ER stress-mediated autophagy promotes Myc-dependent transformation and tumor growth. The Journal of clinical investigation 122, 4621-4634, doi:10.1172/jci62973 (2012).
139 Sheshadri, N. et al. SCCA1/SERPINB3 promotes oncogenesis and epithelial-mesenchymal transition via the unfolded protein response and IL6 signaling. Cancer research 74, 6318-6329, doi:10.1158/0008-5472.can-14-0798 (2014).
140 Lin, Y. G. et al. Targeting the glucose-regulated protein-78 abrogates Pten-null driven AKT activation and endometrioid tumorigenesis. Oncogene 34, 5418-5426, doi:10.1038/onc.2015.4 (2015).
141 Fu, Y. et al. Pten null prostate tumorigenesis and AKT activation are blocked by targeted knockout of ER chaperone GRP78/BiP in prostate epithelium. Proceedings of the National Academy of Sciences of the United States of America 105, 19444-19449, doi:10.1073/pnas.0807691105 (2008).

142 Denoyelle, C. et al. Anti-oncogenic role of the endoplasmic reticulum differentially activated by mutations in the MAPK pathway. Nature cell biology 8, 1053-1063, doi:10.1038/ncb1471 (2006).
143 Huber, A. L. et al. p58(IPK)-mediated attenuation of the proapoptotic PERK-CHOP pathway allows malignant progression upon low glucose. Molecular cell 49, 1049-1059, doi:10.1016/j.molcel.2013.01.009 (2013).
144 Avril, T., Vauleon, E. & Chevet, E. Endoplasmic reticulum stress signaling and chemotherapy resistance in solid cancers. Oncogenesis 6, e373, doi:10.1038/oncsis.2017.72 (2017).
145 Ohashi, A. et al. Aneuploidy generates proteotoxic stress and DNA damage concurrently with p53-mediated post-mitotic apoptosis in SAC-impaired cells. Nature communications 6 (2015).
146 Dongre, A. & Weinberg, R. A. New insights into the mechanisms of epithelial-mesenchymal transition and implications for cancer. Nature reviews. Molecular cell biology, doi:10.1038/s41580-018-0080-4 (2018).
147 Avivar-Valderas, A. et al. PERK integrates autophagy and oxidative stress responses to promote survival during extracellular matrix detachment. Mol Cell Biol 31, 3616-3629, doi:10.1128/mcb.05164-11 (2011).
148 Mujcic, H. et al. Hypoxic activation of the unfolded protein response (UPR) induces expression of the metastasis-associated gene LAMP3. Radiotherapy and oncology : journal of the European Society for Therapeutic Radiology and Oncology 92, 450-459, doi:10.1016/j.radonc.2009.08.017 (2009).
149 Mahadevan, N. R. et al. Transmission of endoplasmic reticulum stress and pro-inflammation from tumor cells to myeloid cells. Proceedings of the National Academy of Sciences of the United States of America 108, 6561-6566, doi:10.1073/pnas.1008942108 (2011).
150 Condamine, T. et al. Lectin-type oxidized LDL receptor-1 distinguishes population of human polymorphonuclear myeloid-derived suppressor cells in cancer patients. Science immunology 1, doi:10.1126/sciimmunol.aaf8943 (2016).
151 Blazanin, N. et al. ER stress and distinct outputs of the IRE1alpha RNase control proliferation and senescence in response to oncogenic Ras. Proceedings of the National Academy of Sciences of the United States of America 114, 9900-9905, doi:10.1073/pnas.1701757114 (2017).
152 Perou, C. M. et al. Molecular portraits of human breast tumours. Nature 406, 747-752, doi:10.1038/35021093 (2000).
153 Qiu, J. et al. Comparison of Clinicopathological Features and Prognosis in Triple-Negative and Non-Triple Negative Breast Cancer. Journal of Cancer 7, 167-173, doi:10.7150/jca.10944 (2016).
154 Prat, A. et al. Clinical implications of the intrinsic molecular subtypes of breast cancer. Breast (Edinburgh, Scotland) 24 Suppl 2, S26-35, doi:10.1016/j.breast.2015.07.008 (2015).
155 Ruan, Q. et al. Development of an anti-angiogenic therapeutic model combining scAAV2-delivered siRNAs and noninvasive photoacoustic imaging of tumor vasculature development. Cancer letters 332, 120-129 (2013).
156 Andruska, N., Zheng, X., Yang, X., Helferich, W. G. & Shapiro, D. J. Anticipatory estrogen activation of the unfolded protein response is linked to cell proliferation and poor survival in estrogen receptor alpha-positive breast cancer. Oncogene 34, 3760-3769, doi:10.1038/onc.2014.292 (2015).

157 Bobrovnikova-Marjon, E. et al. PERK promotes cancer cell proliferation and tumor growth by limiting oxidative DNA damage. Oncogene 29, 3881-3895 (2010).
158 Mujcic, H. et al. Hypoxic activation of the PERK/eIF2alpha arm of the unfolded protein response promotes metastasis through induction of LAMP3. Clinical cancer research : an official journal of the American Association for Cancer Research 19, 6126-6137, doi:10.1158/1078-0432.ccr-13-0526 (2013).
159 Pike, L. R. et al. Transcriptional up-regulation of ULK1 by ATF4 contributes to cancer cell survival. Biochem J 449, 389-400, doi:10.1042/BJ20120972 BJ20120972 [pii] (2013).
160 Nagelkerke, A. et al. Hypoxia stimulates migration of breast cancer cells via the PERK/ATF4/LAMP3-arm of the unfolded protein response. Breast cancer research : BCR 15, R2, doi:10.1186/bcr3373 bcr3373 [pii] (2013).
161 Schaaf, M. B. et al. The autophagy associated gene, ULK1, promotes tolerance to chronic and acute hypoxia. Radiotherapy and oncology : journal of the European Society for Therapeutic Radiology and Oncology 108, 529-534, doi:10.1016/j.radonc.2013.06.015 (2013).
162 Comprehensive molecular portraits of human breast tumours. Nature 490, 61-70, doi:10.1038/nature11412 (2012).
163 Scriven, P. et al. Activation and clinical significance of the unfolded protein response in breast cancer. British journal of cancer 101, 1692-1698, doi:10.1038/sj.bjc.6605365 (2009).
164 Greenman, C. et al. Patterns of somatic mutation in human cancer genomes. Nature 446, 153-158, doi:10.1038/nature05610 (2007).
165 Nik-Zainal, S. et al. Landscape of somatic mutations in 560 breast cancer whole genome sequences. Nature 534, 47-54 (2016).
166 Spiotto, M. T. et al. Imaging the unfolded protein response in primary tumors reveals microenvironments with metabolic variations that predict tumor growth. Cancer research 70, 78-88, doi:10.1158/0008-5472.CAN-09-2747 (2010).
167 Yager, J. D. & Davidson, N. E. Estrogen carcinogenesis in breast cancer. The New England journal of medicine 354, 270-282, doi:10.1056/NEJMra050776 (2006).
168 Lacroix, M. & Leclercq, G. About GATA3, HNF3A, and XBP1, three genes co-expressed with the oestrogen receptor-alpha gene (ESR1) in breast cancer. Molecular and cellular endocrinology 219, 1-7, doi:10.1016/j.mce.2004.02.021 (2004).
169 Carroll, J. S. et al. Chromosome-wide mapping of estrogen receptor binding reveals long-range regulation requiring the forkhead protein FoxA1. Cell 122, 33-43, doi:10.1016/j.cell.2005.05.008 (2005).
170 Ding, L. et al. Ligand-independent activation of estrogen receptor alpha by XBP-1. Nucleic acids research 31, 5266-5274 (2003).
171 Fang, Y. et al. XBP-1 increases ERalpha transcriptional activity through regulation of large-scale chromatin unfolding. Biochemical and biophysical research communications 323, 269-274, doi:10.1016/j.bbrc.2004.08.100 (2004).
172 Hu, R. et al. NF-kappaB signaling is required for XBP1 (unspliced and spliced)-mediated effects on antiestrogen responsiveness and cell fate

decisions in breast cancer. Mol Cell Biol 35, 379-390, doi:10.1128/mcb.00847-14 (2015).
173 Wang, D. Y., Fulthorpe, R., Liss, S. N. & Edwards, E. A. Identification of estrogen-responsive genes by complementary deoxyribonucleic acid microarray and characterization of a novel early estrogen-induced gene: EEIG1. Molecular endocrinology (Baltimore, Md.) 18, 402-411, doi:10.1210/me.2003-0202 (2004).
174 Gomez, B. P. et al. Human X-box binding protein-1 confers both estrogen independence and antiestrogen resistance in breast cancer cell lines. FASEB journal : official publication of the Federation of American Societies for Experimental Biology 21, 4013-4027, doi:10.1096/fj.06-7990com (2007).
175 Sengupta, S., Sharma, C. G. N. & Jordan, V. C. Estrogen regulation of X-box binding protein-1 and its role in estrogen induced growth of breast and endometrial cancer cells. Hormone Molecular Biology and Clinical Investigation 2, doi:10.1515/hmbci.2010.025 (2010).
176 Hetz, C., Chevet, E. & Harding, H. P. Targeting the unfolded protein response in disease. Nature reviews. Drug discovery 12, 703-719, doi:10.1038/nrd3976 (2013).
177 Maurel, M. et al. Controlling the unfolded protein response-mediated life and death decisions in cancer. Seminars in cancer biology 33, 57-66, doi:10.1016/j.semcancer.2015.03.003 (2015).
178 Vincenz, L., Jager, R., O'Dwyer, M. & Samali, A. Endoplasmic reticulum stress and the unfolded protein response: targeting the Achilles heel of multiple myeloma. Molecular cancer therapeutics 12, 831-843, doi:10.1158/1535-7163.MCT-12-0782 (2013).
179 Jiang, D. et al. Identification of Doxorubicin as an Inhibitor of the IRE1α-XBP1 Axis of the Unfolded Protein Response. Scientific reports 6 (2016).
180 Sanches, M. et al. Structure and mechanism of action of the hydroxy aryl aldehyde class of IRE1 endoribonuclease inhibitors. Nature communications 5, 4202 (2014).
181 Ming, J. et al. A novel chemical, STF-083010, reverses tamoxifen-related drug resistance in breast cancer by inhibiting IRE1/XBP1. Oncotarget 6, 40692-40703 (2015).
182 Zhao, N. et al. Pharmacological targeting of MYC-regulated IRE1/XBP1 pathway suppresses MYC-driven breast cancer. The Journal of clinical investigation 128, 1283-1299, doi:10.1172/jci95873 (2018).
183 J.C., O. Venny: An interactive tool for comparing lists with Venn's diagrams., <http://bioinfogp.cnb.csic.es/tools/venny/index.html> (2007-2015).
184 Coelho, D. S. & Domingos, P. M. Physiological roles of regulated Ire1 dependent decay. Frontiers in genetics 5, 76, doi:10.3389/fgene.2014.00076 (2014).
185 Bartels, K., Grenz, A. & Eltzschig, H. K. Hypoxia and inflammation are two sides of the same coin. Proceedings of the National Academy of Sciences of the United States of America 110, 18351-18352, doi:10.1073/pnas.1318345110 (2013).
186 Vander Heiden, M. G., Cantley, L. C. & Thompson, C. B. Understanding the Warburg effect: the metabolic requirements of cell proliferation. Science 324, 1029-1033, doi:10.1126/science.1160809 (2009).

187 Brizel, D. M. et al. Tumor oxygenation predicts for the likelihood of distant metastases in human soft tissue sarcoma. Cancer research 56, 941-943 (1996).
188 Chun, Y. S., Adusumilli, P. S. & Fong, Y. Employing tumor hypoxia for oncolytic therapy in breast cancer. Journal of mammary gland biology and neoplasia 10, 311-318, doi:10.1007/s10911-006-9004-6 (2005).
189 Semenza, G. L. Regulation of oxygen homeostasis by hypoxia-inducible factor 1. Physiology (Bethesda, Md.) 24, 97-106, doi:10.1152/physiol.00045.2008 (2009).
190 Vaupel, P. & Mayer, A. Hypoxia in cancer: significance and impact on clinical outcome. Cancer metastasis reviews 26, 225-239, doi:10.1007/s10555-007-9055-1 (2007).
191 Semenza, G. L. & Wang, G. L. A nuclear factor induced by hypoxia via de novo protein synthesis binds to the human erythropoietin gene enhancer at a site required for transcriptional activation. Mol Cell Biol 12, 5447-5454 (1992).
192 Bruick, R. K. & McKnight, S. L. A conserved family of prolyl-4-hydroxylases that modify HIF. Science 294, 1337-1340, doi:10.1126/science.1066373 (2001).
193 Kamura, T. et al. Activation of HIF1alpha ubiquitination by a reconstituted von Hippel-Lindau (VHL) tumor suppressor complex. Proceedings of the National Academy of Sciences of the United States of America 97, 10430-10435, doi:10.1073/pnas.190332597 (2000).
194 Wang, G. L., Jiang, B. H., Rue, E. A. & Semenza, G. L. Hypoxia-inducible factor 1 is a basic-helix-loop-helix-PAS heterodimer regulated by cellular O2 tension. Proceedings of the National Academy of Sciences of the United States of America 92, 5510-5514 (1995).
195 Foulkes, W. D., Smith, I. E. & Reis-Filho, J. S. Triple-negative breast cancer. The New England journal of medicine 363, 1938-1948, doi:10.1056/NEJMra1001389 (2010).
196 Johnson, A. B., Denko, N. & Barton, M. C. Hypoxia induces a novel signature of chromatin modifications and global repression of transcription. Mutation research 640, 174-179 (2008).
197 Bettigole, S. E. & Glimcher, L. H. Endoplasmic reticulum stress in immunity. Annual review of immunology 33, 107-138, doi:10.1146/annurev-immunol-032414-112116 (2015).
198 Rojas-Rivera, D. et al. When PERK inhibitors turn out to be new potent RIPK1 inhibitors: critical issues on the specificity and use of GSK2606414 and GSK2656157. Cell death and differentiation, doi:10.1038/cdd.2017.58 (2017).
199 Lambert, A. W., Pattabiraman, D. R. & Weinberg, R. A. Emerging Biological Principles of Metastasis. Cell 168, 670-691, doi:10.1016/j.cell.2016.11.037 (2017).
200 Aceto, N. et al. Circulating tumor cell clusters are oligoclonal precursors of breast cancer metastasis. Cell 158, 1110-1122, doi:10.1016/j.cell.2014.07.013 (2014).
201 Korge, B. P. & Krieg, T. The molecular basis for inherited bullous diseases. Journal of molecular medicine (Berlin, Germany) 74, 59-70 (1996).
202 Li, J. Alterations in cell adhesion proteins and cardiomyopathy. World Journal of Cardiology 6, 304-313 (2014).

203 Friedl, P. & Wolf, K. Tumour-cell invasion and migration: diversity and escape mechanisms. Nature reviews. Cancer 3, 362-374, doi:10.1038/nrc1075 (2003).
204 Evans, W. H. & Martin, P. E. Gap junctions: structure and function (Review). Molecular membrane biology 19, 121-136, doi:10.1080/09687680210139839 (2002).
205 Lodish H et al. in Molecular Cell Biology, 4th Edition (W. H. Freeman, 2000).
206 Aktary, Z., Alaee, M. & Pasdar, M. Beyond cell-cell adhesion: Plakoglobin and the regulation of tumorigenesis and metastasis. Oncotarget 8, 32270-32291, doi:10.18632/oncotarget.15650 (2017).
207 Li, J. et al. Cardiac tissue-restricted deletion of plakoglobin results in progressive cardiomyopathy and activation of {beta}-catenin signaling. Mol Cell Biol 31, 1134-1144, doi:10.1128/mcb.01025-10 (2011).
208 McKoy, G. et al. Identification of a deletion in plakoglobin in arrhythmogenic right ventricular cardiomyopathy with palmoplantar keratoderma and woolly hair (Naxos disease). Lancet (London, England) 355, 2119-2124, doi:10.1016/s0140-6736(00)02379-5 (2000).
209 Bierkamp, C., McLaughlin, K. J., Schwarz, H., Huber, O. & Kemler, R. Embryonic heart and skin defects in mice lacking plakoglobin. Developmental biology 180, 780-785, doi:10.1006/dbio.1996.0346 (1996).
210 Lamouille, S., Xu, J. & Derynck, R. Molecular mechanisms of epithelial–mesenchymal transition. Nature reviews. Molecular cell biology 15, 178-196 (2014).
211 Holen, I. et al. Loss of plakoglobin promotes decreased cell-cell contact, increased invasion, and breast cancer cell dissemination in vivo. Breast cancer research : BCR 14, R86 (2012).
212 Goto, W. et al. Circulating tumor cell clusters-associated gene plakoglobin is a significant prognostic predictor in patients with breast cancer. Biomarker Research 5 (2017).
213 Todorović, V. et al. Plakoglobin regulates cell motility through Rho- and fibronectin-dependent Src signaling. Journal of cell science 123, 3576-3586, doi:10.1242/jcs.070391 (2010).
214 Bukholm, I. K., Nesland, J. M. & Borresen-Dale, A. L. Re-expression of E-cadherin, alpha-catenin and beta-catenin, but not of gamma-catenin, in metastatic tissue from breast cancer patients [seecomments]. The Journal of pathology 190, 15-19, doi:10.1002/(sici)1096-9896(200001)190:1<15::aid-path489>3.0.co;2-l (2000).
215 Park, D., Karesen, R., Axcrona, U., Noren, T. & Sauer, T. Expression pattern of adhesion molecules (E-cadherin, alpha-, beta-, gamma-catenin and claudin-7), their influence on survival in primary breast carcinoma, and their corresponding axillary lymph node metastasis. APMIS : acta pathologica, microbiologica, et immunologica Scandinavica 115, 52-65, doi:10.1111/j.1600-0463.2007.apm_524.x (2007).
216 Lee, A. H., Scapa, E. F., Cohen, D. E. & Glimcher, L. H. Regulation of hepatic lipogenesis by the transcription factor XBP1. Science 320, 1492-1496, doi:10.1126/science.1158042 (2008).
217 Bright, M. D., Itzhak, D. N., Wardell, C. P., Morgan, G. J. & Davies, F. E. Cleavage of BLOC1S1 mRNA by IRE1 Is Sequence Specific, Temporally Separate from XBP1 Splicing, and Dispensable for Cell Viability under

Acute Endoplasmic Reticulum Stress. Mol Cell Biol 35, 2186-2202, doi:10.1128/mcb.00013-15 (2015).
218 Bernaudo, S. et al. Cyclin G2 inhibits epithelial-to-mesenchymal transition by disrupting Wnt/β-catenin signaling. Oncogene 35, 4816-4827 (2016).
219 Jiang, Y., Goldberg, I. D. & Shi, Y. E. Complex roles of tissue inhibitors of metalloproteinases in cancer. Oncogene 21, 2245-2252, doi:10.1038/sj.onc.1205291 (2002).
220 Cui, S. et al. The emerging role of inhibitor of growth 4 as a tumor suppressor in multiple human cancers. Cellular physiology and biochemistry : international journal of experimental cellular physiology, biochemistry, and pharmacology 36, 409-422, doi:10.1159/000430108 (2015).
221 Bailey, C. K., Mittal, M. K., Misra, S. & Chaudhuri, G. High motility of triple-negative breast cancer cells is due to repression of plakoglobin gene by metastasis modulator protein SLUG. The Journal of biological chemistry 287, 19472-19486, doi:10.1074/jbc.M112.345728 (2012).
222 Rieger-Christ, K. M. et al. Restoration of plakoglobin expression in bladder carcinoma cell lines suppresses cell migration and tumorigenic potential. British journal of cancer 92, 2153-2159 (2005).
223 Obenauf, A. C. et al. Therapy-induced tumour secretomes promote resistance and tumour progression. Nature 520, 368-372, doi:10.1038/nature14336 (2015).
224 Bhola, N. E. et al. TGF-β inhibition enhances chemotherapy action against triple-negative breast cancer. The Journal of clinical investigation 123, 1348-1358 (2013).
225 Samanta, D., Gilkes, D. M., Chaturvedi, P., Xiang, L. & Semenza, G. L. Hypoxia-inducible factors are required for chemotherapy resistance of breast cancer stem cells. Proceedings of the National Academy of Sciences of the United States of America 111, E5429-5438, doi:10.1073/pnas.1421438111 (2014).
226 Hartman, Z. C. et al. Growth of triple-negative breast cancer cells relies upon coordinate autocrine expression of the proinflammatory cytokines IL-6 and IL-8. Cancer research 73, 3470-3480, doi:10.1158/0008-5472.CAN-12-4524-T (2013).
227 Sansone, P. et al. IL-6 triggers malignant features in mammospheres from human ductal breast carcinoma and normal mammary gland. The Journal of clinical investigation 117, 3988-4002, doi:10.1172/JCI32533 (2007).
228 Acharyya, S. et al. A CXCL1 paracrine network links cancer chemoresistance and metastasis. Cell 150, 165-178, doi:10.1016/j.cell.2012.04.042 (2012).
229 Bhola, N. E. et al. TGF-beta inhibition enhances chemotherapy action against triple-negative breast cancer. The Journal of clinical investigation 123, 1348-1358, doi:10.1172/JCI65416 (2013).
230 Arnal, I. & Wade, R. H. How does taxol stabilize microtubules? Current biology : CB 5, 900-908 (1995).
231 Grimshaw, M. J. et al. Mammosphere culture of metastatic breast cancer cells enriches for tumorigenic breast cancer cells. Breast cancer research : BCR 10, R52, doi:10.1186/bcr2106 (2008).
232 Grivennikov, S. I., Greten, F. R. & Karin, M. Immunity, inflammation, and cancer. Cell 140, 883-899, doi:10.1016/j.cell.2010.01.025 (2010).

233 Eubank, T. D. et al. GM-CSF INHIBITS BREAST CANCER GROWTH AND METASTASIS BY INVOKING AN ANTI-ANGIOGENIC PROGRAM IN TUMOR-EDUCATED MACROPHAGES. Cancer research 69, 2133-2140 (2009).
234 Fujimoto, A. et al. Inhibition of endoplasmic reticulum (ER) stress sensors sensitizes cancer stem-like cells to ER stress-mediated apoptosis. Oncotarget 7, 51854-51864 (2016).
235 Tong, C. W. S., Wu, M., Cho, W. C. S. & To, K. K. W. Recent Advances in the Treatment of Breast Cancer. Frontiers in Oncology 8, doi:10.3389/fonc.2018.00227 (2018).
236 Bergers, G. & Hanahan, D. Modes of resistance to anti-angiogenic therapy. Nature reviews. Cancer 8, 592-603, doi:10.1038/nrc2442 (2008).
237 Henry, K. A., Blank, H. M., Hoose, S. A. & Polymenis, M. The unfolded protein response is not necessary for the G1/S transition, but it is required for chromosome maintenance in Saccharomyces cerevisiae. PLoS One 5, e12732, doi:10.1371/journal.pone.0012732 (2010).
238 Rose, A. A. N., Biondini, M., Curiel, R. & Siegel, P. M. Targeting GPNMB with glembatumumab vedotin: Current developments and future opportunities for the treatment of cancer. Pharmacology & therapeutics 179, 127-141, doi:10.1016/j.pharmthera.2017.05.010 (2017).
239 Noda, Y. et al. GPNMB Induces BiP Expression by Enhancing Splicing of BiP Pre-mRNA during the Endoplasmic Reticulum Stress Response. Scientific reports 7 (2017).
240 Lee, B. R. et al. Elevated endoplasmic reticulum stress reinforced immunosuppression in the tumor microenvironment via myeloid-derived suppressor cells. Oncotarget 5, 12331-12345, doi:10.18632/oncotarget.2589 (2014).
241 Li, J. et al. Targeting Interleukin-6 (IL-6) Sensitizes Anti-PD-L1 Treatment in a Colorectal Cancer Preclinical Model. Medical Science Monitor : International Medical Journal of Experimental and Clinical Research 24, 5501-5508, doi:10.12659/msm.907439 (2018).
242 Sun, L. et al. Gastric cancer mesenchymal stem cells derived IL-8 induces PD-L1 expression in gastric cancer cells via STAT3/mTOR-c-Myc signal axis. Cell death & disease 9, doi:10.1038/s41419-018-0988-9 (2018).
243 Quezada, S. A., Peggs, K. S., Curran, M. A. & Allison, J. P. CTLA4 blockade and GM-CSF combination immunotherapy alters the intratumor balance of effector and regulatory T cells. The Journal of clinical investigation 116, 1935-1945, doi:10.1172/jci27745 (2006).
244 Giavridis, T. et al. CAR T cell-induced cytokine release syndrome is mediated by macrophages and abated by IL-1 blockade. Nature medicine 24, 731-738, doi:10.1038/s41591-018-0041-7 (2018).
245 Li, W. et al. Engineering ER-stress dependent non-conventional mRNA splicing. eLife 7, doi:10.7554/eLife.35388 (2018).

Appendix A: STR-typing of MDA-MB-231 cells

Cell Line Authentication Service
STR Profile Report

Sample Submitted By:	Apoptosis Research Centre National University of Ireland Susan Logue
Email Address:	susan.logue@nuigalway.ie
ATCC Sales Order:	SO0152500
FTA Barcode:	STRA7419
Cell Line Designation:	MDA MB 231
Date Sample Received:	Friday, October 06, 2017
Report Date:	Tuesday, October 10, 2017

Methodology: Seventeen short tandem repeat (STR) loci plus the gender determining locus, Amelogenin, were amplified XVLQJ WKH FRPPHUFLDOO\ DYDLODEOH 3RZHU3OH[Š ' .LW IURP 3URPHJD 7KH FHOO OLQH VDPSOH ZDV SURFHVVHG XVLQJ WKH $%, 3ULVPŠ [O *HQHWLF $QDO\]HU 'DWD ZHUH DQDO\]HG XVLQJ *HQH0DSSHUŠ ,' ; Y software (Applied Biosystems). Appropriate positive and negative controls were run and confirmed for each sample submitted.

Data Interpretation: Cell lines were authenticated using Short Tandem Repeat (STR) analysis as described in 2012 in ANSI Standard (ASN-0002) Authentication of Human Cell Lines: Standardization of STR Profiling by the ATCC Standards Development Organization (SDO) and in Capes-Davis et al., Match criteria for human cell line authentication: Where do we draw the line? Int. J. Cancer. 2012 Nov 8. doi: 10.1002/ijc.27931

ATCC performs STR Profiling following ISO 9001:2008 and ISO/IEC 17025:2005 quality standards.

Technical questions?

ATCC Technical Support
(800) 638-6597 / +1 703-365-2700
STRTechSupport@atcc.org

Ordering questions?

800-638-6597 or 703-365-2700
Fax 703-365-2750
Email: STRtesting@atcc.org

LGC Standards
Excellence through measurement

Cell Line Authentication Service
STR Profile Report

FTA Barcode: STRA7419

ATCC Sales Order: SO0152500

Test Results for Submitted Sample					ATCC Reference Database Profile			
Locus	**Query Profile: MDA MB 231**				**Database Profile: MDA-MB-231; Breast Adenocarcinoma; Human (Homo sapiens)**			
D3S1358	16							
TH01	7	9.3			7	9.3		
D21S11	30	33.2						
D18S51	11	16						
Penta_E	11							
D5S818	12				12			
D13S317	13				13			
D7S820	8	9			8	9		
D16S539	12				12			
CSF1PO	12	13			12	13		
Penta_D	11	14						
Amelogenin	X				X			
vWA	15	18			15	18		
D8S1179	13							
TPOX	8	9			8	9		
FGA	22	23						
D19S433	11	14						
D2S1338	20	21						
Number of shared alleles between query sample and database profile:								14
Total number of alleles in the database profile:								14
Percent match between the submitted sample and the database profile:								100

The allele match algorithm compares the 8 core loci plus amelogenin only, even though alleles from all loci will be reported when available.

NOTE: *Loci highlighted in grey (8 core STR loci plus Amelogenin) can be made public to verify cell identity. In order to protect the identity of the donor,* ***please do not publish*** *the allele calls from all the STR loci tested.*
Electropherograms showing raw data are attached.

Explanation of Test Results
Cell lines with 80% match are considered to be related; i.e., derived from a common ancestry. Cell lines with between a 55% to 80% match require further profiling for authentication of relatedness.

☐ The submitted sample profile is human, but not a match for any profile in the ATCC STR database.

☒ The submitted profile is an exact match for the following ATCC human cell line(s) in the ATCC STR database (8 core loci plus Amelogenin): HTB-26

☐ The submitted profile is similar to the following ATCC human cell line(s):

☐ An STR profile could not be generated.

Additional Comments:

Submitted sample, STRA7419 (MDA MB 231), is an exact match to ATCC cell line HTB-26 (MDA-MB-231).

e-Signature, Technician:	snicholson 10/10/2017
e-Signature, Reviewer:	kkindig 10/10/2017

LGC Standards
Excellence through measurement

Cell Line Authentication Service
STR Profile Report

FTA Barcode: STRA7419

ATCC Sales Order: SO0152500

Addendum: Comparative Output from the ATCC STR Profile Database

% Match	$7&&Š &DW No.	Designation	D5S818	D13S317	D7S820	D16S539	vWA	THO1	AMEL	TPOX	CSF1PO
100	STRA7419	MDA MB 231	12	13	8,9	12	15,18	7,9.3	X	8,9	12,13
100	HTB-26	MDA-MB-231; Breast Adenocarcinoma; Human (Homo sapiens)	12	13	8,9	12	15,18	7,9.3	X	8,9	12,13

Definitions of terms used in this report:

Peak Area Difference (PAD):
Refers to a heterozygous peak imbalance.
Two alleles at a single locus should amplify in a similar manner; and therefore produce peaks of similar height and area. Peaks which are above threshold (50 rfu) but are not of similar area, within 50% of each other, are referred to as a PAD. Due to their nature cell lines do not amplify in the same manner as a sample taken from a fresh buccal swab. PAD is far more common in cell line samples.

Stutter:
A stutter peak is a small peak which occurs immediately before the true peak. It is defined as being a single repeat unit smaller than the true peak. The stutter peak should be less than 15% of the true peak. The stutter is caused by the polymerase.

+4 Peak:
A +4 is similar to a stutter but occurs immediately after the true peak. A stutter peak should be less than 5% for a homozygous and 10% for a heterozygous.

Below Threshold Peak(s):
Cell lines can produce unusual profiles and occasionally a peak will amplify poorly and be below threshold. Where we find a below threshold peak which we believe is valid we indicate it as a below threshold peak. Our cell line analysis criteria, Homozygous and Heterozygous peaks must be equal to or above the set height threshold for it to be considered a true peak.

Ladder/ Off Ladder Peak(s):
The allelic ladder consists of most or all known alleles in the population and allows for precise assignment of alleles. Those which do not align are termed µoff ladder.

Artifact:
A non-allelic product of the amplification process, an anomaly of the detection process, or a by-product of primer synthesis

Pull-up:
A term used to describe when signal from one dye color channel produces artificial peaks in another, usually adjacent, color.

Spike:
An extraneous peak resulting from dust, dried polymer, an air bubble, or an electrical surge.
Dye blob:
Free dye not coupled to primer that can be injected into the capillary (A known and documented dye blob is often found at the D3S1358 locus.)

Germany

LGC Standards GmbH
Mercatorstrasse 51
46485 Wesel
Germany

Tel: +49 (0)281 9887 0
Fax: +49 (0)281 9887 199
Email: de@lgcstandards.com

Italy

LGC Standards S.r.l.
Via Venezia, 23
20099 Sesto San Giovanni
Italy

Tel: +39 02 2412 6830
Fax: +39 02 2412 6831
Email: it@lgcstandards.com

Spain

LGC Standards S.L.U.
C/Salvador Espriu 59, 2ž
SODQWD
08005 Barcelona
(VSDxD

Tel: +34 93 308 4181
Fax: +34 93 307 3612
Email: es@lgcstandards.com

France

LGC Standards SARL
6, Rue Alfred Kastler
B.P. 83076
67123 MOLSHEIM
FRANCE

7pO 33 (0)3 88 04 82 82
Fax: +33 (0)3 88 04 82 90
Email: fr@lgcstandards.com

Poland

LGC Standards Sp. z o.o.
ul. M. Konopnickiej 1
']LHNDQyZ /HÖQ\
05-092 ˆomianki
Poland

Tel: +48 (0)22 751 31 40
Fax: +48 (0)22 751 58 45
Email: pl@lgcstandards.com

UK

LGC Standards
Queens Road
Teddington
Middlesex
TW11 0LY, UK

Tel.: +44 (0)20 8943 8480
Fax: +44 (0)20 8943 7554
Email:uksales@lgcstandards.com


Applied Biosystems
GeneMapper® ID-X 1.2
Project: 20171009-SN-STR
Sample Name
SQ
STRA7419_MDA MB 231
D3S1358
TH01
D21S11
D18S51
Penta_E
90
150
210
270
330
390
450
3900
2600
1300
0
16
7
9.3
30
33.2
11
16
11
STRA7419_MDA MB 231
D5S818
D13S317
D7S820
D16S539
CSF1PO
Penta_D
90
150
210
270
330
390
450
3900
2600
1300
0
12
13
8
9
12
12
13
11
14

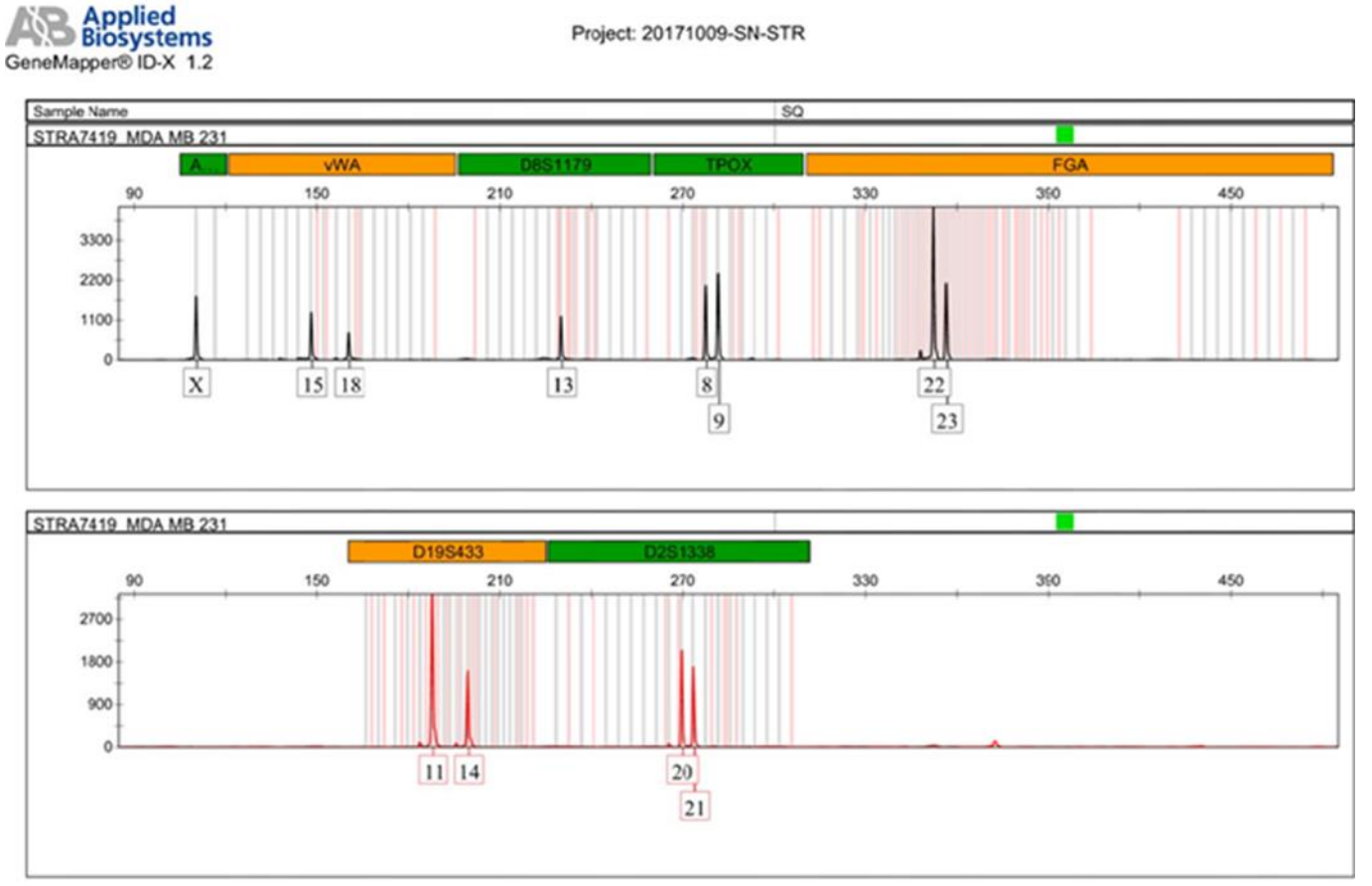
Applied Biosystems
GeneMapper® ID-X 1.2
Project: 20171009-SN-STR
Sample Name
SQ
STRA7419_MDA MB 231
A...
vWA
D8S1179
TPOX
FGA
90
150
210
270
330
390
450
3300
2200
1100
0
X
15
18
13
8
9
22
23
STRA7419_MDA MB 231
D19S433
D2S1338
90
150
210
270
330
390
450
2700
1800
900
0
11
14
20
21

Appendix B: Patient Information

ASLAB ID	TUM/TAN	Type	TUMOUR TYPE	TUMOURGRADE	PREDOMINANT HISTOLOGICAL INVASIVE TYPE	OESTROGEN RECEPTOR ALPHA	PROGESTERONE RECEPTOR	Her-2/Neu Hercept test	Breast Cancer Subtype	TRU TUMOUR SIZE IN mm
1	TUM	TNBC	Invasive	3	Ductal	Negative	Negative	Negative	Basal	30
2	TUM	TNBC	Invasive	3	Ductal	Negative	Negative	Negative	Basal	35
3	TUM	TNBC	Invasive	3	Ductal	Negative	Negative	Negative	Basal	15
4	TUM	TNBC	Invasive	3	Ductal	Negative	Negative	Negative	Basal	63
5	TUM	TNBC	NA	NA	NA	NA	NA	NA	NA	
6	TUM	LUMINAL	Invasive	2	Ductal	Positive	Positive	Negative	Luminal A	3
7	TUM	LUMINAL	Invasive	2	Ductal	Positive	Positive	Negative	Luminal A	29
8	TUM	LUMINAL	Invasive	2	Ductal	Positive	Positive	Negative	Luminal A	21
9	TUM	LUMINAL	Invasive	3	Ductal	Positive	Positive	Negative	Luminal A	23
10	TAN									
11	TAN									
12	TAN									
13	TAN									

Appendix C: Complete Gene Lists from MicroArray

MKC8866 24 h - Normoxia			MKC8866 24 h - Hypoxia		
genesymbol	LOG2 Fold Change	negative LOG10 p-value	genesymbol	LOG2 Fold Change	negative LOG10 p-value
DDIT4	1.22588	2.79197	INSIG1	1.370997	4.433297
DNAH11	1.151973	3.649607	DDIT4	1.09381	3.323597
SLC2A12	1.099632	2.761064	LOC100127888	1.083211	3.197184
SOX4	1.0044	2.562645	SOX4	1.043923	3.162205
HSD17B7P2	1.003853	3.417687	SCD	1.010336	2.821727
MIR210HG	1.002719	4.37355	SCD	0.988812	2.46549
CCNG2	0.988454	2.75266	LIPG	0.98666	4.918684
LIPH	0.973367	4.598125	ALDOC	0.966768	2.711639
-	0.963058	2.95074	CCNG2	0.948816	2.781577
PIK3C2B	0.955905	5.414724	linc-DHRS7B (lincRNA)	0.914452	3.026606
-	0.923909	2.374912	SLCO4A1	0.891133	2.778211
RGCC	0.919495	3.301024	HMGCS1	0.863614	2.375915
PCDHB12	0.914702	2.247404	SPNS2	0.857367	3.242889
-	0.914396	3.874681	-	0.825482	4.611909
HMGCS1	0.906952	2.223245	MIR210HG	0.825366	3.361797
SCD	0.900983	2.327128	TMEM154	0.814332	2.867371
INSIG1	0.891871	1.867904	RGCC	0.806668	3.910554
LIPG	0.864669	2.498071	DYRK1B	0.806575	3.954128
NDRG1	0.834045	2.757198	-	0.80333	3.65395
METTL7A	0.832259	4.392245	PIK3C2B	0.796777	3.96882
C20orf96	0.820388	3.880285	SPAG4	0.780604	3.193399
TMEM154	0.818138	4.971201	NDRG1	0.766799	4.208876
FBXL20	0.806834	2.983392	ITGB4	0.751656	3.476168
PNRC1	0.805454	2.60191	PLLP	0.738801	3.491005
SPRY1	0.805389	3.986436	LIPH	0.725634	4.423994
LPIN1	0.804363	3.779384	DBP	0.725044	2.368186
MSMO1	0.79951	3.136962	DNAH11	0.724917	1.420042

KDM3A	0.782584	2.882141	DMBT1	0.719701	3.389976
SLCO4A1	0.776936	2.908604	TRERF1	0.716546	4.61399
PPFIA4	0.7623	2.787425	PFKFB4	0.715873	3.282107
SCD	0.742861	2.274162	FBXL20	0.715483	3.791723
TNFSF10	0.739922	1.392127	AHNAK2	0.713989	3.270724
PFKFB4	0.736102	3.060508	-	0.709165	1.657513
DMBT1	0.729774	3.652083	LDLR	0.704806	3.986339
P4HA1	0.727693	3.288891	SLC2A12	0.701876	2.02023
TP53INP1	0.724938	2.372091	PNPLA3	0.695813	2.761095
KLHL24	0.71981	2.172347	HSD17B7P2	0.688083	3.083375
BHLHE41	0.717093	2.339838	LRP1	0.686754	2.620674
TRERF1	0.705541	4.815293	METTL7A	0.678489	2.971312
VLDLR	0.705239	2.52023	KRT19	0.676811	3.083118
FAM115C|LOC154761|FAM115D	0.699744	3.600864	-	0.676041	2.593627
	0.69567	3.358291	ORAI3	0.668488	3.353162
SPAG4	0.690565	2.753135	JUP	0.667771	3.439349
TRAJ17|TRAC|TRAV20	0.685596	1.507721	MSMO1	0.666348	3.403071
LOC154761	0.681056	2.013968	TENC1	0.661229	3.617609
SLC16A13	0.673861	1.858544	RASSF4	0.659587	3.390727
CNTNAP3|CNTNAP3B	0.671824	2.622237	CRLF2	0.657681	2.815657
LOC100127888	0.667977	2.930937	MUC1	0.657017	2.846731
PDK1	0.666593	4.496804	PPL	0.654412	2.711766
FLJ35776	0.664089	2.407611	RIMKLA	0.647517	2.978281
SH3TC2	0.661779	3.348377	LPIN1	0.646503	3.450407
TRANK1	0.660434	3.246377	UCN2	0.643037	2.368087
FDFT1	0.655215	2.469342	ZMYM3	0.642325	2.453965
	0.652016	3.77308	PCDHB12	0.63928	1.357739
PDK3	0.651169	3.912441	C6orf223	0.637178	2.736012

MAML3	0.649308	4.328511	TP53INP1	0.629816	3.153354
ARHGAP5-AS1	0.648003	2.261425	FDFT1	0.629181	3.606781
CYP51A1|LRRD1	0.647665	2.003867	PNRC1	0.614442	2.905966
IDH1	0.639994	4.325884	TRANK1	0.608583	3.091644
FUT11	0.634904	2.097691	SLC16A13	0.608313	2.955218
INSIG2	0.625276	3.662207	ARHGAP5-AS1	0.605265	3.000708
ANKRD20A5P	0.622293	3.484639	YPEL3	0.601904	1.970967
ORAI3	0.609377	2.470462	IQSEC2	0.59973	3.302495
DBP	0.602126	1.803592	LSS	0.598838	3.337691
ANKRD37	0.596878	1.912576	MAML3	0.595058	3.827216
PLD1	0.591992	2.742301	RALGDS	0.59292	2.383935
CRLF2	0.590788	3.072292		0.592369	2.685009
KCNN4	0.588154	2.847027	SH3TC2	0.589859	3.863745
GDPD1	0.584642	3.506124		0.585185	1.651203
FAM63A	0.582454	3.555609	-	0.583461	3.252226
PHF21A	0.581517	3.747171	F11R	0.581258	3.003799
PLLP	0.581488	2.997228	-	0.58018	1.706881
KIAA0430	0.580998	2.85765	FAM46C	0.577604	3.735011
KIAA1217	0.578024	4.39507	linc-SCYL1-2 (lincRNA)	0.577035	2.159976
ETV1	0.576934	3.094078	KCNN4	0.573148	2.865961
MIR604	0.575611	2.040747	ROBO4	0.571501	1.541638
	0.57137	3.242837	MOB3A	0.564709	2.65514
	0.570165	1.775308	SNX33	0.564155	3.579445
FAM46C	0.569431	2.762969	SREBF2	0.564057	2.603812
TNIK	0.568828	3.09188	SPRY1	0.562437	2.956605
DYRK1B	0.568646	2.861921	GPER	0.562073	3.163979
LGR4	0.568493	2.789602	LAMA5	0.561861	3.001271
KAT6B	0.567741	3.208395	SPDEF	0.55836	1.952
PRICKLE2	0.565994	3.195873	FAM117B	0.5563	2.685737

IDI1	0.565965	2.736468	IDH1	0.553011	3.421501
FAM13A	0.564451	4.042057		0.551604	1.698364
ANG|RNASE4	0.563629	2.455479	NDP	0.549809	2.409206
ZNF608	0.562296	2.816439	LOC154761	0.547851	3.079678
PPL	0.56194	2.740622	CNIH3|LOC100506354	0.546433	3.421955
BNIP3|BNIP3P1	0.559721	3.460639	BPHL|LOC100130927	0.544246	2.699289
SQLE	0.558378	1.721876	IZUMO4	0.543436	3.217803
JUP	0.556546	2.617399	ANG|RNASE4	0.542084	2.344565
PFKFB3	0.556168	1.473566	MIR4640|DDR1	0.541951	3.199311
	0.555538	1.806203	TCEA3	0.539693	2.686446
	0.555262	1.785447	SLC29A2	0.539665	2.475738
PCDHB14	0.554981	1.641726	DHCR7	0.535881	2.823429
SLC12A6	0.552544	3.040468	CCNA1	0.533244	2.486863
FAM117B	0.548027	3.894032	ACSF2	0.53264	2.808858
ZMYM3	0.545868	3.444357	ARTN	0.529552	4.013386
	0.54584	3.614636	FLJ35776	0.529462	2.633605
	0.545492	2.302196	SNX21	0.526859	3.185282
TMCC3	0.543962	3.39871	ABTB1	0.52354	2.053204
WWTR1-IT1	0.539793	3.924578	PPFIA4	0.522262	3.471238
SPNS2	0.538715	3.687574	LOXL4	0.515761	1.952978
BCL9	0.535387	3.460427	SLC25A23	0.515647	2.86689
	0.535058	1.586501	RPL23AP82	0.513976	2.204899
NUDT7	0.534918	1.885563	MVK	0.513554	2.715707
KCTD12	0.534528	2.17853	CLCN6	0.513524	2.734212
EGLN3	0.533592	2.227055	BCAS3	0.513462	2.928976
ANKZF1	0.531342	2.646311	CLDN4	0.506926	3.106047
MVK	0.528982	2.961749	FAM63A	0.505283	2.727418
PROS1	0.527219	1.4995	KIAA0430	0.50452	3.071274
LSS	0.526289	1.945188	SH3D21|LOC100127947	0.503976	2.990453

CLCN6	0.524773	1.55385	SLC9A3R1|MIR3615	0.503484	1.674617
	0.524573	1.55946	SIN3B	0.502933	2.600647
KIAA1147	0.52339	2.971382	FAM214B	0.499383	2.073744
CCL28	0.521363	3.211846		0.49859	2.166318
DNAH2	0.514318	3.391981	DPYSL2	0.496939	3.755468
DHCR7	0.514011	1.492354	ZMYND8	0.49258	2.969698
MOB3A	0.513689	2.376161	RHOF|TMEM120B	0.491201	2.897458
RASSF4	0.508483	2.796057	-	0.490655	1.323003
DDX58	0.507799	2.454881	SLC4A11	0.488583	2.63954
LMBRD1	0.505143	3.051207	MT1F	0.487657	2.968497
PCDHGB8P	0.498729	2.551469	FAM225A|FAM225B	0.487176	2.210126
FAM225A|FAM225B	0.496786	2.938812	ZNF608	0.487105	1.958204
CDON	0.496456	2.327853	TMEM92	0.486957	2.600984
PITPNC1	0.493903	1.820672	GXYLT2	0.485925	3.241198
MANSC1	0.490398	2.088075	-	0.485866	2.574121
KRT19	0.489915	2.836806	SUFU	0.483044	2.806734
STARD4	0.489739	1.737543	TMEM140	0.480115	2.459453
TRIM2	0.488243	1.559956	BCL3	0.478714	3.184959
TNFRSF10D	0.488217	1.576215	RHBDF1	0.478707	1.669675
CRYZ	0.48593	2.912001	linc-CALML5 (linoRNA)	0.478414	2.121631
IQSEC2	0.485754	2.629824	ING4	0.478178	2.548178
BCAS3	0.485417	2.746738	BTBD2	0.475473	2.405422
PLXNB3|SRPK3	0.485391	3.684025	MIR3907	0.474682	2.274746
C4orf34	0.484864	1.924274	ENO2	0.473237	2.691407
DHCR24	0.483823	1.521915	EGLN3	0.472975	2.364221
FLJ27352	0.483711	1.534893		0.471092	1.782964
SVIL	0.482621	2.998357	WDTC1	0.470818	2.557684
GXYLT2	0.482536	2.71982	misc_RNA	0.470527	1.447256

MLLT3	0.480575	1.893754	MST1R	0.468765	2.744878
AHNAK2	0.480085	1.977995	IGKC|IGKV1-17	0.468759	1.615223
KLHL4	0.479859	1.314977	CALCOCO1	0.468713	3.184593
LOC100507459	0.478652	1.757029	ADAM8	0.467909	1.852663
LPIN2	0.477819	2.204391	HEXIM2	0.467696	2.092648
MKNK2	0.47703	1.967248	PYROXD2|MIR1287	0.467219	3.089409
HMGCR	0.47489	1.693253	LOC253039	0.464965	1.937227
LOC100508120	0.474586	2.357757	RAB3D	0.464101	2.166648
SAT1	0.474182	1.79181	ZNF362	0.463713	2.608129
	0.473891	1.607496	SCAND2	0.463193	1.903502
ARID5B	0.472096	2.686726	MAGED2	0.462601	2.398732
TDRKH	0.471783	3.425361	CST7	0.462017	3.223796
LDLR	0.468105	2.25858	LOC146880	0.46133	1.807353
	0.467405	1.496009	LOC100508120	0.461297	1.475619
TENC1	0.466705	2.608539	PRICKLE2	0.460946	3.360369
	0.464173	1.718547	MXI1	0.458283	3.255358
MEGF9	0.463468	2.471957	FEZF1-AS1	0.456281	2.356404
RPL23AP82	0.462853	1.36014	SLC2A3	0.456226	2.096628
CARD6	0.461343	1.761548	TMCC3	0.452354	2.977163
RALGDS	0.460306	2.260647	KIF3C	0.45215	2.171326
ING4	0.458882	2.479572	MTMR11	0.451972	2.311883
SH3PXD2A	0.458282	3.629013	ARRB1	0.45161	1.826273
SHC3	0.45824	1.503565	MKNK2	0.45045	2.519377
TMEM87B	0.456799	2.955846	GM2A	0.449978	2.88619
LAMA5	0.453109	3.150512	TMC6	0.449598	2.609799
PCDHGA6|PCDHGB2|PCDHGB6|PCDHGA3|PCDHGA4|PCDHGA7|PCDHGA8|PCDHGA9|PCDHGB4|PCDHGC4|PCDHGB5|PCDH	0.450126	2.762731	AMPD3	0.4484	1.926135

GA1|PCDHGA10|PCDHGA11|PCDHGA12|PCDHGA2|PCDHGA5|PCDHGB3|PCDHGB7|PCDHGC3|PCDHGB1|PCDHGC5					
ENO1-IT1	0.449944	2.056033	PGAM1|PGAM4	0.447862	1.948872
IGFBP1	0.449831	3.593589	BHLHE41	0.445404	2.44772
LGALSL	0.449722	3.213074	PCSK9	0.44517	2.507141
GPR39	0.448388	1.966045	NIPSNAP1	0.444493	2.378167
ALDOC	0.447586	1.649638	C14orf159	0.443948	2.121373
PIM1	0.446792	2.547432	BCKDHA	0.44348	1.881335
GFPT2	0.446203	2.051057	PRKD2	0.442878	2.610636
ENO2	0.446191	1.637231	ARHGAP40	0.44196	2.663881
GALM	0.446181	2.926512	PLEKHA8P1	0.441143	2.458786
EGLN1	0.445102	2.67055	NPAS2	0.439909	2.791815
RDH11	0.443981	2.571655	MANSC1	0.439299	1.803197
ARHGAP26	0.443699	3.37212	DNAH2	0.438615	2.992891
CHD6	0.442967	2.862384	SFN	0.437996	2.538056
DLG3	0.441278	2.258917	PHF21A	0.437105	2.896826
	0.441278	3.02288	GNE	0.435469	2.625302
LOC644704	0.440674	2.327652	DDR1|MIR4640	0.434963	2.858888
KIF3C	0.440411	1.873737	ANKZF1	0.434522	2.032468
SC5DL	0.439948	2.284673	MPI	0.434116	2.03063
SLC35D2	0.438557	2.349992	CA12	0.432789	3.258751
CNTNAP1	0.438344	1.838291	MMAB	0.432305	1.669327
RIN2	0.437944	2.705849	KDM5B	0.431981	3.072627
CLDN4	0.437048	1.552962	PFKL	0.431378	2.024055
PLEKHA2	0.43627	3.029278	LOC644704	0.431209	1.444122
SSBP2	0.436145	2.335224	DDR1|MIR4640	0.430119	2.913753
	0.436144	1.99606	DDR1|MIR4640	0.429642	2.907018
SLC29A2	0.435436	3.680348	ZMIZ1	0.429527	2.038961

ST6GALNAC2	0.434957	1.306476	TMEM53	0.429417	1.733885
PBX1	0.433389	3.176089		0.42838	1.30689
DHCR24	0.432148	1.689133	DNAJB5	0.428033	2.537939
SORL1	0.432076	2.262949	GFPT2	0.426386	2.204491
FGD6	0.431655	1.448654	SREBF1	0.425621	1.995592
OCLN|LOC647859	0.430699	2.202191	C9orf89	0.425311	3.117418
OSMR	0.43043	3.20107	PPP1R3G	0.42506	1.876296
FZD1	0.429534	2.269779	BST2	0.424171	1.514575
SCD5	0.428987	2.041269	ARMCX1	0.423731	3.170278
DPYSL2	0.426889	3.607658	NUDT7	0.422086	2.59984
SLFN5	0.426275	1.50875	CORO2A	0.421688	2.543396
SLC25A27	0.425796	1.40121	PDK1	0.421558	2.259658
IL31RA	0.425465	2.416164	OLFML2A	0.421326	1.697236
ENDOD1	0.425127	2.51763	MAP3K12	0.420784	2.583088
C14orf1	0.423929	2.213806	KIAA1217	0.420412	2.16999
ANGPTL2	0.423358	1.551485	PGPEP1|FKBP8	0.420071	2.497989
LOC253039	0.421167	2.665575	DDAH2	0.419888	2.441935
OLFML2A	0.420429	2.989093	DDAH2	0.419357	2.431428
PCDHB13	0.420326	1.351271	DDAH2	0.419342	2.44082
GATSL1|GATSL2	0.42021	1.993824	SORL1	0.419332	3.376219
GPER	0.420129	3.350842	DDAH2	0.419125	2.343279
MXI1	0.420115	3.173845	GATSL1|GATSL2	0.419076	2.802644
BCL3	0.418946	1.943596	IRF9	0.416901	2.142762
AMPD3	0.418141	1.753449	ZHX2	0.416755	1.623145
F11R	0.41754	2.939591	DDAH2	0.416073	2.393099
ACOT13	0.415043	2.923034	TBC1D8	0.415828	1.682883
MAP3K13	0.4143	3.168638	FAM115C|LOC154761|FAM115D	0.415101	2.632108
RAB38	0.413306	1.477142	HFE	0.414907	3.326296
MAP3K12	0.412999	2.366914	SLC1A1	0.414894	2.107663

REPS2	0.410459	2.209238	TMEM45A	0.414461	2.312262
NPPA-AS1	0.409422	1.328052	GGT2|GGT1|SNRPD3	0.414438	1.569768
PCSK9	0.409382	2.677709	SCNN1A	0.414317	2.024306
SLC1A1	0.409369	2.591952	TIMP4	0.413595	2.282224
GPR137B	0.408781	2.506069		0.413563	2.477126
RNF122	0.408522	1.383359	ZBTB22	0.412994	2.782794
MIR421	0.408321	2.470834	ZBTB22	0.412991	2.790834
ZFP90	0.407394	1.459771	ZBTB22	0.412376	2.776304
PLOD2	0.405293	1.89296	ZBTB22	0.412353	2.790649
LOC100216001	0.405055	1.477432	KANK2	0.411836	2.229631
SH3D21|LOC100127947	0.404658	1.580146	TUBB3	0.410663	2.132179
USP28	0.404313	2.854143	ZFYVE1	0.409962	2.338193
TBC1D19	0.403931	1.788669	GPR39	0.409814	2.250828
ACSF2	0.403921	1.728311	F13A1	0.4093	1.97062
SLC6A9	0.403808	1.869672	ANO8	0.40921	1.661314
NAPEPLD	0.402801	1.811018	GALM	0.408999	1.925414
PTX3	0.401457	1.844287	ARHGEF2	0.408819	1.843766
	0.399708	1.87487	CLDN7	0.407676	1.655929
GM2A	0.39872	2.216331		0.40713	1.898879
C11orf54	0.398499	2.427332	VPS39	0.406128	2.272988
YEATS2	0.398472	1.659851	SLC25A1	0.405963	2.54339
PGK1|LOC100653302|LOC100652805	0.398328	3.032645	THAP8	0.404645	1.50458
BBS2	0.39733	2.723102	PINK1|PINK1-AS	0.403616	2.626233
EDEM2|MT1P3	0.397319	1.345099	CTDSPL	0.403545	2.458784
	0.396602	2.447344	FADS2	0.403262	2.155601
ARHGAP40	0.395837	2.602243	BBS2	0.400815	1.996225
LOC100505828|MGST3	0.39559	2.135917	PDK3	0.400496	1.799515
SPDEF	0.395242	1.729862	SOX12	0.400102	1.547684

IRF2BP2	0.394712	1.79579	BCL9	0.398918	2.062277
ATP7A	0.394509	2.486597	RAB5B	0.39874	2.46796
GOLPH3L	0.394183	2.367197	NAT14	0.398576	1.516908
SREBF2	0.394151	1.593215	EPHB4	0.398273	2.230543
TNRC6B	0.393138	2.379612	DHCR24	0.397639	2.710244
AGFG2	0.392032	1.980618	FAM20C	0.397182	1.968783
PLEKHA8P1	0.390795	1.482207	LZTS2	0.397054	2.275885
SEMA4D	0.390634	2.619125	PLOD1	0.397001	2.24782
	0.390621	2.673835	MIR4294	0.396368	1.830481
NDP	0.389333	1.889707	LOC389602	0.396249	2.668246
	0.388729	3.278054	LPIN2	0.395983	2.553351
TMEM14A	0.388215	2.78584	RNF122	0.395515	2.718425
MIR1299	0.388183	1.380374	DNASE2	0.393946	1.755641
IL17RD	0.388007	2.072443	CAPN10	0.392975	2.265235
ZCCHC24	0.387346	3.171465	FBXL2	0.392693	1.470941
NIPSNAP1	0.386907	2.185201	PYCARD	0.392104	2.213352
TGFBR2	0.386734	3.139517	FAM100B	0.391021	1.324103
ATP2B4	0.385906	2.221124	P4HA1	0.39077	3.049595
TCEA3	0.384652	1.754936	EIF2C4	0.390477	1.778964
GBE1	0.384075	1.714253	TGFBR2	0.389777	2.639693
RHOT1	0.383928	2.469342	TBC1D17|MIR4750	0.389652	2.391215
ACSS2	0.38338	2.088844	OCEL1	0.388943	2.361003
LOC100132815	0.382851	2.135757	BNIP3|BNIP3P1	0.388517	2.8988
ALDH6A1	0.382738	2.526959	PIM1	0.388171	2.460202
CNIH3|LOC100506354	0.382615	3.34885	ZER1	0.387564	1.98043
FLVCR2	0.382213	2.236905	ICAM1	0.387465	1.694002
SNX21	0.382082	2.305088	ST6GALNAC2	0.387069	2.105245
MST1R	0.38046	1.934638	CYP27A1	0.386325	2.33565
BACE1-AS	0.380167	2.442555	snoRNA	0.385643	1.718749

TCEAL8	0.380105	1.993974	IL17RC	0.385326	1.868653
BTBD2	0.379786	2.455307	GSN	0.383358	3.103315
CTPS2	0.378889	2.282535	SLC35D2	0.383197	2.771781
SNHG1	-0.37857	2.738038	TNS4	0.382627	1.987893
BIRC2	-0.37892	1.865243	TUBGCP2|LOC100506167	0.382507	2.448807
EIF5A2	-0.38062	1.357562	CD24	0.381825	1.602074
TEAD4	-0.38115	1.771139	CYP51A1|LRRD1	0.381233	2.340794
ADAT2	-0.38161	3.460174	CNTNAP1	0.38084	1.853256
UGCG	-0.38191	2.698474	ARHGAP27	0.380275	2.514095
RRP1	-0.38201	2.263566	ENO1-IT1	0.380098	1.828298
NOC3L	-0.38296	2.02686	ZNF395|FBXO16	0.379997	1.949198
FOSL1	-0.38318	1.597284	C6orf1	0.379378	2.003745
PAWR	-0.38387	1.553122	IFI6	0.379173	1.643836
SLC5A6	-0.38391	1.773812	GALNT6	0.37886	1.749365
DDX31	-0.38505	2.124018	SEMA4D	0.378692	2.379499
LOC100505573	-0.38602	2.832385	DDR1|MIR4640	0.378615	2.406932
AGMAT	-0.38646	1.919846	CCNJL	0.378585	2.123955
TOMM40	-0.38695	1.782189	FOS	-1.38225	2.295916
UTP15	-0.38725	3.012561		-1.02276	4.542594
BRIX1	-0.38792	1.762542	SERPINE1	-0.95723	3.838066
	-0.38922	2.143969	LOC730755|KRTAP2-4	-0.93778	2.462585
PPRC1	-0.38934	1.984067	LACC1	-0.91087	1.303064
LOC100128881	-0.38935	1.721438		-0.86276	1.339838
POLR3D	-0.38953	2.006307	KIAA0020	-0.8548	1.683473
MB21D2	-0.3905	1.681158	ZNHIT6	-0.84648	1.92844
PWP2	-0.39101	1.678658	SNORD78	-0.84623	2.073551
TGFB2	-0.39173	1.471343	SKIL	-0.8338	1.485421
ARRDC4	-0.39489	1.830177	POLR3G	-0.81825	1.881153
MRTO4	-0.39532	1.98297	SERPINB2|SERPI	-0.81211	3.102811

			NB10		
TIMM8A	-0.39599	2.30422	LOC100133106	-0.81088	1.795657
FOXC1	-0.39622	2.631102	NOC3L	-0.80436	1.462515
MYBBP1A	-0.39888	1.650804	SLC30A1	-0.80164	1.806514
SNORA71B|LOC388796	-0.39974	2.390523		-0.80066	1.737849
	-0.39978	1.740402	CYP1B1	-0.79704	1.933642
FZD7	-0.39984	2.611633	LOC728643	-0.78659	1.529126
HIST1H2BM	-0.40236	1.341169	AMIGO2	-0.77282	3.397709
USP36	-0.40237	1.807818	URB2	-0.7709	2.914005
MAK16	-0.40252	3.33604	DDX21	-0.76957	2.927552
PNPT1	-0.40299	2.736455	CYP1A1	-0.76196	4.072006
TAF1D|MIR1304|SNORD5|SNORA32|SNORA40|SNORA18|SNORA8	-0.40606	1.323545	ZNF451	-0.75568	1.396737
UBIAD1	-0.40805	1.949518	TAF1D|MIR1304|SNORD5|SNORA32|SNORA40|SNORA18|SNORA8	-0.7465	1.349323
C10orf2	-0.4083	2.38395		-0.741	1.891841
TPRA1	-0.40852	2.015968	UTP15	-0.74003	2.558012
BYSL	-0.40968	2.521617	GCLM	-0.73595	1.608615
PPAT	-0.41034	2.738132	RRS1	-0.73531	2.613793
URB1	-0.41125	2.709045	LTV1	-0.73473	3.391665
QTRTD1	-0.41133	2.627637	WDR43	-0.73446	1.849956
BOP1	-0.41188	1.668417	SNAPC1	-0.73386	1.755771
WDR3	-0.4125	2.56514	RRP15	-0.72973	2.29515
SLC25A33	-0.41336	2.959164	PNO1	-0.71801	4.015358
RPL12	-0.4134	2.147933		-0.71571	2.149036
TOX	-0.41513	2.857622	FST	-0.71471	4.419966
TMEM5	-0.41567	2.755506	SNORD14E	-0.70081	2.537728
DKC1|SNORA56	-0.41584	2.427215	RIOK1	-0.69734	3.832013

NIP7	-0.41634	2.713082	IQCB1	-0.69631	1.665209
UTP14A	-0.41667	2.066935	PNPT1	-0.69559	2.515359
MARS2	-0.41773	2.912348	UTP20	-0.68376	1.58723
NOP56|SNORD86|MIR1292|SNORD110|SNORD57	-0.4182	2.383447	ADAT2	-0.68354	2.016691
RIOK1	-0.41909	2.622259	SNORD18B|SNORD18C|SNORD18A|SNORD16|RPL4	-0.68331	1.348243
NOG	-0.42168	1.338319	SDAD1	-0.66294	1.334508
DNTTIP2	-0.42276	1.446849	SNORD11	-0.65562	1.483174
SNHG15	-0.42464	2.156783	FAM72D	-0.64818	1.403573
NFKB1	-0.4256	3.634797	C12orf4	-0.6448	1.957059
MKI67IP	-0.42985	2.795218	MIR548AL	-0.64268	2.806726
	-0.43301	2.437504	CHAC2	-0.63789	2.566895
YRDC	-0.43642	2.253124	TUBE1	-0.62237	2.175024
SNORD12C	-0.4373	1.663631	BIRC2	-0.62198	1.304607
TAF4B	-0.43739	2.793889	snoRNA	-0.61354	2.426496
SNORD69	-0.43742	2.676376	EXO1	-0.61183	2.508273
SNORA9|SNHG15	-0.43927	2.259422	GPCPD1	-0.61095	1.845038
CCDC41	-0.44041	1.536368	DNAJB9	-0.6103	2.993941
HES1	-0.44141	1.729708	PAWR	-0.61019	1.336522
ANKRD1	-0.44552	3.190216	SNORA27|SNORD102|RPL21	-0.60944	1.407581
SNORA45	-0.44559	2.999137	MAGOHB	-0.60786	1.66111
METTL1	-0.45033	2.870735	SLC7A2	-0.60711	2.361429
GTPBP4	-0.45093	3.064294	ANGPTL4	-0.60322	2.593818
DPH2	-0.45272	1.806066	MAK16	-0.60132	2.541483
SELRC1	-0.45624	3.114274	PRAMEF3	-0.59959	1.987102
LOC100507303	-0.45727	1.426567	TMEM168	-0.59703	1.471696
NEGR1	-0.45737	1.509103	RND3	-0.59334	1.598217
SNORD75	-0.45794	3.500331	PPAT	-0.59253	2.379232

CD3EAP	-0.45827	1.636584	TFAM	-0.59127	1.407376
FSTL3	-0.46004	2.969355	DDX10	-0.58743	1.772982
POP1	-0.46035	2.518816	ACTR3B	-0.58716	1.917962
RRP15	-0.4627	2.980104	NUDCD1	-0.587	1.750314
SNHG8	-0.46305	2.753994	SCARNA27	-0.58476	1.319114
SMAD7	-0.46525	1.47151	GPATCH4	-0.57872	2.852917
	-0.46768	1.819837	DNAJC2	-0.57769	1.320776
NUFIP1	-0.46836	2.823519	NMD3	-0.57725	1.536625
ZNHIT6	-0.46855	2.294548	TIPIN	-0.57573	2.876638
WDR4	-0.46987	2.138898	EID3	-0.57432	1.410171
TAF1D|MIR1304|SNORD5|SNORA32|SNORA40|SNORA18|SNORA8	-0.47811	1.705915	SNORA76	-0.57411	2.198326
HIST2H3D	-0.47968	1.374602	RNF219	-0.5731	1.426857
SLC7A5	-0.47996	2.760756	MND1	-0.57131	1.880444
LTV1	-0.48127	3.396995	QTRTD1	-0.57037	2.500918
GPATCH4	-0.48168	2.584377	FAM196B	-0.56728	3.594025
	-0.48309	1.319734		-0.56501	1.849933
	-0.48428	3.053273	ZNF485	-0.56364	2.324554
RRP12	-0.48514	1.634099	FGF5	-0.56211	2.456477
FAM196B	-0.4882	1.69938	LIAS	-0.56158	2.362417
	-0.48998	3.072223	EPT1	-0.55828	2.021492
AEN	-0.49411	3.361518	PDSS1	-0.55584	3.159993
NOL6	-0.4976	2.295309	ZNF239	-0.55471	3.473551
FGF5	-0.49952	3.811017	ENAH	-0.55439	1.398439
LOC388796	-0.5017	2.310719	ADAMTS6	-0.55414	1.471436
MIR22HG	-0.50683	3.237979	EIF3J	-0.55407	2.131432
SNHG12	-0.50702	2.688098	linc-AGMAT3 (linc+K114RNA)	-0.55279	2.817562
SNAPC1	-0.50741	2.446229	ZNF699	-0.55269	2.377716
WDR43	-0.51238	3.018046	GTPBP4	-0.55093	3.043528

GPR110	-0.51262	1.709504	METTL12	-0.54921	1.990006
SLC7A6	-0.51884	2.685112	C1orf135	-0.54818	2.469338
RPL22L1	-0.51998	2.888366	MPHOSPH10	-0.54683	1.444088
ESF1	-0.52489	1.436956	GTF2F2	-0.54681	1.839605
TINAGL1	-0.52493	3.060178	CD3EAP	-0.5443	2.208775
BIRC3	-0.52708	1.355245	GNL3|SNORD19B	-0.54323	3.493692
NOP2	-0.52718	2.855146	LOC100507303	-0.54321	2.112399
KIAA0020	-0.529	2.456735	SEC11C	-0.53971	1.944079
CCRN4L	-0.5296	2.96913	TBC1D4	-0.53884	1.894903
F3	-0.53107	2.646354	TAF13	-0.53832	1.730593
URB2	-0.53275	1.918435	IMPA1	-0.53758	1.548282
MFSD2A	-0.53325	3.417734	ZNF330	-0.53603	2.083572
VDR	-0.53358	2.43406	EPB41L4A-AS1	-0.53571	2.801984
SRFBP1	-0.53473	1.648428	MIR22HG	-0.53518	2.449473
PRMT3	-0.53597	2.779339	CCRN4L	-0.53353	2.278935
PNO1	-0.54052	2.911707	THUMPD2	-0.53118	1.485127
CHORDC1	-0.54228	1.490678	SUV39H2	-0.52951	2.288722
LOC100509671	-0.54813	2.717382	SNORD75	-0.52895	2.482524
DDX21	-0.56159	3.076576	TAF4B	-0.52784	2.389547
CCDC99	-0.56593	1.657873	CDCA7	-0.5275	2.141606
	-0.56617	3.443648	LOC643650	-0.52682	1.775839
SNORD14E	-0.57347	4.125463	MINA	-0.52531	3.150707
NOP16	-0.5776	3.771756	SNORA74A	-0.52488	1.747762
PXK	-0.58513	3.105853	RPF2	-0.52448	2.61702
THBS1	-0.58571	3.147045	RPIA	-0.52317	1.886864
LOC643650	-0.58705	3.589015	ING3	-0.52309	1.977364
SNORD18B|SNORD18C|SNORD18A|SNORD16|RPL4	-0.58775	1.751484	RPL22L1	-0.52219	2.787699
KCNQ5-IT1	-0.59159	1.81168	DUSP1	-0.52109	2.951337
PMEPA1	-0.61492	1.961347	ZMAT3	-0.52045	1.78131

FJX1	-0.62409	3.153232	SNHG1	-0.51933	2.727188
SNORA74A	-0.6242	2.14607	PPA1	-0.51851	1.834512
RRS1	-0.6343	3.327403	XPO4	-0.51828	1.802748
SNORD78	-0.63907	4.310304	WDR89	-0.51704	1.452672
METTL12	-0.65148	2.702257	CCNE2	-0.51686	1.644386
LOC100133106	-0.67776	2.499639	ZWILCH	-0.51591	1.815354
	-0.68817	3.473789	lincRNA	-0.51547	1.75757
SKIL	-0.6941	2.667885	SPCS3	-0.51499	1.394663
	-0.70286	2.162304	GAN	-0.51484	2.203386
LACC1	-0.75065	2.444775	UBIAD1	-0.51427	2.175121
	-0.77079	2.78285	WDR35	-0.51419	1.424687
	-0.78477	3.656701	C14orf149	-0.51387	1.513582
SHISA2	-0.81781	2.177912	SNHG5	-0.51325	2.524911
AMIGO2	-0.84445	3.366779	SNORD51	-0.51197	1.85117
SERPINE1	-0.97375	3.692842	CCDC75	-0.51164	1.542319
LOC730755|KRTAP2-4	-0.97419	2.132607	CRY1	-0.51057	2.398724
FST	-0.98464	4.736901	FASTKD3	-0.51038	3.192055
SERPINB2|SERPINB10	-1.00899	2.519683	MKI67IP	-0.51	3.129807
LOC728643	-1.03113	2.67314	ENTPD7	-0.50918	1.961855
CYP1B1	-1.07389	4.219522	PXK	-0.50906	1.904179
CYP1A1	-1.40576	3.71772	KLHL8	-0.50863	1.78862
				-0.50666	1.812988
			NUFIP1	-0.50655	2.115948
			NUP54	-0.50573	1.455779
			PAK1IP1	-0.50403	3.259789
			RPL12	-0.50184	1.318086
			HES1	-0.4999	2.688025
			WDR3	-0.49989	3.287737
			HEATR1	-0.4985	1.76739

ME2	-0.49798	1.542003
CHRNA5	-0.49725	2.238109
	-0.49555	1.86164
BRIX1	-0.49535	2.160599
MRPL42	-0.49252	1.725863
ZNF639	-0.49198	2.039324
VRK1	-0.49174	1.650834
NOL10	-0.49149	2.405325
ZNF26|LOC100287515	-0.49112	1.340632
UTP14A	-0.49099	2.339685
LYAR	-0.49087	2.515445
SLC25A33	-0.49024	1.557573
CASP3	-0.49016	1.569701
NOP16	-0.48982	1.95332
MRPL1	-0.48956	1.47177
GNL2	-0.48864	2.32583
OXCT1	-0.48854	2.885979
C12orf5	-0.4879	2.213162
MYL12B	-0.48789	2.127682
BYSL	-0.48626	1.882697
THBS1	-0.48574	3.023357
DSCC1	-0.48476	2.023912
MIOS	-0.48466	1.940006
GTF2H2B|GTF2H2C|GTF2H2D	-0.48458	1.579595
PDCD1LG2	-0.48377	2.287393
ARRDC4	-0.48153	2.255028
PUS3	-0.48146	2.260402
ncrna:snoRNA	-0.48129	2.812919
FAM13B	-0.47996	1.95652
SLC25A20	-0.47796	1.972702

C11orf82	-0.47696	1.4479
CLSPN	-0.47577	1.976099
TAF1D|MIR1304|SNORD5|SNORA32|SNORA40|SNORA18|SNORA8	-0.47537	1.381396
LOC728463	-0.4751	1.978936
NAF1	-0.47378	1.657189
NSUN6	-0.47366	1.71133
NOL6	-0.47329	1.776164
DDX18	-0.47276	1.662641
RFC3	-0.47267	2.128019
F3	-0.47164	2.043713
SNORA75	-0.47143	1.576325
NOP58	-0.47055	1.498273
YTHDC1	-0.47051	1.587482
METTL1	-0.46932	1.867429
EOGT	-0.46922	1.424606
RBM26-AS1	-0.46815	1.499957
SLC25A32	-0.46611	2.395147
C18orf21	-0.46503	1.772595
LOC100133920	-0.46491	1.854317
FRMD6	-0.46376	1.876733
ZFAND1	-0.46339	1.342731
MARS2	-0.4631	2.912389
ZNF878	-0.46245	1.716925
GNPNAT1	-0.46205	2.749013
TIMM8A	-0.4613	2.619034
CCNJ	-0.46047	2.06945
TMEM38B	-0.45999	1.380556
LLPH|TMBIM4	-0.45884	2.696027
AMD1	-0.45881	2.131757

FASTKD2	-0.45879	1.558261
	-0.45642	2.069426
NAA25	-0.45502	1.926289
PMEPA1	-0.45381	2.491878
NOLC1	-0.45334	2.170851
ADRB2	-0.45264	3.397036
SNORD69	-0.45187	2.276877
GFM1	-0.4515	1.876245
MFSD2A	-0.45026	2.115762
	-0.44995	1.305756
SLC22A4	-0.4492	1.844467
C10orf2	-0.44814	2.064662
MRPS25	-0.44362	2.924682
C6orf228	-0.44325	1.357024
SNORA13	-0.44273	2.357732
VPS36	-0.44056	1.310238
LONRF3	-0.44024	3.525227
RGS2	-0.4401	2.294821
PITPNB|LOC100507669	-0.43828	2.161338
NOP2	-0.43793	2.047687
TGDS	-0.43776	1.67601
SNRPD1	-0.43675	2.080262
FJX1	-0.43647	2.072068
LINC00702	-0.436	1.991611
GLIPR1	-0.43555	1.372924
YRDC	-0.4344	1.458189
PHLPP2	-0.43432	3.707824
PRMT3	-0.43426	1.920407
TOMM70A	-0.43243	2.133629
ORC5	-0.43226	2.2113

CDRT1	-0.43222	1.501329
RSBN1L	-0.43182	1.360429
RNFT1	-0.43168	1.728923
AIMP1	-0.43049	1.972937
POP1	-0.43005	2.981544
MIR3137	-0.43002	1.345344
DIMT1	-0.42875	3.145301
C3orf52	-0.42831	1.324958
ASNSD1	-0.42824	1.936036
MAD2L1	-0.42707	1.717592
MBLAC2	-0.42695	1.372851
SLC25A19	-0.42676	2.226224
	-0.42619	1.6186
RIOK2	-0.42532	1.393314
MIS12	-0.42405	2.339434
MRPS35	-0.42316	1.83542
NKRF	-0.42294	3.150984
C19orf48	-0.42252	1.40379
DKC1|SNORA56	-0.42229	2.401255
LOC202181	-0.42213	1.656707
RPS27	-0.42211	1.511122
NKIRAS1	-0.42188	2.539084
SRP19	-0.4204	1.806834
RNU1-19P	-0.41936	1.680364
SLC35D1	-0.41876	1.768565
IFRD1	-0.41871	2.323663
MDN1	-0.41754	2.77951
DPH5	-0.41577	2.227628
EIF2A	-0.41534	1.317919
C2orf47	-0.41526	1.712394
TIMM9	-0.41515	1.651375

FOXC1	-0.415	2.24925
GTPBP8	-0.41475	1.845988
NAV3	-0.41472	2.059629
NOL11	-0.41468	2.543775
SNORA45	-0.41462	1.736517
	-0.41438	1.866867
BLOC1S2	-0.41344	1.760946
DPH2	-0.41329	2.069921
PUS7	-0.41274	2.36551
POLR1B	-0.41188	2.417867
IPO11|KIF2A	-0.41093	1.476507
URB1	-0.41076	1.833789
SCML2	-0.41019	1.827222
MPHOSPH6	-0.41019	1.851733
RHOBTB3	-0.40941	1.507475
MIR17HG|MIR92A1|MIR20A|MIR19A|MIR18A|MIR19B1	-0.40866	1.507295
NFKB1	-0.40837	2.741055
TXLNG	-0.40721	1.495442
RBL1	-0.40685	1.47857
ZNRF3	-0.40635	1.591301
WDR75	-0.40445	1.742637
42066	-0.40295	2.526986
LSM6	-0.40257	1.594438
CTPS1	-0.40255	2.632042
NSUN2	-0.40222	2.994922
PAPD5	-0.40177	1.521463
ZNF600	-0.40096	1.487521
RABGGTB|SNORD45C|SNORD45A|SNORD45B	-0.4007	2.113254
MTIF2	-0.40045	1.663793

GEMIN5	-0.39967	2.431977
ncrna:snoRNA	-0.39915	1.876407
BCCIP	-0.39912	2.044795
MTHFD2	-0.39854	1.974567
PWWP2A	-0.39751	1.347617
ORMDL1	-0.39684	1.897742
ZNF121	-0.39648	1.394076
BMS1	-0.39557	1.656209
SFXN4	-0.39517	1.334878
SNORD14A	-0.39297	1.654703
TDG	-0.39256	2.333773
RSL24D1	-0.39184	1.729951
FAM72C	-0.39159	2.017035
CDKL1	-0.39154	2.757821
SLC35G1	-0.39153	2.28032
EIF2S1	-0.39054	1.951059
SNORD100|SNORA33	-0.39028	1.605931
TMEM5	-0.39024	2.975244
ASAP1	-0.38973	2.060816
SNORD12C	-0.38874	1.424016
	-0.38871	1.598224
MRPL19	-0.38852	1.553064
LOC442075	-0.38829	2.776852
SNORA9|SNHG15	-0.38801	1.810767
SNHG8	-0.38787	1.719062
SSR3	-0.38763	2.110704
METTL21D	-0.38721	1.535307
GAR1	-0.38717	2.047991
PRPF18	-0.38647	1.396601
SNRPF	-0.38607	1.383562

PDCL3|LOC285359	-0.38582	1.748674
C12orf45	-0.38567	2.432039
SNORD18C|RPL4|SNORD18B|SNORD18A|SNORD16	-0.38539	2.659551
SLC33A1	-0.38498	2.276481
CHCHD1	-0.38497	1.350949
ZNF844	-0.38475	2.193976
ARMC8	-0.38447	1.509719
AGAP6	-0.38428	1.601762
GPAM	-0.38255	2.193199
RRN3	-0.3809	1.481614
DESI1	-0.37951	1.978548